Distortion-Based Crest Factor Reduction Algorithms in Multi-Carrier Transmission Systems

A Dissertation
Presented to
The Academic Faculty

by

Chunming Zhao

In Partial Fulfillment
of the Requirements for the Degree
Doctor of Philosophy in the
School of Electrical and Computer Engineering

Georgia Institute of Technology
December 2007

Distortion-Based Crest Factor Reduction Algorithms in Multi-Carrier Transmission Systems

Approved by:

Professor G. Tong Zhou, Advisor
School of Electrical and Computer Engineering
Georgia Institute of Technology

Professor Ye (Geoffrey) Li
School of Electrical and Computer Engineering
Georgia Institute of Technology

Professor Xiaoli Ma
School of Electrical and Computer Engineering
Georgia Institute of Technology

Professor Ming Yuan
School of Industrial and Systems Engineering
Georgia Institute of Technology

Professor J. Stevenson Kenney
School of Electrical and Computer Engineering
Georgia Institute of Technology

Date Approved: 19 October 2007

To my grandmother,

my wife,

and other family members,

for their love and encouragement

ACKNOWLEDGEMENTS

This dissertation has been accomplished with accompany and support of many people. It is my pleasure to express my gratitude to all of them.

First and foremost, I would like to express my sincere appreciation and gratitude to my advisor, Dr. G. Tong Zhou. She taught me how to start academic pursuits step by step. From her, I learned a lot and improved a lot especially in critical thinking and algorithm developing. Without her encouragement and help I can not complete this work. My time in our group was really happy and will sit in my mind forever.

Next, I would like to thank my thesis defense committee members: Dr. Xiaoli Ma, Dr. J. Stevenson Kenney, Dr. Ye (Geoffrey) Li and Dr. Ming Yuan for helping me a lot to improve the quality of the dissertation.

I would also like to thank my group members: Hua Qian, Ning Chen, Chunpeng Xiao, Vince Emanuele, Thao Tran, Robert Baxley, Kun Shi and Qijia Liu, for their kind helps and valuable discussions. Sharing happiness with them make my study full of fun. Special appreciation is given to Robert Baxley for our happy collaborations related to the topic of this dissertation.

Last but not least, I would like to express my gratitude to my family. I would like to thank my grandmother and my parents for their love and support. Letting them feel proud of me is the biggest power for me to work hard. I would like to thank my sister for her encouragements. Special thanks to my wife, Yao Xin, for her love and accompany. She takes care of me since I met her.

TABLE OF CONTENTS

LIST OF TABLES

LIST OF FIGURES

LIST OF ABBREVIATIONS

3GPP	3rd Generation Partnership Project.
ACE	Active Constellation Extension.
ADC	Analog-to-Digital Converter.
AWGN	Additive White Gaussian Noise.
BER	Bit Error Rate.
CCDF	Complementary Cumulative Distribution Function.
CDMA	Code Division Multiplexing Access.
CF	Crest Factor.
CFR	Crest Factor Reduction.
CP	Cyclic Prefix.
CR	Clipping Ratio.
CSI	Channel State Information.
DAC	Digital-to-Analog Converter.
DMT	Discrete Multi-Tone.
DSL	Digital Subscriber Line.
EDGE	Enhanced Data rates for GSM Evolution.
EVM	Error Vector Magnitude.
FFT	Fast Fourier Transform.
GSM	Global System for Mobile.
ICI	Inter-Carrier Interference.
IDFT	Inverse Discrete Fourier Transform.
IFFT	Inverse Fast Fourier Transform.
ISF	Identical Scaling Factor.
ISI	Inter-Symbol Interference.
LAN	Local Area Network.
LTE	Long-Term Evolution.
MAN	Metropolitan Area Network.

MIMO Multiple-Input Multiple-Output.

MSF Multiple Scaling Factors.

NLNST Nonlinear Non-Symmetric Transform.

OFDM Orthogonal Frequency Division Multiplexing.

OFDMA Orthogonal Frequency Division Multiplexing Access.

PA Power Amplifier.

PAR Peak-to-Average Power Ratio.

PDF Probability Density Function.

PSD Power Spectrum Density.

PSK Phase-Shift Keying.

PSNR Peak Signal-to-Noise Ratio.

PTS Partial Transmit Sequence.

QAM Quadrature Amplitude Modulation.

SISO Single-Input Single-Output.

SLM Selected Mapping.

SNDR Signal-to-Noise-and-Distortion Ratio.

SNR Signal-to-Noise Ratio.

WiMAX Worldwide Interoperability for Microwave Access.

SUMMARY

With the increasing demand for information transmission, fast, reliable and flexible data communication is highly required. Orthogonal frequency division multiplexing (OFDM) is a powerful multi-carrier scheme in the frequency-selective environment, combating multi-path fading by transmitting data in parallel sub-channels. OFDM sub-carriers are mutually orthogonal to eliminate the inter-carrier interference (ICI). The introduction of a cyclic prefix (CP) removes the inter-symbol interference (ISI) and allows the channel matrix to be in the diagonal shape, greatly simplifying the equalization. Combining with multiple-input multiple-output (MIMO) scheme, MIMO-OFDM can provide either higher data rate or better signal quality than the single-input single-output (SISO) OFDM. Because of these excellent properties, OFDM has been adopted by several standards [1,3,4,6] as the physical-layer transmission scheme.

However, the time-domain OFDM signal exhibits high peaks because of its Gaussian-like distribution. When the OFDM signal goes through a power amplifier (PA), for example, high peaks will be clipped, thus increasing the bit error rate (BER) and causing interference to other users. To avoid such nonlinear distortions, the signal has to be backed off to the linear region, reducing the power efficiency of the PA. The envelope variation can be quantified by the peak-to-average power ratio (PAR) or the crest factor (CF). Since PAR = CF^2, PAR and CF are the same in the dB scale. Hence, these two are not distinguished in the dissertation.

PAR reduction, or crest factor reduction (CFR), is an efficient solution for the high-PAR problem, attracting a lot of research efforts. CFR techniques can be divided into two categories, distortion-based CFR and distortionless-based CFR, depending on whether extra distortion will be introduced. Each category has advantages and disadvantages. Distortion-based CFR methods are simple, usually without receiver-side processing. The downside is

that distortions will be generated both in-band and out-of-band, significantly deteriorating the link quality. On the other hand, distortionless-based CFR methods, while requiring intensive computations and involving receiver-side processing, maintain system performance without degradation. In this dissertation, we will investigate several aspects related to distortion-based CFR techniques.

Before we set forth to find efficient CFR methods, it is better to investigate what is the proper PAR metric. This is worthwhile, especially for MIMO-OFDM systems where several different metrics are used without justifications. To increase the average power efficiency, PAR metrics should be derived for different linear scaling scenarios in different MIMO-OFDM configurations.

Another important aspect of distortion-based CFR algorithm is to choose efficient metrics to describe the performance degradation. A popular figure of merit, error vector magnitude (EVM), can be used to evaluate in-band distortions introduced in a communication system. Compared with BER, EVM not only quantifies the distortions, but also attributes the source of distortion to phase noise, modulator imbalances, power amplifier nonlinearities, and so on [7, 22]. To guarantee reliable transmissions, EVM thresholds are specified in various standards. Statistical analysis of EVM is performed to provide concrete thresholds for the amount of allowable distortions from each source to meet EVM requirements.

Existing distortion-based CFR techniques are reviewed in the dissertation. After analyzing these schemes, we find that signals after processing may violate the in-band EVM threshold and the out-of-band spectrum mask requirement; hence, additional processing is required to reduce such distortions. Therefore, we propose a novel distortion-based CFR method, constrained clipping, to include in-band and out-of-band distortion control mechanisms. Moreover, constrained clipping has low computational complexity and requires no receiver-side processing, making it easy to be implemented.

Finally, the signal-to-noise-and-distortion ratio (SNDR) analysis for transceiver nonlinearities in the additive white Gaussian noise (AWGN) channel is investigated to setup a platform for comparing two CFR algorithms: clipping and companding. Closed-form SNDR

expression is derived by utilizing the Bussgang Theorem and complex polynomial approximations. Additionally, the SNDR analysis can help us determine the optimal nonlinearity at the receiver to maximize the transceiver SNDR when the transmitter nonlinearity is known.

CHAPTER I

INTRODUCTION

1.1 Motivations

Multi-carrier transmission is a popular choice in modern communication systems, such as discrete multi-tone (DMT) in digital subscriber line (DSL) and orthogonal frequency division multiplexing (OFDM) in wireless LAN, wireless MAN and 3GPP long term evolution (LTE). In multi-carrier systems, information data are generated in the frequency domain, transformed to the time domain, and sometimes spread to the space domain if multiple antennas are used.

Time-domain multi-carrier signals usually exhibit large amplitude variations, which can be approximately described by the Gaussian distribution. This is an undesirable property because it will involve the nonlinear distortion, lower the power efficiency, and increase the implementation cost, when the high-PAR signal passes through the transmitter front-end, which is usually modeled as a peak-power limited channel. We choose peak-to-average power ratio (PAR) or crest factor (the square root of PAR) to delineate the power or envelope variations of multi-carrier signals.

When the input power drives the transmitter front-end (such as power amplifier (PA)) into the nonlinear region, peaks of the signal will be clipped, which will generate nonlinear distortions both in the signal bandwidth and in the adjacent channels. To avoid such distortions, the common solution is to back off the signal down to the linear region. However, with the unreduced PAR, the obtained power efficiency of the PA is usually pretty low. Another motivation of CFR is to efficiently utilize the dynamic range of digital-to-analog converter (DAC) or analog-to-digital converter (ADC), because the high peaks rarely occur. With a powerful PAR reduction technique, we can expect high power efficiency, low nonlinear distortion, and small dynamic-range requirement of the analog components. Therefore, it is worthwhile to investigate the CFR as a useful tool to boost the performance of multi-carrier

systems.

The definition of PAR in SISO-OFDM systems is clear because PAR has straightforward relationship with the performance-evaluating metrics; however, when the MIMO-OFDM signal is considered, the confusion appears. Different PAR metrics are used in the literature, such as the individual branch PAR, the maximum PAR on different antenna branches, and the arithmetic average PAR on different antenna branches. Usually, one definition is just adopted without giving the necessary justifications. This motivates us to study what is the meaningful PAR definition in MIMO-OFDM systems by considering the purpose of designing CFR, such as the power efficiency improvement.

Distortion-based CFR techniques have many advantages for the system implementation, such as simple structure, low computational complexity, and no side information transmission. However, these nonlinear CFR operations may greatly degrade the link quality. So, additional operations are required to control the in-band and out-of-band distortions. For the in-band part, we can rely on the EVM analysis to relate the performance degradation to various distortion mechanisms and control the EVM to satisfy the standard requirements. Spectral mask is a deterministic metric to constrain the out-of-band spectrum regrowth.

SNDR analysis is a useful tool to study the nonlinearity in the transmission link, for example, clipping with a specific gain was proved to be the optimal nonlinearity to maximize the SNDR in the linear receiver configuration [75]. Nonetheless, when transceiver nonlinearities are of interest, such as companding CFR algorithms, we need to generalize the SNDR analysis. Based on the SNDR of transceiver nonlinearities, clipping and companding can be compared to determine which one has better error performance when they meet the same peak-power constraint.

1.2 Objective

The objective of this dissertation is to design, analyze and compare distortion-based crest factor reduction algorithms in OFDM and MIMO-OFDM systems.

First, we aim to clarify the definitions of PAR in MIMO-OFDM systems based on the power efficiency consideration. These proper PAR metrics should be used by CFR system

designers to maximize the power efficiency of the PA.

Second, EVM analysis will be performed in OFDM systems to calculate theoretical EVM values for various distortion mechanisms. For each distortion, we expect to derive the concrete threshold for the amount of allowable distortion to satisfy the requirement of the standard.

Third, new signal processing operations are needed to cope with the in-band and out-of-band degradations introduced by the clipping-based CFR algorithm. We should add necessary constraints on the in-band EVM and out-of-band power spectrum density (PSD), and design efficient mechanisms to meet the requirements.

Finally, we are interested in comparing two powerful CFR algorithms, clipping and companding. SNDR analysis is used as a tool to exploit the transceiver nonlinearities, such as the transmitter compressing function and the receiver expanding function in the companding scheme.

1.3 Outline

The outline of the rest of this dissertation is as follows:

Necessary backgrounds are introduced in Chapter 2, including the generation of OFDM signals, PAR definitions, distortion-evaluating metrics and review of existing distortion-based CFR techniques.

From Chapter 3 to Chapter 6, several important aspects of the distortion-based CFR algorithms are analyzed. First, in Chapter 3, we investigate the proper PAR metrics in MIMO-OFDM systems based on the power efficiency improvement consideration. Depending on different linear scaling scenarios, different PAR definitions are shown to be appropriate.

Chapter 4 presents the EVM analysis to cope with various distortion mechanisms in OFDM systems, including clipping, nonlinear power amplifier, phase noise, and gain/phase imbalances.

A novel CFR technique, constrained clipping, is proposed in Chapter 5, where the

performance and the computational complexity are also demonstrated. Based on the simulation results, constrained clipping is shown to be able to achieve large PAR reduction while satisfying the in-band EVM and out-of-band spectral mask requirements. Moreover, the proposed algorithm is extended to the multiple-user OFDM case, which is adopted in the mobile WiMAX standard.

In Chapter 6, the SNDR for transceiver nonlinearities in the AWGN channel is studied. Closed-form SNDR expression is obtained based on the Bussgang Theorem and complex polynomial approximations. Moreover, the receiver nonlinearity can be optimized to maximize the SNDR when the transmitter nonlinearity is known. The comparison of clipping and companding is also included in this chapter.

Finally, we summarize the dissertation in Chapter 7.

CHAPTER II

BACKGROUND

2.1 Introduction

In this chapter, necessary background is introduced as the basis for detailed descriptions in the dissertation. We briefly review the OFDM system, which is chosen as the exemplary multi-carrier transmission scheme. Next, the definition of PAR is given, and the high-PAR problem is analyzed, motivating us to study efficient CFR algorithms. A large number of studies on CFR can be found in the literature; however, distortion-based methods are of our interest because of their effectiveness and simplicity. In-band and out-of-band metrics are required to evaluate the performance degradation introduced by additional nonlinear components in the distortion-based CFR algorithms. By analyzing these metrics, we can control the degree of nonlinearity to achieve the tradeoff between the CFR performance and other metrics, such as bit error rate (BER) and spectral regrowth. Clipping and companding algorithms are reviewed as examples of distortion-based CFR methods.

2.2 OFDM Systems

Multi-carrier modulation stems from the single-carrier transmission scheme. The single-carrier complex baseband signal can be expressed as

$$x(t) = \sum_{i=-\infty}^{\infty} X_i g(t - iT), \tag{2.1}$$

where X_i is the ith complex constellation point with symbol duration T, and $g(t)$ is the pulse-shaping function. A multi-carrier signal can be obtained by using N different shaping functions as [19, 38]

$$x(t) = \sum_{i=-\infty}^{\infty} \sum_{k=-N/2}^{N/2-1} X_{i,k} g_k(t - iT). \tag{2.2}$$

Nyquist criterion should be satisfied by $\{g_k(t)\}_{k=-N/2}^{N/2-1}$ to avoid interference [19]. OFDM is constructed by using the complex exponential orthogonal functions,

$$g_k(t) = \frac{1}{\sqrt{N}} e^{j2\pi kt/T} u(t), \tag{2.3}$$

which is time-limited because $u(t)$ is the rectangular window with width T. If sampling the ith OFDM symbol at rate N/T, we can obtain the ith Nyquist-rate sampled $x(t)$ as

$$x_{i,n} = \frac{1}{\sqrt{N}} \sum_{k=-N/2}^{N/2-1} X_{i,k} e^{j2\pi kn/N}, \quad 0 \le n \le N-1. \tag{2.4}$$

It is clear that (2.4) can be implemented by the inverse discrete Fourier transform (IDFT), which was first analyzed by Weinstein and Ebert [93] in 1971. With the help of the fast Fourier transform (FFT) technique, OFDM can be easily implemented with reasonable complexity. Usually, $X_{i,k}$ is referred as the frequency-domain sample, and $x_{i,n}$ (or $x(t)$) is the corresponding time-domain sample (or symbol).

A cyclic prefix (CP) is usually inserted to remove the inter-symbol interference (ISI); hence, OFDM can be processed block by block, allowing us to remove the symbol index i from now on. Because CP is a repetition of part of the OFDM block, it will not change the PAR value. Therefore, we do not consider the CP and denote the continuous-time signal by

$$x(t) = \frac{1}{\sqrt{N}} \sum_{k=-N/2}^{N/2-1} X_k \, e^{\frac{j2\pi kt}{T}}, \qquad t \in (0, T], \tag{2.5}$$

and the discrete-time Nyquist-rate samples by

$$x_n = \frac{1}{\sqrt{N}} \sum_{k=-N/2}^{N/2-1} X_k e^{j2\pi kn/N}, \quad 0 \le n \le N-1. \tag{2.6}$$

Based on the central limit theorem, x_n is approximately i.i.d. complex Gaussian distributed with significant envelope variations. When N is large, the real and imaginary parts of x_n both have zero mean and variance σ^2. Also, we have $E[|X_k|^2] = E[|x_n|^2] = 2\sigma^2$. It is easy to check that the envelope and power of x_n satisfy the Rayleigh distribution and the exponential distribution, respectively.

OFDM can provide high spectral efficiency, robust resistance to multi-path fading, and simple equalization structure. These attractive properties make OFDM one of the candidates for various high-speed wireless standards. For example, the IEEE 802.11 standard

has an OFDM option [1], and WiMAX (IEEE 802.16) also uses OFDM or multiple-user OFDM [4]. Additionally, OFDM has been adopted by digital audio broadcasting (DAB) [6] and digital video broadcasting (DVB) [3] standards.

Based on the simple OFDM structure, researchers have constructed other OFDM-based systems, such as coded OFDM [103], multiple-input multiple-output (MIMO) OFDM [17,82, 96], multi-carrier code division multiplexing access (CDMA) [39], and orthogonal frequency division multiplexing access (OFDMA) [54]. Among these schemes, MIMO-OFDM will be further studied in the dissertation; hence, for clarification, simple OFDM is also referred as the single-input single-output (SISO) OFDM.

A MIMO system can either improve the signal quality by maximizing the spatial diversity (space-time coding [9,85], space-frequency coding [52]) or increase the system throughput by using layered transmission [32] or exploiting channel state information (CSI) at the transmitter [68]. MIMO-OFDM [17, 82, 96] combines OFDM with multiple transmit and receive antennas to achieve higher data rate or improve the link reliability. In the next generation wireless LAN (IEEE 802.11n), 3G LTE, and future 4G standards, MIMO-OFDM has been proposed as the physical-layer transmission technique [23, 29].

2.3 PAR Definition in OFDM Systems

2.3.1 PAR Definition in SISO-OFDM Systems

Peak-to-average power ratio (PAR) is the most popular metric used to evaluate the dynamic range of the time-domain OFDM signal. If $x(t)$ in (2.5) goes through the power amplifier (PA) without proper scaling, high peaks may be clipped, thus increasing the BER and causing interference to other users. To avoid such nonlinear distortions, $x(t)$ has to be backed off to the linear region of the PA, reducing the power efficiency of the system. PAR in the continuous-time form is defined as

$$\text{PAR}\{x(t)\} = \frac{\max\limits_{t\in(0,T]} |x(t)|^2}{E[|x(t)|^2]}, \tag{2.7}$$

where $E[\cdot]$ is the expectation operation. Because the numerator in (2.7) is random, PAR is a random variable as well; its complementary cumulative distribution function (CCDF)

can be approximated by

$$\Pr\{\text{PAR}\{x(t)\} > \gamma\} = 1 - \exp\left\{-b(N)e^{-\gamma}\right\}, \tag{2.8}$$

where $b(N) = N\sqrt{\frac{\pi}{3}\ln N}$ [92]. Other studies on PAR distributions of continuous-time OFDM signals can be found in [33, 58, 66, 100].

Usually, it is difficult to evaluate the maximum value of a continuous-time signal; hence, the sampled version is of practical interest. For the Nyquist-rate samples, PAR can be written as

$$\text{PAR}\{x_n\} = \frac{\max_{0\le n\le N-1}|x_n|^2}{E[|x_n|^2]}. \tag{2.9}$$

For large N values, the CCDF of PAR for the Nyquist-rate sampling is

$$\Pr\{\text{PAR}\{x_n\} > \gamma\} = 1 - (1 - e^{-\gamma})^N. \tag{2.10}$$

Since Nyquist-rate samples may miss the peaks of the continuous-time signal, it is desirable to show CFR performance on over-sampled signals [10, 11, 55, 60, 67]. It is typical to use an over-sampling factor of $L \geq 4$ so that the PAR before the digital-to-analog converter (DAC) can accurately describe the continuous-time PAR [81]. Frequency-domain zero-padding can be used to generate the over-sampled sequences. For distortion-based CFR methods, over-sampling is also necessary to examine the out-of-band spectral characteristics of the signal after CFR.

Let us define the in-band indices to be the set

$$\mathcal{I} : [-N/2, N/2 - 1],$$

and the out-of-band indices to be the set

$$\mathcal{O} : [-LN/2, -N/2 - 1] \cup [N/2, LN/2 - 1].$$

The zero-padded version of X_k is denoted by $\{X_k^{(L)}\}_{k=-LN/2}^{LN/2-1}$, where

$$X_k^{(L)} = \begin{cases} X_k, & k \in \mathcal{I}, \\ 0, & k \in \mathcal{O}. \end{cases} \tag{2.11}$$

Thus, the over-sampled discrete-time symbol $x_n^{(L)}$ can be calculated as follows:

$$x_n^{(L)} = \frac{1}{\sqrt{LN}} \sum_{k=-LN/2}^{LN/2-1} X_k^{(L)} \, e^{j\frac{2\pi kn}{LN}}, \quad 0 \le n \le LN-1. \tag{2.12}$$

We define the PAR of the over-sampled symbol as

$$\mathrm{PAR}\{x_n^{(L)}\} = \frac{\max_{0\le n\le LN-1} |x_n^{(L)}|^2}{E[|x_n^{(L)}|^2]}. \tag{2.13}$$

2.3.2 PAR Definition in MIMO-OFDM Systems

Some CFR methods for SISO-OFDM have been extended to MIMO-OFDM; for example, selected mapping (SLM) [31, 42, 53], partial transmit sequence (PTS) [12], cross-antenna rotation and inversion [84], active constellation extension (ACE) [48], and convex optimization [8]. Several novel PAR reduction methods that are unique to MIMO-OFDM have also been proposed, for example, unitary rotation [51], and spatial shifting [80].

Before we set forth to solve the CFR problem, we need to first define the PAR metric for MIMO-OFDM. Suppose there are M transmit antennas in the system; hence, M high power amplifiers will be needed, one in front of each antenna. The mth branch signal $x_m(t)$ has a PAR value defined as

$$\mathrm{PAR}_m = \frac{\max\limits_{t\in(0,T]} |x_m(t)|^2}{E[|x_m(t)|^2]}. \tag{2.14}$$

The definition in (2.14) is sufficient if we just extend the CFR method for SISO-OFDM directly to MIMO-OFDM. Intuitively, however, the direct extension may not be the best solution. It would be better to implement CFR in MIMO-OFDM by considering the signals in all M branches together. In such a way, we hope to either reduce the complexities or utilize the spatial freedom given by the multiple antennas, such as in [12,51,53]. Hence, the PAR metric, related to branch PAR values $\{\mathrm{PAR}_m\}_{m=1}^M$, is of particular interest, .

For MIMO-OFDM systems, several PAR metrics exist [12,51,53,80], such as the average branch PARs

$$\mathrm{PAR}_{\mathrm{ave}} = \frac{1}{M} \sum_{m=1}^{M} \mathrm{PAR}_m, \tag{2.15}$$

and the maximum branch PARs

$$\mathrm{PAR}_{\mathrm{max}} = \max_{1\le m\le M} \mathrm{PAR}_m, \tag{2.16}$$

and it is not clear why these are meaningful definitions. In Chapter 3, proper PAR metrics will be analyzed based on the power efficiency considerations and different MIMO-OFDM system configurations.

2.4 Performance-Evaluating Metrics

In this dissertation, we are interested in studying distortion-based CFR algorithms, such as clipping and companding. Before reviewing these CFR methods, performance-evaluating metrics, e.g. error vector magnitude (EVM), spectral mask, and signal-to-noise-and-distortion ratio (SNDR), are introduced in this section.

2.4.1 Error Vector Magnitude

EVM is a popular figure of merit for evaluating in-band distortions in a communication system. Compared with BER, EVM not only quantifies the distortions, but also attributes the source of distortion to phase noise, modulator imbalances, power amplifier nonlinearities, and so on [7, 22]. EVM is more useful than BER when performing real-world RF design and troubleshooting. A number of studies on simulations and measurements of EVM have been proposed [46, 49, 95]. EVM analysis for distortions in an 8-PSK system, a GSM EDGE system, a wideband code-division multiple-access (CDMA) system, and a general linear single-carrier transmit-receive system have been investigated in [34, 61, 71, 89], respectively. With its excellent troubleshooting capability, EVM has been adopted by many communication standards, such as wideband CDMA, wireless LAN, and wireless MAN. EVM has also been taken into account when formulating CFR algorithms, such as in [8, 14].

Figure 2.1 illustrates the EVM concept. Denote by X_k the reference signal, Y_k its distorted version, and $D_k = Y_k - X_k$ the error signal (vector). The so-called EVM is defined as [4]

$$\text{EVM} = \frac{1}{S_{max}} \sqrt{\frac{1}{N} \sum_{k \in \mathcal{I}} |Y_k - X_k|^2} = \frac{1}{S_{max}} \sqrt{\frac{1}{N} \sum_{k \in \mathcal{I}} |D_k|^2}, \tag{2.17}$$

where $S_{\max}$ is the maximum amplitude of the constellation points that define X_k, and N is the number of points in a measurement. Since X_k is a random variable, EVM is a random

variable as well. The following quantity

$$Z = \frac{1}{N} \sum_{k=0}^{N-1} \frac{|D_k|^2}{S_{\max}^2} \tag{2.18}$$

conveys information about sample-averaged normalized error powers. Z is of interest, because it is much easier to be theoretically analyzed than the EVM value in (2.17).

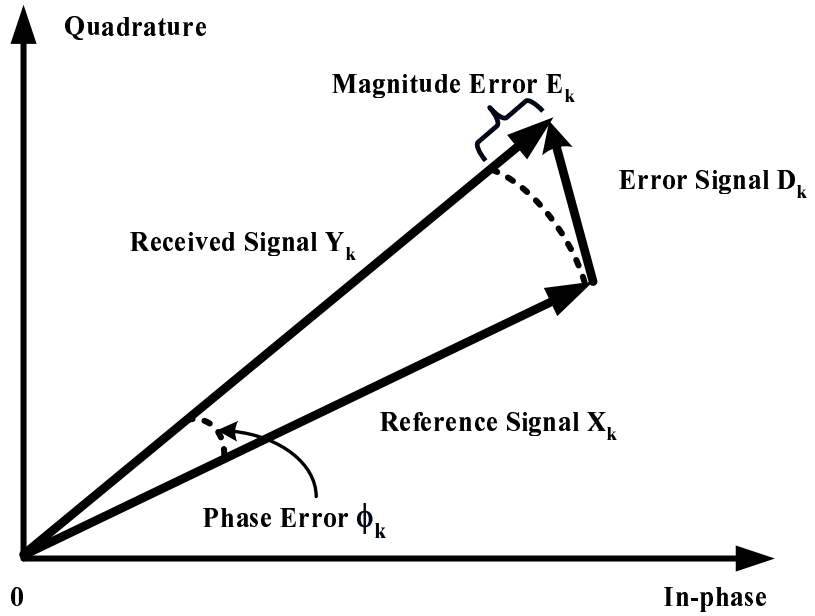

Figure 2.1: Illustration of the EVM definition, including the magnitude error E_k and the phase error ϕ_k.

Two related parameters are the magnitude error $E_k = |Y_k| - |X_k|$ and the phase error $\phi_k = \angle Y_k - \angle X_k$, which are useful to identify the phase-related distortion.

EVM of the transmitted signal should not be larger than a threshold specified by the standard. For example, EVM thresholds for various modulation schemes in WiMAX standard [4] are given in Table 2.1, where $S_{\max}$ values are also presented.

Table 2.1: S_{max} and EVM thresholds for various modulation schemes.

Modulation	BPSK	QPSK	16QAM	64QAM
S_{max}	1	$\sqrt{2}$	$\sqrt{18}$	$\sqrt{98}$
EVM Threshold	23%	12%	6%	3%

In Chapter 4, EVM analysis in OFDM systems is performed, where we relate the theoretical EVM values to various distortion parameters to provide us guidelines for controlling

the severity of distortions. Moreover, EVM is chosen by the constrained clipping technique in Chapter 5 as the in-band metric to design a powerful distortion-based CFR algorithm.

2.4.2 Spectral Mask

Nonlinear devices may broaden the spectrum of the signal, which is usually called the spectrum regrowth. We need to control this out-of-band distortion; otherwise, the systems at the adjacent frequency bands will face large interference. Spectral mask is used as the evaluation metric and always specified in the standards. For example, the spectral mask used in WiMAX [4] system is illustrated in Fig. 2.2. We will compare the power spectrum density (PSD) of the transmitted signal to this deterministic spectral mask to constrain the spectrum regrowth in Chapter 5.

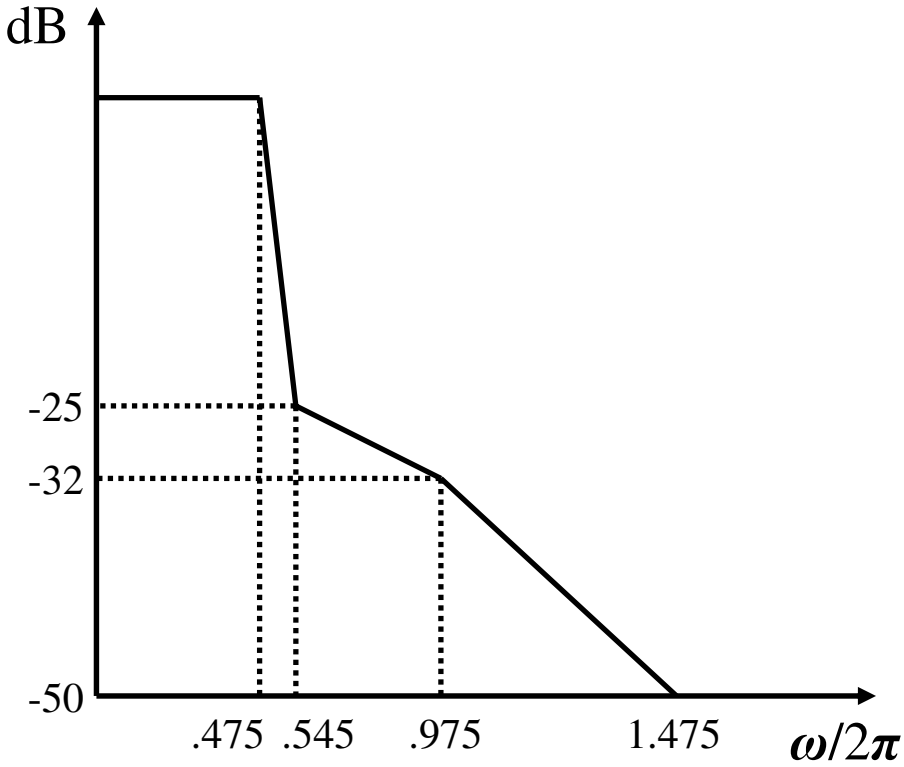

Figure 2.2: Spectral mask for the WiMAX standard [4].

2.4.3 Signal-to-Noise-and-Distortion Ratio

Signal-to-noise ratio (SNR) is commonly adopted to describe the harshness of the additive white Gaussian noise (AWGN) channel and has the deterministic relationship with BER to

evaluate the reception reliability. When the link nonlinearity is not negligible, the signal passed through the nonlinear device can be decomposed into a linear part and an uncorrelated distortion part, by utilizing Bussgang Theorem [20]. Therefore, when taking the nonlinear distortion into consideration, the signal-to-noise-and-distortion ratio (SNDR) is a proper performance-evaluating metric in the AWGN channel [25, 65, 67, 75]. Previous studies confine the nonlinearity only at the transmitter. Shown in Fig. 2.3 is the baseband structure when the transmitter nonlinearity $g(\cdot)$ is considered.

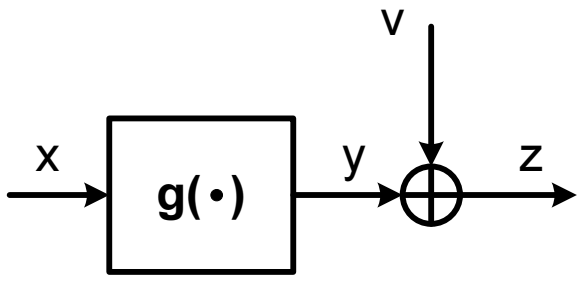

Figure 2.3: Baseband structure of linear receiver a transmitter nonlinearity $g(\cdot)$ in the AWGN channel.

For the linear receiver, using the Bussgang Theorem [20], any nonlinear function can be decomposed as follows:

$$y = g(x) = \alpha x + d, \tag{2.19}$$

where

$$\alpha = \frac{E[x^* y]}{\sigma_x^2} \tag{2.20}$$

is chosen so that $E[x^* d] = 0$ ($E[\cdot]$ is the expectation operation, $(\cdot)^*$ denotes the complex conjugate, and σ_x^2 is the signal power). The distortion power is

$$E[|d|^2] = E[|y|^2] - |\alpha|^2 \sigma_x^2 = E[|y|^2] - \frac{|E[x^* y]|^2}{\sigma_x^2}. \tag{2.21}$$

Because v and d are uncorrelated, the total degradation power is $E[|d|^2] + \sigma_v^2$, where σ_v^2 is the noise power. Therefore, we define SNDR as

$$\text{SNDR} = \frac{|\alpha|^2 \sigma_x^2}{E[|d|^2] + \sigma_v^2}. \tag{2.22}$$

Substituting α and $E[|d|^2]$ into (2.22),

$$\text{SNDR} = \frac{|E[x^* y]|^2}{\sigma_x^2 E[|y|^2] - |E[x^* y]|^2 + \sigma_x^2 \sigma_v^2}, \tag{2.23}$$

with

$$E[x^*y] = E[x^*g(x)] = \int_{\mathcal{R}(x)} g(x)x^* f_x(x)dx, \tag{2.24}$$

$$E[|y|^2] = E[|g(x)|^2] = \int_{\mathcal{R}(x)} |g(x)|^2 f_x(x)dx, \tag{2.25}$$

where $\mathcal{R}(x)$ is the range of x, and $f_x(x)$ is the probability density function (PDF) of x. This expression is also used in [25, 65, 67, 75].

However, the SNDR analysis for the linear receiver is not sufficient to deal with the transceiver nonlinearities. For example, in order to evaluate the performance of companding PAR reduction algorithms [41, 43, 90, 91], it is necessary to take into account both the transmitter compressing nonlinearity and the receiver expanding nonlinearity. In Chapter 6, SNDR analysis is provided in the AWGN channel for transceiver nonlinearities. Based on the closed-form SNDR expression, we can analyze the degree of nonlinearities and optimize the transceiver design.

2.5 Distortion-Based CFR Algorithms

Many CFR techniques have been proposed in the literature, which can be mainly separated into two categories: distortion-based and distortionless-based techniques. Distortionless-based methods have significant CFR performance without causing nonlinear distortion; however, they typically incur large computational complexities and sometimes side information transmission. Moreover, these methods usually require receiver-side modifications that may be incompatible to existing communication systems. Such approaches include selected mapping [13, 15], partial transmit sequence [40, 50, 56, 62, 97], tone injection, tone reservation, and coding (see [36, 57, 86] and references therein).

On the other hand, distortion-based CFR algorithms generally require less computational complexity and do not require receiver-side modification, such as clipping [67, 75], companding [41, 43, 90, 91], active constellation extension (ACE) [47], and generalized ACE methods [26, 79]. Therefore, it is possible for some distortion-based CFR algorithms to be implemented at the base station of an existing mobile communications network without requiring modifications to individual handsets. However, distortion-based methods may

degrade the system performance by the additional nonlinear operations; hence, we should carefully control the degree of nonlinearity.

In this section, we will review two typical distortion-based CFR techniques, clipping and companding. Clipping contains several different implementations, and we will introduce (i) simple clipping and its modifications, including ACE and clipping plus filtering; (ii) optimal clipping. Similarly, several different companding schemes, e.g. μ-law, A-law, nonlinear non-symmetric transform (NLNST) and exponential transform, will also be covered.

2.5.1 Simple Clipping

Polar clipping $x_n^{(L)}$ in (2.12) with threshold A_{max} yields

$$\bar{x}_n^{(L)} = \begin{cases} x_n^{(L)}, & |x_n^{(L)}| \le A_{max}, \\ A_{max}\ e^{j\angle x_n^{(L)}}, & |x_n^{(L)}| > A_{max}. \end{cases} \tag{2.26}$$

To compare the performance for different over-sampling rates, clipping ratio (CR) is always used, which can be written as

$$\Omega = \frac{A_{max}\sqrt{L}}{\sigma\sqrt{2}}. \tag{2.27}$$

The frequency-domain clipped signal is

$$\bar{X}_k^{(L)} = \frac{1}{\sqrt{LN}} \sum_{n=0}^{LN-1} \bar{x}_n^{(L)}\ e^{-j\frac{2\pi kn}{LN}}, \quad -\frac{LN}{2} \le k \le \frac{LN}{2} - 1. \tag{2.28}$$

The clipping operation in (2.26) generates both in-band and out-of-band distortions in $\bar{X}_k^{(L)}$. In-band distortion is observed when $\bar{X}_k^{(L)} \neq X_k$ for $k \in \mathcal{I}$. Out-of-band spectral regrowth is revealed since $\bar{X}_k^{(L)} \neq 0$ for $k \in \mathcal{O}$, reminding that we have defined $\mathcal{I} : [-N/2, N/2-1]$ and $\mathcal{O} : [-LN/2, -N/2-1] \cup [N/2, LN/2-1]$ in Section 2.3. These are in contrast to the unclipped signal $X_k^{(L)}$ described in (2.11).

Denote by

$$\begin{aligned} D_k &= \bar{X}_k^{(L)} - X_k^{(L)}, \quad k \in \mathcal{I} \\ &= \bar{X}_k^{(L)} - X_k, \quad k \in \mathcal{I} \end{aligned} \tag{2.29}$$

the error vector at the kth subcarrier in-band. The formula for calculating the EVM varies depending on communication standards [2, 4, 5]. As an example, let us use the EVM metric

defined in the WiMAX standard (c.f. eq. (2.17)),

$$\text{EVM}\{\bar{x}_n^{(L)}\} = \frac{1}{S_{max}}\sqrt{\frac{1}{N}\sum_{k\in\mathcal{I}}|D_k|^2} = \frac{1}{S_{max}}\sqrt{\frac{1}{N}\sum_{k\in\mathcal{I}}|\bar{X}_k^{(L)} - X_k|^2}. \tag{2.30}$$

In other words, EVM is a scaled root-mean-squared (rms) distance between the desired constellation points X_k and the positions of the signal $\bar{X}_k^{(L)}$, $k \in \mathcal{I}$.

The EVM calculated according to (2.30) is only for one symbol period. When the measured period contains several OFDM symbols, the EVM should be calculated as the average EVM, i.e., $E[\text{EVM}]$. An approximation of the average EVM is $\sqrt{E[Z]}$, where Z is given in (2.18). It is much easier to derive $\sqrt{E[Z]}$ theoretically than $E[\text{EVM}]$.

A comparison of the true value of the average EVM and its approximation is given in Fig. 2.4 for different clipping ratios. Nyquist-rate sampling ($L = 1$) and four-time over-sampling ($L = 4$) are both presented in the simulation. QPSK modulation is used, and the corresponding EVM threshold is 12%. From Fig. 2.4, $\Omega \geq 3.6$ dB and $\Omega \geq 3.0$ dB are required to satisfy the standard's requirement for $L = 1$ and $L = 4$, respectively. Two conclusions can be drawn: (i) the approximation $\sqrt{E[Z]}$ is very close to $E[\text{EVM}]$ around the interested range of Ω and (ii) clipping the over-sampled signal incurs less in-band distortion than clipping the Nyquist-rate signal, which was also verified in [55].

The influence of simple clipping on the out-of-band PSD performance is evaluated in Fig. 2.5. A four-time over-sampled QPSK signal is used in the simulation. Even with the clipping ratio as high as 7 dB, the spectral mask requirement is still violated. Combining Fig. 2.4 and Fig. 2.5, we can imagine that the CFR performance of the simple clipping may be very limited if both in-band and out-of-band requirements need to be satisfied.

Simple clipping has low complexity and requires no receiver-side modification and thus is very likely to be incorporated into existing systems. However, simple clipping generates both in-band and out-of-band distortions, violating the requirements of the standard. We have to explore additional signal processing techniques to reduce such distortions.

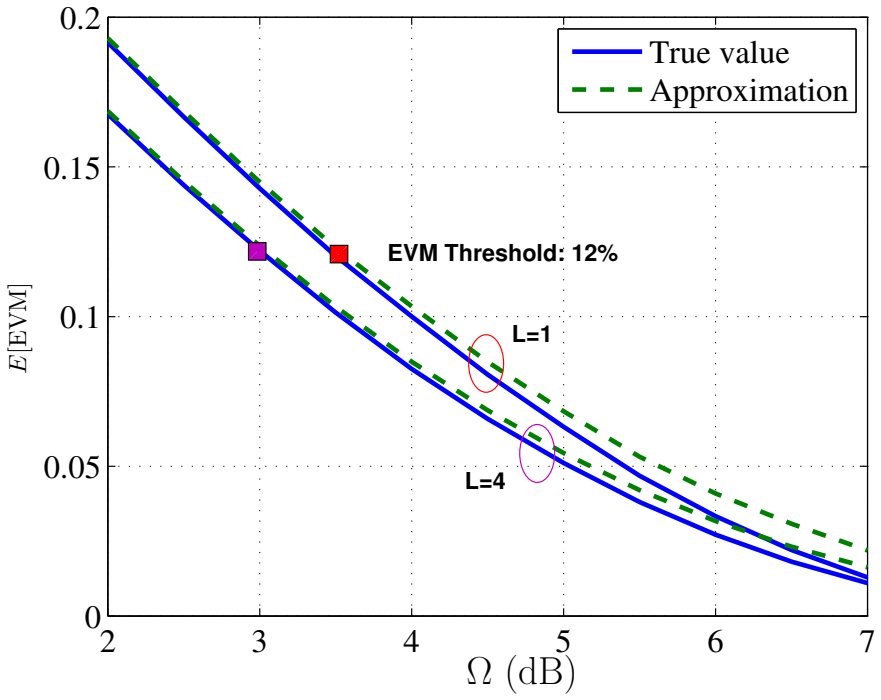

Figure 2.4: Average EVM and its approximation under different clipping ratios. Nyquist-rate sampling and four-time over-sampling are included, $N = 128$.

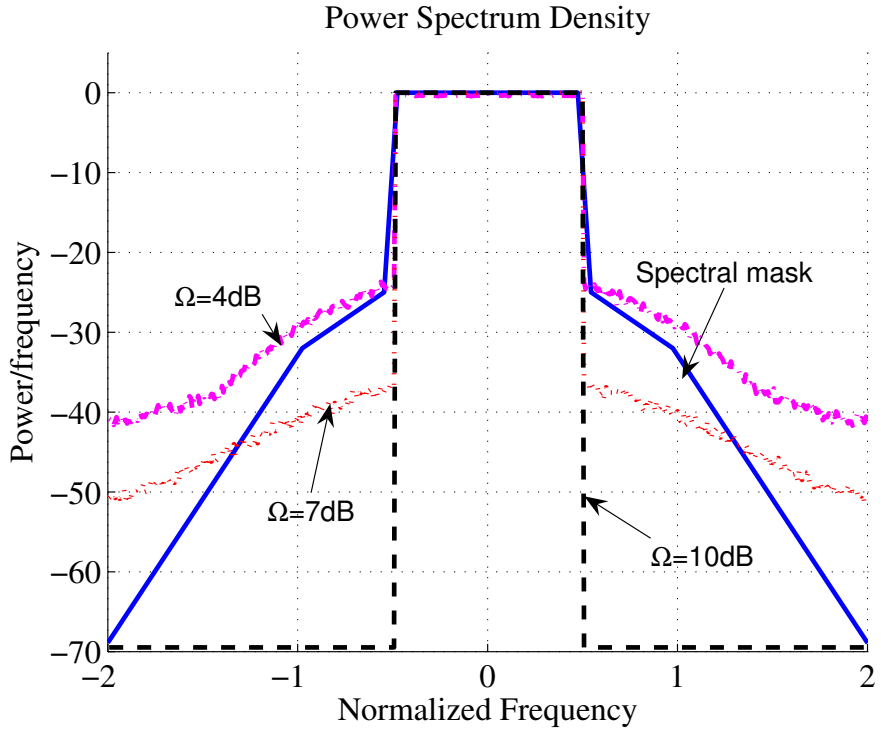

Figure 2.5: PSD plots of clipped signals with different clipping ratios, $N = 128$. Spectral mask is also included to check the severity of the spectrum regrowth.

2.5.1.1 In-Band Clipping Distortion Reduction

Various signal processing techniques have been proposed to reduce the in-band distortion introduced by simple clipping. These algorithms can be classified into two groups: receiver-based clipping noise mitigation and transmitter-based constellation modification.

Clipping noise mitigation methods, such as [21, 45], aimed at regenerating the in-band distortion at the receiver and removing it from the received signal. Iterations are usually needed to obtain accurate estimation of the clipping noise. Nevertheless, in coded OFDM systems, it is not necessary to design a stand-alone clipping noise mitigation unit, because the iterative procedure may be absorbed by the decoder or the clipping noise can be greatly recovered by the powerful channel codec [63, 78].

Constellation modification mainly refers to active constellation extension (ACE) [47] and generalized ACE [26, 79]. After clipping, $\bar{X}_k^{(L)}$ is constrained into a certain region by comparing with the designed bound to reduce the in-band distortion. Without involving receiver-side processing, constellation modification methods are more applicable to real-system implementation. However, there are several problems with these methods: (i) all the in-band distortion reduction methods have not considered the out-of-band spectral regrowth; (ii) these algorithms can not achieve satisfactory PAR reduction and BER simultaneously by a single iteration in general which requires iterative operations; and (iii) the computational complexities are high.

2.5.1.2 Out-of-Band Distortion Reduction

Clipping with filtering is usually used to deal with the out-of-band radiation. Filtering can be implemented either in the time domain [55] or the frequency-domain [10]. For example, one well-known method to deal with the out-of-band spectral regrowth is to set $\bar{X}_k^{(L)} = 0$, $\forall k \in \mathcal{O}$; this is the so-called frequency-domain filtering method proposed by J. Armstrong [10]. However, this simple scheme has several disadvantages. With Armstrong's method, nothing is done to control the in-band EVM. The out-of-band spectral regrowth stays far below the spectral mask, essentially wasting energy that is allotted by the standard that could be used for CFR. After filtering, the PAR is always larger than that of the simple

clipping method, i.e., peak regrowth occurs. To improve the CFR performance, repeated clipping and filtering was proposed in [11]; however, the iterative processing still can not fulfill the in-band EVM requirement.

Figure 2.6 is a plot of the probability of an OFDM symbol (QPSK modulation, $N = 256$) having the EVM exceeding the allowed 6%. Even for modest clipping (> 7 dB), there is a non-zero probability that some of the symbols will exceed the allotted EVM.

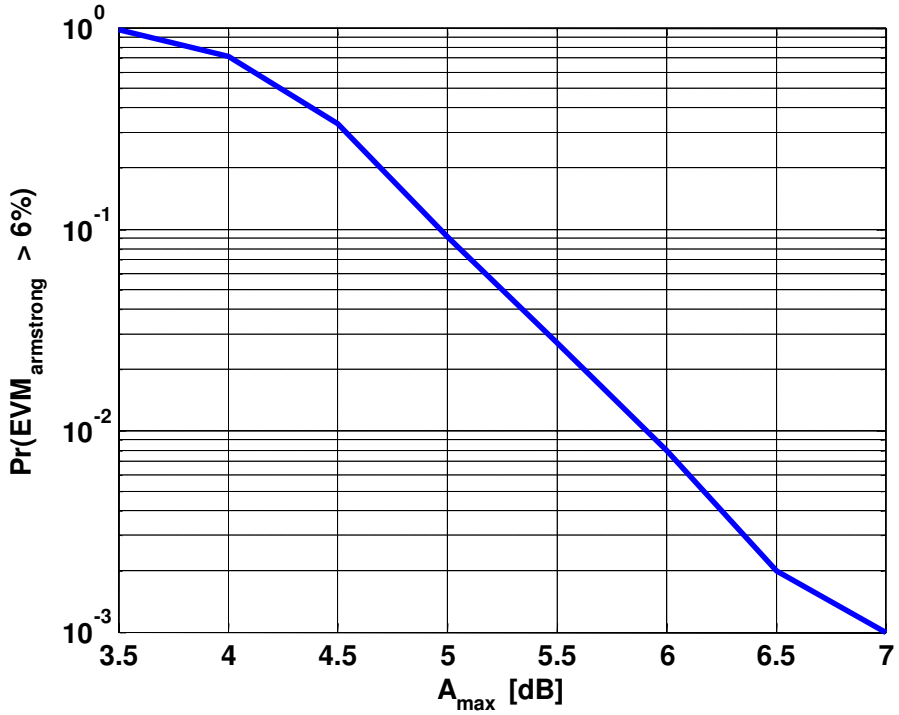

Figure 2.6: Probability that the Armstrong's method will exceed the EVM threshold with $N = 256$. EVM threshold is 6%.

Based on the analysis in Section 2.5.1.1 and Section 2.5.1.2, we can see that it is necessary to design a new clipping based CFR algorithm to solve the above problems. In Chapter 5, the constrained clipping CFR algorithm is proposed to efficiently reduce PAR with satisfied in-band and out-of-band distortion-control capability. It is a one-shot procedure, which has low computational complexity.

2.5.2 Optimal Clipping

In the optimal clipping method [75],

$$g(x) = \begin{cases} \frac{B}{\eta}x, & |x| \leq \eta, \\ B\ e^{j\angle x}, & |x| > \eta, \end{cases} \tag{2.31}$$

where η is the clipping threshold and B is the maximum amplitude of the output, i.e., $|g(x)| \leq B$. It has been proved in [75] that the nonlinearity in (2.31) can maximize the SNDR in the linear receiver case. Optimal η depends on the knowledge of the channel noise and the peak-power limitation. If the input signal x is complex Gaussian distributed, the SNDR-optimizing clipping threshold is

$$\tilde{\eta} = U^{-1}\left(\frac{B}{\sigma_v^2}\right), \tag{2.32}$$

where

$$U(\eta) = \frac{2\eta}{\sqrt{\pi}\mathrm{erfc}(\eta)}. \tag{2.33}$$

Under the peak power constraints,

$$\mathrm{PSNR} = \frac{B}{\sigma_v^2} \tag{2.34}$$

is chosen because the transmitted signal will always be linearly scaled to its peak amplitude to achieve the maximum power efficiency [64]. Because $U(\eta)$ is a monotonicly increasing function, the optimal SNDR has one-to-one relationship with the PSNR. The closed-form optimal SNDR is presented in Theorem 1 of [75], see [75] for details.

To utilize the optimal clipping, the noise power should be known at the transmitter, which requires some feedback of channel state information (CSI) from the receiver. Moreover, the optimal clipping is derived based on the sample-based framework that is different from the block-based transmission scheme used in OFDM. See [16] for the discussion about this difference.

The optimal clipping in [75] considered the AWGN channel only, and was extended to the multi-path fading channels in [74] where clipping with a special gain (different with $\tilde{\eta}$ in (2.32)) was shown still optimal in terms of SNDR.

2.5.3 Companding

For the companding scheme, different pairs of inverse functions have been proposed, and usually, the transmitter nonlinearity $g(\cdot)$ is compressing to reduce the PAR and the receiver nonlinearity $s(\cdot)$ is expanding to recover the signal.

Different companding schemes include the μ-law compander [90]

$$|g_\mu(x)| = \frac{B\ \ln\left[1+\mu\frac{|x|}{B}\right]}{\ln(1+\mu)}, \tag{2.35}$$

$$|s_\mu(w)| = \frac{B\exp\left[\frac{|w|\ln(1+\mu)}{B}\right]-B}{\mu}, \tag{2.36}$$

the A-law compander [91]

$$|g_A(x)| = \begin{cases} \frac{\mu_A|x|}{1+\ln\mu_A}, & 0\le|x|\le\frac{B}{\mu_A}, \\ \frac{B+B\ln(\frac{\mu_A|x|}{B})}{1+\ln\mu_A}, & \frac{B}{\mu_A}\le|x|\le B, \end{cases}, \tag{2.37}$$

$$|s_A(w)| = \begin{cases} \frac{(1+\ln\mu_A)|w|}{\mu_A}, & 0\le|w|\le\frac{B}{\mu_A}, \\ \frac{B\exp[|w|\frac{1+\ln\mu_A}{B}-1]}{\mu_A}, & \frac{B}{\mu_A}\le|w|\le B, \end{cases}, \tag{2.38}$$

the nonlinear non-symmetric transform compander (NLNST) [41]

$$|g_N(x)| = \zeta\frac{\theta\ \ln\left[1+\mu_N\frac{|x|}{\theta}\right]}{\ln(1+\mu_N)}, \tag{2.39}$$

$$|s_N(w)| = \frac{\theta\exp\left[\frac{|w|\ln(1+\mu_N)}{\theta}\right]-\theta}{\mu_N}, \tag{2.40}$$

and the exponential transform compander [43]

$$|g_e(x)| = \sqrt[c]{\beta\left[1-\exp\left(-\frac{2|x|^2}{\sigma_x^2}\right)\right]}, \tag{2.41}$$

$$|s_e(w)| = \sqrt{-\frac{\sigma_x^2}{2}\ln\left(1-\frac{|w|^c}{\beta}\right)}. \tag{2.42}$$

The parameters μ, μ_A, μ_N, θ and c are companding factors, which control the shapes of companding functions. ζ and β are scaling factors to keep $|g(x)|\le B$ satisfied. In Fig. 2.7 and Fig. 2.8, the above companding function pairs with typical companding factors are plotted. The used companding factors are $\mu = 2$ for the μ-law scheme, $\mu_A = 2$ for the A-law scheme, $\mu_N = 2$ and $\theta = 0.75B$ for the NLNST scheme, and $c = 2$ for the

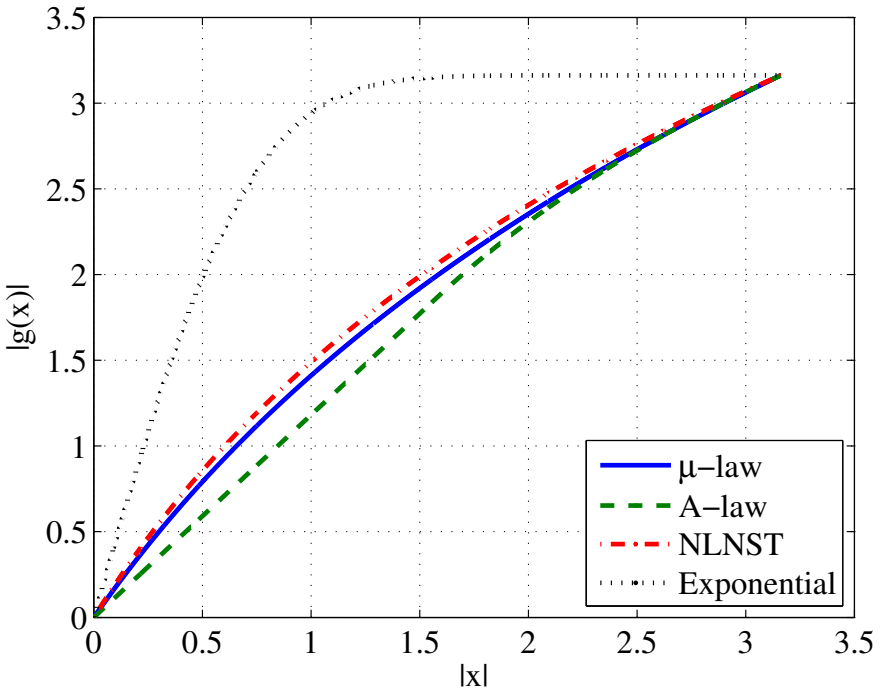

Figure 2.7: Transmitter AM-AM characteristics of different compressing functions $g(\cdot)$, including μ-law, A-law, NLNST and exponential transform.

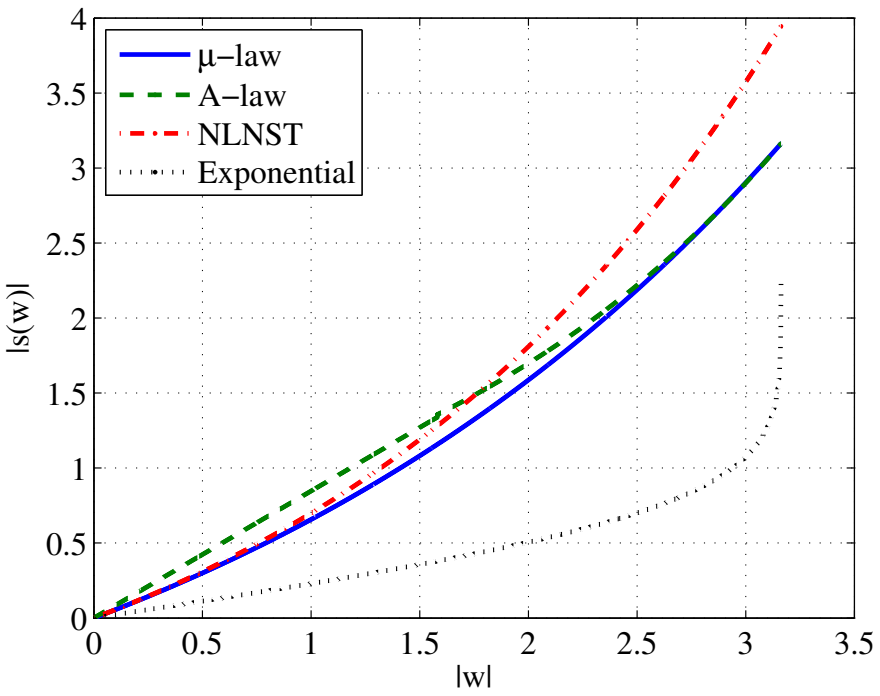

Figure 2.8: Receiver AM-AM characteristics of different expanding functions $s(\cdot)$, including μ-law, A-law, NLNST and exponential transform.

exponential scheme. The maximum amplitude is set to be $B = \sqrt{10}$. Moreover, the scaling factors are $\zeta = \ln(1 + \mu_N)/(0.75\ln(1 + \mu_N/0.75)) = 1.1274$ for the NLNST scheme and $\beta = B^c/(1 - \exp(-2B^2/\sigma_x^2)) = 10$ for the exponential scheme, respectively.

In Chapter 6, a structure is proposed to study the SNDR of transceiver nonlinearities where companding functions can be regarded as the special case. We will compare the performance of clipping and companding from the viewpoint of SNDR.

CHAPTER III

MIMO-OFDM PAR DEFINITION

3.1 Introduction

Multiple-input multiple-output (MIMO) is a promising technique to boost the transmission system performance, either improving the diversity order by the space-time coding or increasing the channel capacity by the spatial multiplexing or transmitter beamforming [9, 32]. Applying OFDM modulation in the MIMO system, the benefits of MIMO can be easily realized in the frequency-selective fading channel. However, due to the existence of the OFDM, the high-PAR problem still exists.

The goal of PAR reduction in this chapter is focused on improving the overall system power efficiency. For SISO-OFDM systems, there is a straightforward relationship between PAR and efficiency. For MIMO-OFDM, however, it is not obvious how the multiple branch PARs should be combined into a single metric that reflects the overall system power efficiency. In fact for MIMO-OFDM, different PAR metrics have been used by different authors [12, 51, 53, 80], and it is not clear why those are meaningful metrics. The objectives of this chapter are three-fold: 1) to clarify how PAR is related to power efficiency in a MIMO-OFDM system, 2) to analyze the mean power efficiency realized by different MIMO-OFDM systems, and 3) to define PAR metrics that maximize the power efficiency for MIMO-OFDM.

3.2 SISO Linear Scaling

It is well known that the PA is a peak power limited device. Figure 3.1 shows the input-output characteristic of an ideal linear PA, achievable by predistorting a nonlinear PA [44]. The DC to RF power conversion efficiency is defined as

$$\eta = \frac{P_{\text{o,avg}}}{P_{\text{dc}}}, \tag{3.1}$$

where $P_{\text{o,avg}}$ is the average output power, and P_{dc} is the power drawn from the DC source.

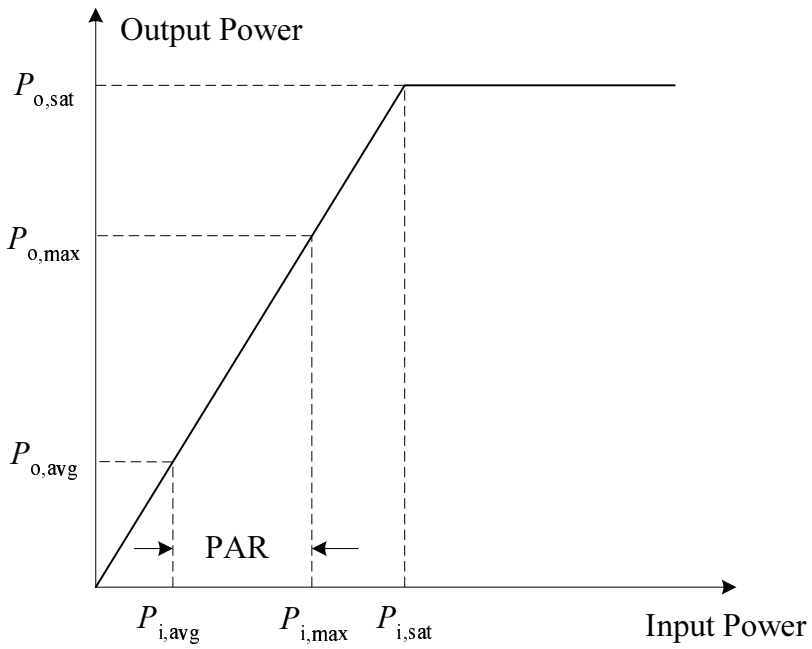

Figure 3.1: An ideal linear PA characteristic. The average PA input power is $P_{\text{i,avg}}$; the maximum PA input power is $P_{\text{i,max}}$. To avoid nonlinear distortions, we need $P_{\text{i,max}} \leq P_{\text{i,sat}}$. The PA is maximally efficient if $P_{\text{i,max}} = P_{\text{i,sat}}$.

If the signal is to be linearly amplified and the maximum power efficiency is to be delivered, the input signal should have its peak power $P_{\text{i,max}}$ positioned exactly at the PA input saturation level $P_{\text{i,sat}}$. The linear scaling technique [64] can be used to scale the peak power of the input signal to the saturation level; the scaling factor can be obtained as

$$\zeta = \frac{P_{\text{i,sat}}}{\max\limits_{t\in(0,T]} |x(t)|^2}. \tag{3.2}$$

Thus, $\sqrt{\zeta}\ x(t)$ is the PA input signal. During each OFDM symbol period, ζ remains constant, but will vary from symbol to symbol. Multiplication by $\sqrt{\zeta}$ has an effect similar to that of flat fading. At the receiver, the scaling factor can be treated as part of the channel and compensated for by conventional channel estimation and equalization techniques.

For signals with linear amplification (c.f. Fig. 3.1), we have

$$\frac{P_{\text{o,max}}}{P_{\text{o,avg}}} = \frac{P_{\text{i,max}}}{P_{\text{i,avg}}} = \text{PAR}. \tag{3.3}$$

A class A PA has $P_{\text{dc}} = 2P_{\text{o,sat}}$, where $P_{\text{o,sat}}$ is the output saturation level of the PA. To exploit the maximum efficiency of the PA without causing distortions, we set $P_{\text{i,max}} = P_{\text{i,sat}}$,

or, $P_{\text{o,max}} = P_{\text{o,sat}}$. As such, the efficiency of a class A PA is

$$\eta = \frac{P_{\text{o,avg}}}{P_{\text{dc}}} = \frac{P_{\text{o,avg}}}{2P_{\text{o,max}}} = \frac{P_{\text{i,avg}}}{2P_{\text{i,max}}} = \frac{0.5}{\text{PAR}}. \tag{3.4}$$

The above relationship clearly indicates that the power efficiency can be increased by reducing the PAR of the input signal.

The CCDF of PAR of the continuous-time signal is given in (2.8), from which the probability density function (PDF) of PAR can be derived as

$$f_{\text{PAR}}(\gamma) = b(N)e^{-\gamma}e^{-b(N)e^{-\gamma}}. \tag{3.5}$$

3.3 MIMO Linear Scaling

In this section, the linear scaling scheme of [64] is extended to MIMO-OFDM. The following two scenarios are possible: 1) a branch-independent scaling factor c is used for all the M branches, 2) branch-dependent scaling factors $\{d_m\}_{m=1}^{M}$ are used so that each branch has a unique scaling factor. We will show that these scenarios will justify different PAR metrics that are meaningful from the power efficiency point of view.

The power efficiency of the mth PA in the MIMO-OFDM system can be written as

$$\eta_m = \frac{P_{\text{o,avg}}^{(m)}}{P_{\text{dc}}}, \tag{3.6}$$

where $P_{\text{o,avg}}^{(m)}$ is the average output power of the mth PA. For the MIMO-OFDM system, assume that the DC power of each PA is P_{dc}. The total DC power consumed by M such transmit PAs is then MP_{dc}. The overall DC to RF power conversion efficiency for the M PAs is

$$\bar{\eta} = \frac{\sum_{m=1}^{M} P_{\text{o,avg}}^{(m)}}{MP_{\text{dc}}} = \frac{1}{M}\sum_{m=1}^{M}\eta_m, \tag{3.7}$$

which is the average of the power efficiencies at the M branches.

3.3.1 Identical Scaling Factor (ISF) Case

When a MIMO-OFDM system uses channel state information (CSI) at the transmitter to beam form the transmitted signal, it is only possible to apply an identical scaling factor across all transmit branches without disrupting data transmission. By placing the largest

of all M signal peaks at the saturation point of the PA, the scaling factor is obtained as

$$c = \frac{P_{\text{i,sat}}}{\max_{1\le m\le M}\{\max\limits_{t\in(0,T]}|x_m(t)|^2\}}. \tag{3.8}$$

Hence, the mth branch PA input signal is $\sqrt{c}\,x_m(t)$. Assume that $E[|x_m(t)|^2]$ are same for all m, then $\eta_1 = \eta_2 = \cdots = \eta_M$. Define

$$\bar{m} = \arg\max_{1\le m\le M}\{\text{PAR}_m\}, \tag{3.9}$$

i.e., the $\bar{m}$th branch has

$$\text{PAR}_{\bar{m}} = \max_{1\le m\le M}\text{PAR}_m. \tag{3.10}$$

Hence, the corresponding efficiency is

$$\eta_{\bar{m}} = \frac{0.5}{\text{PAR}_{\bar{m}}}. \tag{3.11}$$

Therefore, the overall efficiency is

$$\bar{\eta}^{(\text{is})} = \eta_{\bar{m}} \tag{3.12}$$

according to (3.7). In other words, the power efficiency in the ISF case is determined by the worst-case branch PAR. Accordingly, the PAR metric in an ISF MIMO-OFDM system is the *worst branch* PAR; i.e.,

$$\text{PAR}^{(\text{is})} = \text{PAR}_{\bar{m}}. \tag{3.13}$$

This is the metric that should be minimized in order to achieve maximum transmit power efficiency for the overall MIMO system.

If the signal modification is linear, as is the case in beamforming, the PAR distribution in each branch, given by (3.5), will remain unchanged. When the M PARs are mutually independent, the CCDF of the PAR in (3.13) is

$$\Pr\{\text{PAR}_{\bar{m}} > \gamma\} \;=\; 1 - \left(\exp\left\{-b(N)e^{-\gamma}\right\}\right)^M. \tag{3.14}$$

From (3.14), the PDF of $\text{PAR}_{\bar{m}}$ is

$$f_{\text{PAR}_{\bar{m}}}(\gamma) = Mb(N)e^{-\gamma}e^{-Mb(N)e^{-\gamma}}. \tag{3.15}$$

With this, we can write

$$\begin{aligned} E\left[\bar{\eta}^{(\mathrm{is})}\right] &= E\left[\eta_{\bar{m}}\right] = 0.5E\left[\frac{1}{\mathrm{PAR}_{\bar{m}}}\right] \\ &= \int_{e^{-1}}^{0} \frac{Mb(N)e^{-Mb(N)u}}{2\log(u)}du, \end{aligned} \tag{3.16}$$

which has no closed form solution, but can be evaluated numerically.

3.3.2 Multiple Scaling Factors (MSF) Case

In MIMO systems where no *a priori* information about the channel is used in the transmitter, (e.g. space-time block codes), it is possible to apply a scaling factor to each branch independently. Similar to the SISO case, each of these scaling factors can be viewed as part of the MIMO channel and can be equalized at the receiver. Denote the scaling factor on the mth branch by

$$d_m = \frac{P_{\mathrm{i,sat}}}{\max\limits_{t\in(0,T]} |x_m(t)|^2}. \tag{3.17}$$

Then, the mth branch PA input signal becomes $\sqrt{d_m}\ x_m(t)$. After the linear scaling, the peak powers of all branches are positioned at $P_{\mathrm{i,sat}}$ and the branch power efficiency can be written as

$$\eta_m = \frac{0.5}{\mathrm{PAR}_m}, \quad 1 \le m \le M. \tag{3.18}$$

Substituting η_m into (3.7), we can obtain the overall MIMO system power efficiency as

$$\bar{\eta}^{(\mathrm{ms})} = \frac{0.5}{M}\sum_{m=1}^{M}\frac{1}{\mathrm{PAR}_m}. \tag{3.19}$$

In the spirit of (3.4), if we define a MIMO PAR metric $\mathrm{PAR}^{(\mathrm{ms})}$ such that $\bar{\eta}^{(\mathrm{ms})} = 0.5/\mathrm{PAR}^{(\mathrm{ms})}$, then

$$\mathrm{PAR}^{(\mathrm{ms})} = \left(\frac{1}{M}\sum_{m=1}^{M}\frac{1}{\mathrm{PAR}_m}\right)^{-1}. \tag{3.20}$$

Thus, for a MIMO system that allows for independent scaling on each branch, the *harmonic average* of the branch PARs is the proper PAR metric. Note that in this configuration, each branch delivers the same peak power but different average powers on a per-block basis.

With the help of (3.7) and (3.5), we can express the expected value of $\bar{\eta}^{(\mathrm{ms})}$ as

$$E\left[\bar{\eta}^{(\mathrm{ms})}\right] = \frac{0.5}{M}\sum_{m=1}^{M}E\left[\frac{1}{\mathrm{PAR}_m}\right] = \int_{e^{-1}}^{0}\frac{b(N)e^{-b(N)u}}{2\log(u)}du, \tag{3.21}$$

which can be evaluated numerically.

Figure 3.2 is a plot of the mean power efficiency for several different MIMO-OFDM configurations. The figure shows that the MSF configuration performs the best regardless of the number of transmit antennas. On the other hand, the ISF system power efficiency degrades as the number of transmit antennas increases. This makes intuitive sense since under the MSF configuration it is possible to extract the most power efficiency out of each branch, whereas the ISF system efficiency is heavily influenced by the branch with the largest PAR.

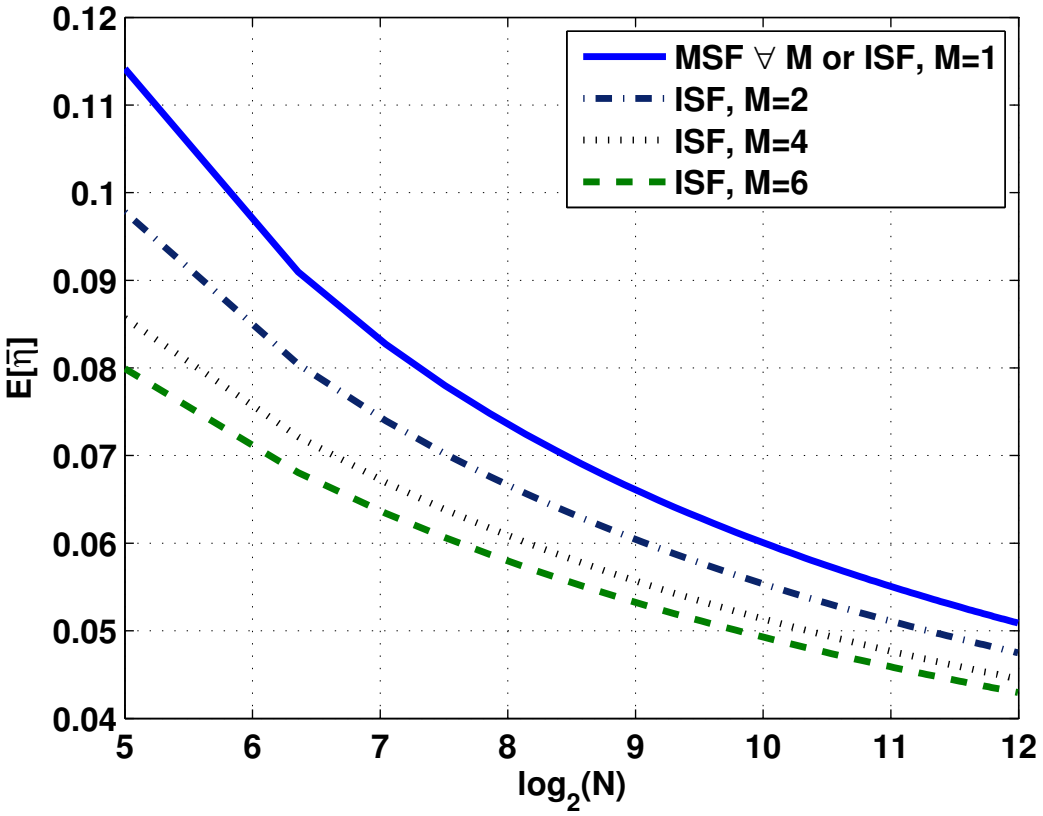

Figure 3.2: MIMO power efficiency under the MSF and ISF configurations.

3.3.3 Efficiency Improvement Example

It is worthwhile to study the efficiency improvement that can be realized when the proper metrics are used in MIMO PAR reduction schemes. As an example, consider concurrent selected mapping (cSLM) [53], where each mapping is generated by applying the same

phase sequence across all M antenna branches. The mapping that produces the minimum arithmetic-average PAR is then selected for transmission.

In Fig. 3.3, cSLM is used as an example to illustrate the importance of using proper PAR metrics in achieving the maximum overall power efficiency. For the plot, $N = \{32, 1024\}$ and $D = \{2, 8, 64\}$, where D is the number of signal mappings in cSLM. The solid curves show the percent power efficiency improvement when the ISF metric given in (3.13) is used instead of arithmetic average branch PARs [53] under the ISF scenario. Similarly, the dashed curves demonstrate the percent power efficiency improvement in the MSF scenario when the harmonic average metric in (3.20) is used as the selection metric instead of the worst branch PAR [84].

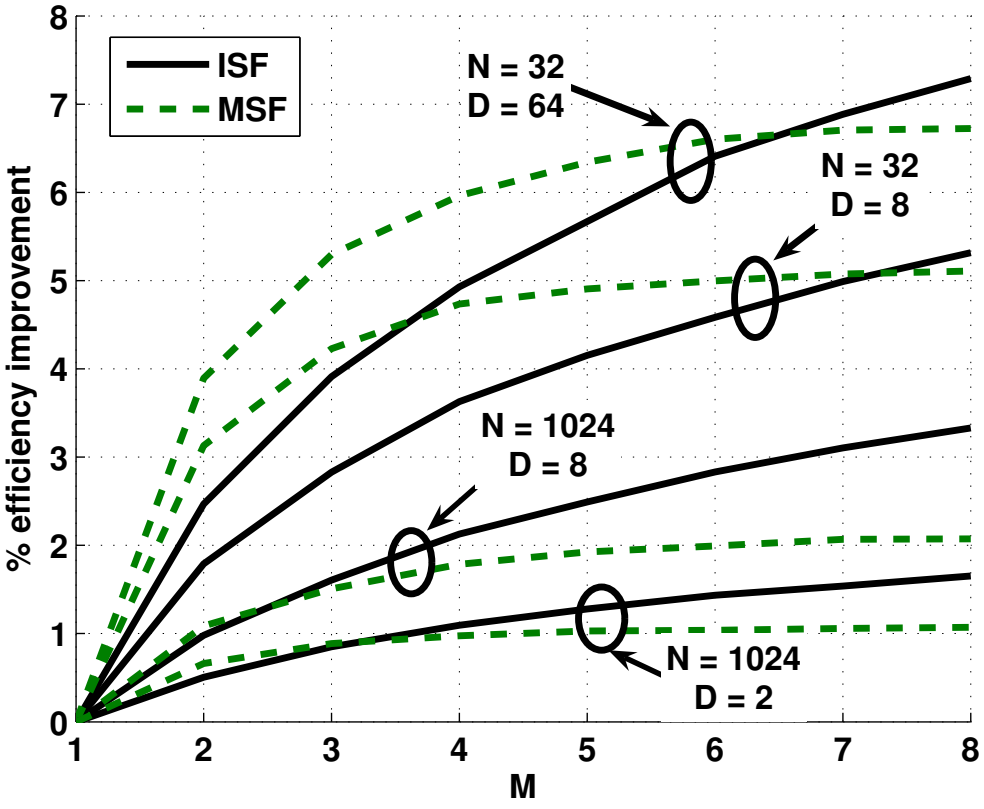

Figure 3.3: Percent power efficiency improvement when the proper PAR metric is applied to cSLM.

3.4 Conclusions

In this chapter, we derived the power efficiency maximizing PAR metrics for MIMO-OFDM systems. Under two different system setups, we obtained the relationship between the branch PARs and the overall power efficiency. For each case we have provided the metric that can be used by PAR reduction system designers to maximize the power efficiency. For the ISF case, the PAR metric is defined as the maximum of the branch PARs as in (3.13). For the MSF case, the proper PAR metric should be the harmonic average of the individual branch PARs as defined in (3.20). In some papers, for example, [53], [12], and [80], the *arithmetic average* of the branch PARs was used as the metric for PAR reduction – we fail to relate such PAR metric to meaningful physical mechanisms.

CHAPTER IV

EVM ANALYSIS IN OFDM SYSTEMS

4.1 Introduction

The objectives of the EVM analysis are twofold. First, statistical analyses are carried out for various distortion mechanisms. Second, we will apply the derived theoretical results to check whether the EVM of OFDM signals satisfies the standard requirement. It is anticipated that the proposed theoretical derivations will simplify OFDM EVM evaluation by avoiding the necessity of costly hardware tests and/or software simulations.

4.2 EVM and its Approximated Distribution

The definition of EVM for the WiMAX standard has been given in Chapter 2, which is repeated here for convenience

$$\text{EVM} = \frac{1}{S_{max}}\sqrt{\frac{1}{N}\sum_{k\in\mathcal{I}}|Y_k - X_k|^2} = \sqrt{\frac{\frac{1}{N}\sum_{k=1}^{N}|D_k|^2}{S_{\max}^2}}, \tag{4.1}$$

where the root mean square error is normalized by the maximum amplitude of the constellation points $S_{\max}$. This is different from the EVM definition in the IEEE 802.11 standard, where the normalization factor is the average amplitude of the constellation points. Moreover, we have shown that the following quantity

$$Z = \text{EVM}^2 = \frac{1}{N}\sum_{k=0}^{N-1}\frac{|D_k|^2}{S_{\max}^2} \tag{4.2}$$

conveys information about sample-averaged normalized error powers. Z is of interest, because it is much easier to be theoretically analyzed than the EVM value in (4.1).

Recall that x_n is the Nyquist-rate time-domain sample. When N is large, the real and imaginary parts of x_n are approximately i.i.d. Gaussian distributed with zero mean and variance σ^2. Also, we have $E[|X_k|^2] = E[|x_n|^2] = 2\sigma^2$. Denote by $d_n = y_n - x_n$ ($d_n = \text{IDFT}\{D_k\}$ and $y_n = \text{IDFT}\{Y_k\}$) the error vector in the time domain. As shown in

Section 2.4, we have $E[\text{EVM}] \approx \sqrt{E[Z]}$. Using Parseval's Theorem, we can rewrite (4.2) as

$$Z = \frac{1}{N} \sum_{n=0}^{N-1} \frac{|d_n|^2}{S_{\max}^2}. \tag{4.3}$$

During transmission, the OFDM signal x_n may experience various distortions. The specified EVM thresholds are given in Table 2.1 for the WiMAX system. If the dB scale is concerned, $E[Z]$ should not exceed -18.4dB for QPSK or -24.4dB for 16QAM.

Observing (4.2) and (4.3), we can find that Z is composed of the summation of N random variables with identical distribution. Suppose these random variables are also independent; then the central limit theorem can be applied when N is large. Thus, Z approximates the Gaussian distribution with the probability density function

$$f_Z(z) = \frac{1}{\sqrt{2\pi}\zeta} e^{-\frac{(z-\mu)^2}{2\zeta^2}}, \tag{4.4}$$

where $\mu = E[Z] = E[|d_n|^2]/S_{max}^2$ is the mean and $\zeta^2 = Var[Z] = Var[|d_n|^2]/(N \cdot S_{max}^4)$ is the variance ($Var[\cdot]$ is the variance operation). For various distortion mechanisms, we only need to calculate μ and ζ^2 to obtain the distribution of Z.

A series of troubleshooting measurements was presented in [7, 22] to identify the distortion source according to different symptoms. Detailed μ values are calculated for different distortions in the following descriptions. We then demonstrate that it is possible to use the EVM-related parameters to diagnose the source of distortion. Also, based on theoretical values of μ, we are able to derive the limiting values for phase noise, clipping level, PA nonlinearity coefficient and gain/phase imbalance that result in permissable EVM.

4.3 EVM Analysis of Phase Noise

According to [7]: "Different error mechanisms will affect a signal in different ways, perhaps in magnitude only, phase only, or both simultaneously.... Thus, the first diagnostic step is to resolve EVM into its magnitude and phase error components and compare their relative sizes." So, when $E[|\phi_k|] >> E[|E_k|]$, some sort of unwanted phase distortion is the dominant error. However, the inverse statement is not always true for OFDM systems [22], i.e., phase noise may not always have $E[|\phi_k|] >> E[|E_k|]$. We will demonstrate this using the phase noise distortion mechanism.

From [34, 88, 94], the baseband phase noise model is

$$y_n = x_n \cdot e^{j\theta_n}, \tag{4.5}$$

where θ_n is the phase noise at the nth sample. Suppose θ_n is small, so that $e^{j\theta_n} \approx 1 + j\theta_n$. Then, in the frequency domain, we have

$$Y_k = X_k + jX_k\Theta + \mathrm{ICI}_k, \tag{4.6}$$

where

$$\Theta = \frac{1}{\sqrt{N}} \sum_{n=0}^{N-1} \theta_n$$

is the common phase error (CPE), and ICI_k is the inter-carrier interference (ICI) at the kth sub-carrier.

When the phase noise variations are much slower than the OFDM period, the CPE dominates over the ICI. In this case,

$$Y_k = X_k(1 + j\Theta); \tag{4.7}$$

hence, we have

$$|E_k| = ||Y_k| - |X_k|| = |X_k|(\sqrt{1 + \Theta^2} - 1), \tag{4.8}$$

and

$$|\phi_k| = |\angle Y_k - \angle X_k| = |\tan^{-1}\Theta|. \tag{4.9}$$

When $|\Theta|$ is small, $E[|E_k|] \approx 0 << E[|\phi_k|] \approx |\Theta|$. So the condition $E[|\phi_k|] >> E[|E_k|]$ is satisfied no matter what the modulation scheme is used.

If both the CPE and the ICI should be considered, the analysis becomes complicated; hence, we rely on the simulations to check the relationship between $E[|\phi_k|]$ and $E[|E_k|]$. From [94], θ_n can be regarded as Gaussian distributed with zero mean and variance σ_θ^2. Define

$$\lambda = \frac{E[|\phi_k|]}{E[|X_k|]}, \tag{4.10}$$

which should be larger than 5 when we say $E[|\phi_k|] >> E[|E_k|]$ [7]. Shown in Fig. 4.1 are the λ curves changing with σ_θ^2 for various modulation schemes. Clearly, $E[|\phi_k|] >> E[|E_k|]$

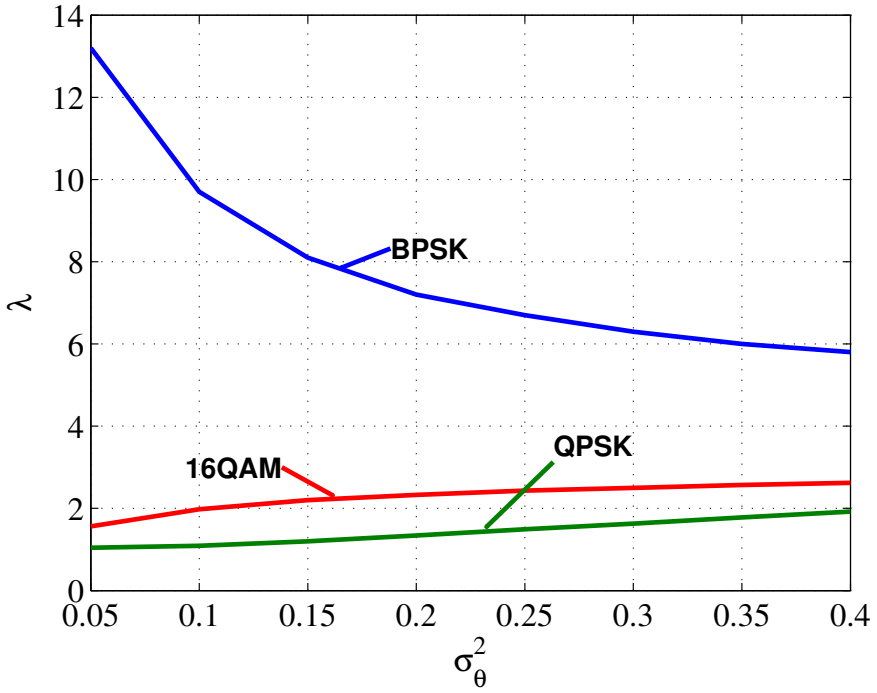

Figure 4.1: Relationship between $\lambda = E[|\phi_k|]/E[|X_k|]$ and the phase noise variance for various modulation schemes: QPSK, 16QAM and 64QAM, $N = 2048$.

is only valid for the BPSK modulation. For QPSK and 16QAM, the average phase error and the average magnitude error are at similar levels.

Suppose $|E_k| \approx 0$, i.e., $|Y_k| \approx |X_k|$,

$$Z = \frac{1}{N} \sum_{k=0}^{N-1} \frac{2(1 - \cos\phi_k)|X_k|^2}{S_{\max}^2}. \tag{4.11}$$

Because ϕ_k and $|X_k|$ are independent random variables,

$$\mu = \frac{2(1 - E[\cos\phi_k])E[|X_k|^2]}{S_{\max}^2} = \frac{2(1 - E[\cos\phi_k])}{\gamma}, \tag{4.12}$$

where $\gamma = S_{\max}^2/(2\sigma^2)$ is the PAR of the constellation for X_k. Phase noise ϕ_k is assumed to be a Gaussian random variable with zero mean and variance σ_ϕ^2, so [34], [35, page 483]

$$E_{\phi_k}[\cos\phi_k] = \int_{-\infty}^{+\infty} \cos\phi_k \cdot \frac{1}{\sqrt{2\pi}\sigma_\phi} e^{-\frac{\phi_k^2}{2\sigma_\phi^2}} d\phi_k = e^{-\frac{\sigma_\phi^2}{2}}. \tag{4.13}$$

Hence,

$$\mu = \frac{2(1 - e^{-\frac{\sigma_\phi^2}{2}})}{\gamma}. \tag{4.14}$$

By observing (4.14), we find that μ increases with the phase noise power σ_ϕ^2. In Fig. 4.2, μ vs. σ_ϕ^2 for different modulation schemes are shown. To satisfy the requirement of the standard, σ_ϕ^2 should be less than or equal to 0.014, 6.5×10^{-3} and 2.1×10^{-3} for QPSK, 16QAM and 64QAM, respectively.

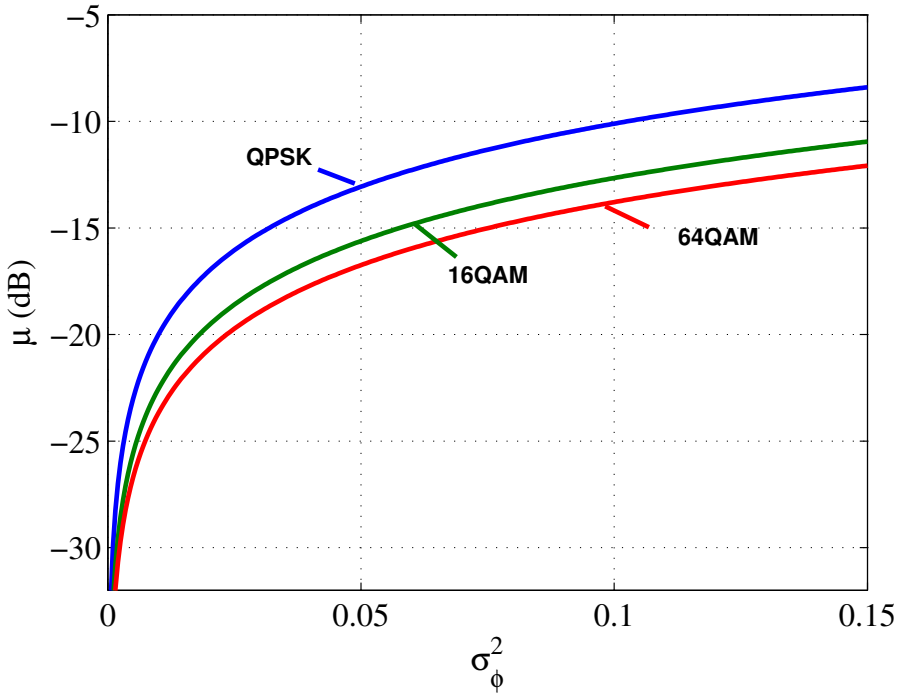

Figure 4.2: Theoretical μ with different σ_ϕ^2 values for various modulation schemes: QPSK, 16QAM and 64QAM.

4.4 EVM Analysis of Amplitude Clipping

Based on the polar clipping model in (2.26), the magnitude of the time-domain clipping noise d_n can be written as

$$|d_n| = |y_n - x_n| = \begin{cases} 0, & |x_n| \le A_{max} \\ |x_n| - A_{max}, & |x_n| > A_{max} \end{cases}, \tag{4.15}$$

where $|x_n|$ has the Rayleigh distribution

$$f_{|x_n|}(r) = \frac{r}{\sigma^2} e^{-r^2/2\sigma^2}, r \ge 0. \tag{4.16}$$

Hence, the average power of the clipping noise d_n is

$$\begin{aligned} E[|d_n|^2] &= \int_{A_{max}}^{\infty} (r - A_{max})^2 f_{|x_n|}(r) dr \\ &= 2\sigma^2 e^{-A_{max}^2/2\sigma^2} - \sigma A_{max}\sqrt{2\pi}\ \text{erfc}\left(\frac{A_{max}}{\sigma\sqrt{2}}\right). \end{aligned} \tag{4.17}$$

Substituting (4.17) into (4.3), we obtain

$$\mu = \frac{E[|d_n|^2]}{S_{max}^2} = \frac{e^{-A_{max}^2/2\sigma^2}}{\gamma} - \frac{\frac{A_{max}}{\sigma}\sqrt{\frac{\pi}{2}}\ \text{erfc}(\frac{A_{max}}{\sigma\sqrt{2}})}{\gamma}. \tag{4.18}$$

The result in (4.17) was also derived in [89] using a conditional probability method.

Figure 4.3 presents theoretical values of μ when the number of subcarriers N is 128. The solid line is obtained from (4.18) for the QPSK constellation ($\sigma = 1$, $S_{\max} = \sqrt{2}$), while the dashed line is for the 16QAM constellation ($\sigma = \sqrt{5}$, $S_{\max} = \sqrt{18}$). If we are to use (4.18) to select the clipping ratio $\Omega = \frac{A_{max}}{\sqrt{2}\sigma}$ to meet 802.16 EVM requirements [4], we find that $\Omega \geq 3.6$dB for QPSK and $\Omega \geq 4.6$dB for 16QAM are necessary.

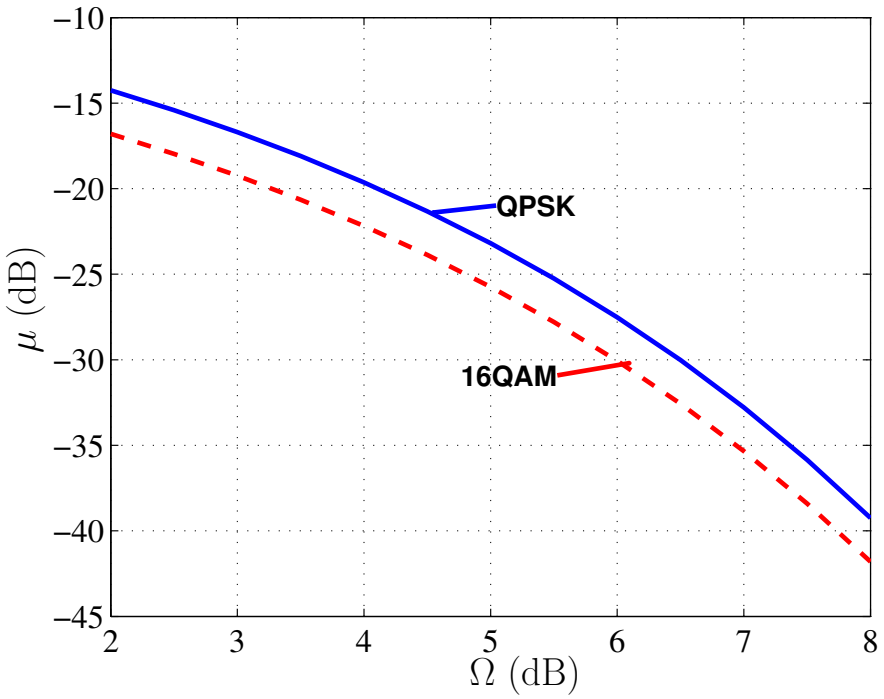

Figure 4.3: Theoretical μ as a function of the clipping ratio Ω for QPSK and 16QAM.

4.5 EVM Analysis of Baseband Polynomial Model for Nonlinearities of the PA

The power amplifier (PA) is an essential component in communication systems. However, the inherent nonlinearity in PAs introduces in-band distortion and out-of-band spectral regrowth. A baseband polynomial model is a convenient way to describe nonlinearities [101].

The baseband polynomial model including both the odd-order and the even-order terms can be written as [27]

$$y_n = \sum_{k=1}^{K} b_k \; x_n \; |x_n|^{k-1}, \tag{4.19}$$

where x_n is the baseband PA input signal, y_n is the baseband PA output signal, K is the polynomial order which is an integer, and b_k are polynomial coefficients.

The time-domain nonlinear distortion term can be written as

$$d_n = \sum_{k=1}^{K} \frac{b_k}{b_1} \; x_n \; |x_n|^{k-1} - x_n = \sum_{k=2}^{K} c_k \; x_n \; |x_n|^{k-1}, \tag{4.20}$$

where $c_k = b_k/b_1, \forall k \geq 2$.

The magnitude square of d_n can be further expressed as

$$\begin{aligned} |d_n|^2 &= \left| \sum_{k=2}^{K} c_k \; x_n \; |x_n|^{k-1} \right|^2 \\ &= \left(\sum_{k=2}^{K} c_k \; |x_n|^{k-1} \right) \cdot \left(\sum_{l=2}^{K} c_l \; |x_n|^{l-1} \right)^* \cdot |x_n|^2 \\ &= \sum_{k=2}^{K} \sum_{l=2}^{K} c_k \; c_l^* \; |x_n|^{k+l}, \end{aligned} \tag{4.21}$$

where $(\cdot)^*$ is the complex conjugate operation. Because $|x_n|$ has the Rayleigh distribution, the mth order moment of $|x_n|$ is [70, page 148]

$$E[|x_n|^m] = 2^{\frac{m}{2}} \Gamma\left(\frac{m+2}{2}\right) \sigma^m = \begin{cases} m!!\sigma^m, & m \text{ even}, \\ \sqrt{\frac{\pi}{2}} m!!\sigma^m, & m \text{ odd}, \end{cases} \tag{4.22}$$

where $\Gamma(\cdot)$ is the Gamma function and (.)!! is the double factorial operation. By combining

(4.21) and (4.22), the statistical expectation of Z is

$$\begin{aligned}\mu &= \frac{E[|d_n|^2]}{S_{max}^2} \\ &= \frac{\sum_{k=2}^{K}\sum_{l=2}^{K} c_k\ c_l^*\ E[|x_n|^{k+l}]}{S_{max}^2} \\ &= \frac{\sum_{k=2}^{K}\sum_{l=2}^{K} c_k\ c_l^*\ 2^{\frac{k+l}{2}}\Gamma(\frac{k+l+2}{2})\sigma^{k+l}}{S_{max}^2}. \end{aligned} \tag{4.23}$$

If the band-pass signal is of interest, only the odd-order terms need to be considered in (4.19). In this case, the polynomial coefficients $b_k, k = 1, 3, \cdots, K$ are real numbers for strictly memoryless PA and complex numbers for quasi-memoryless PA. Hence, (4.23) becomes

$$\mu = \frac{\sum_{k=3,\ k\ \text{odd}}^{K}\sum_{l=3,\ l\ \text{odd}}^{K} c_k c_l^*(k+l)!!\sigma^{k+l-2}}{\gamma}. \tag{4.24}$$

From (4.24), we can observe that the distortion depends on the signal variance, the polynomial coefficients, and the polynomial order. For example, if only the third-order nonlinearity is present, we have $\mu = 24|c_3|^2\sigma^4/\gamma$. Hence, EVM would increase with the degree of nonlinearity $|c_3|^2$. The polynomial coefficients can be obtained from either measured AM/AM and AM/PM curves of the PA by applying the polynomial fitting, or the odd-order intercept points and 1-dB compression point by solving a system of equations [101].

To demonstrate the relationship between μ and related parameters, numerical examples are presented by setting σ^2 to be one. For a fixed $c_3 = -0.02$, μ decreases with γ. Three γ's corresponding to QPSK, 16QAM, and 64QAM are shown in Fig. 4.4. By comparing μ with the threshold, only QPSK satisfies the requirement of the standard when $c_3 = -0.02$. For the 16QAM and 64QAM constellations, $|c_3|$ must be smaller than 0.02 to meet the EVM requirement.

Shown in Fig. 4.5 is the relationship between μ and $|c_3|$ for different modulation schemes. To satisfy the requirement of the standard, $|c_3|$ should not be larger than 0.025, 0.017 and 0.009 for QPSK, 16QAM and 64QAM, respectively.

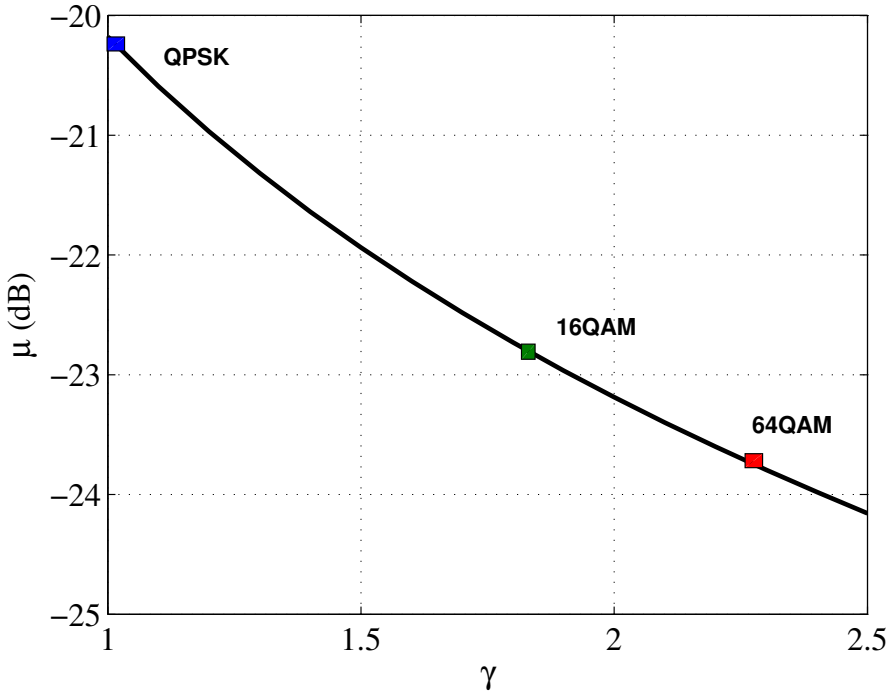

Figure 4.4: Theoretical μ with different γ values, where the cubic nonlinear coefficient is $c_3 = -0.02$.

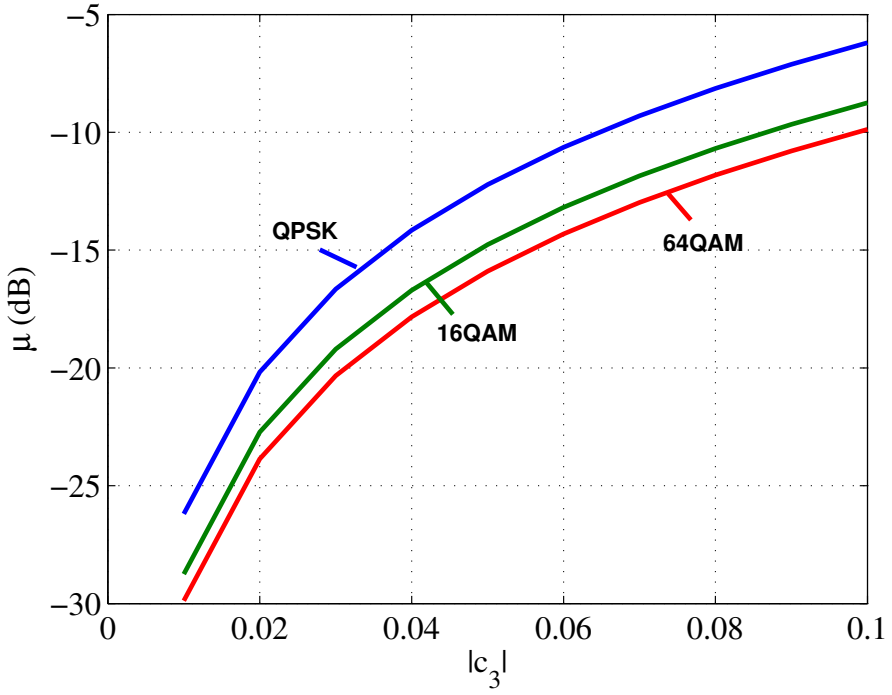

Figure 4.5: Theoretical μ with different $|c_3|$ values for various modulation schemes: QPSK, 16QAM and 64QAM.

4.6 EVM Analysis of Gain/Phase Imbalances

Gain/phase imbalances occur in the front-end analog processing that will distort the in-band OFDM signals [77, 88]. The imbalances can be characterized by two parameters: the gain imbalance ϵ and the phase imbalance $\Delta\phi$. The baseband model can be written as:

$$y_n = \alpha \cdot x_n + \beta \cdot x_n^*, \tag{4.25}$$

where

$$\alpha = \cos\Delta\phi + j\epsilon \sin\Delta\phi,$$

and

$$\beta = \epsilon \cos\Delta\phi - j \sin\Delta\phi.$$

If no imbalance exists, i.e., $\epsilon = 0$, $\Delta\phi = 0$, then $\alpha = 1$ and $\beta = 0$ and (4.25) reduces to $y_n = x_n$.

The distortion signal can be expressed as

$$d_n = y_n - x_n = \eta \cdot x_n + \beta \cdot x_n^*, \tag{4.26}$$

where $\eta = \alpha - 1$. So the distortion power is

$$\begin{aligned} E[|d_n|^2] &= E\left[(\eta \cdot x_n + \beta \cdot x_n^*) \cdot (\eta \cdot x_n + \beta \cdot x_n^*)^*\right] \\ &= (|\eta|^2 + |\beta|^2)E[|x_n|^2] + \eta\beta^* E[x_n^2] + \eta^*\beta E[(x_n^*)^2]. \end{aligned} \tag{4.27}$$

Based on the assumption that x_n is circular complex Gaussian distributed, $E[x_n^2] = E[(x_n^*)^2] = 0$. Hence,

$$\mu = \frac{|\eta|^2 + |\beta|^2}{\gamma} = \frac{\epsilon^2 + 2(1 - \cos\Delta\phi)}{\gamma}. \tag{4.28}$$

The contours of μ with different gain and phase imbalances are plotted in Fig. 4.6 for the QPSK modulation. We can see that EVM increases with gain/phase imbalances. The regions below the solid line indicate the allowed gain/phase imbalance combinations to satisfy the standard's requirements.

The symptom of gain/phase imbalances in OFDM systems is the constellation state spreading, which is different from that of the single-carrier systems [22]. Hence, it is difficult

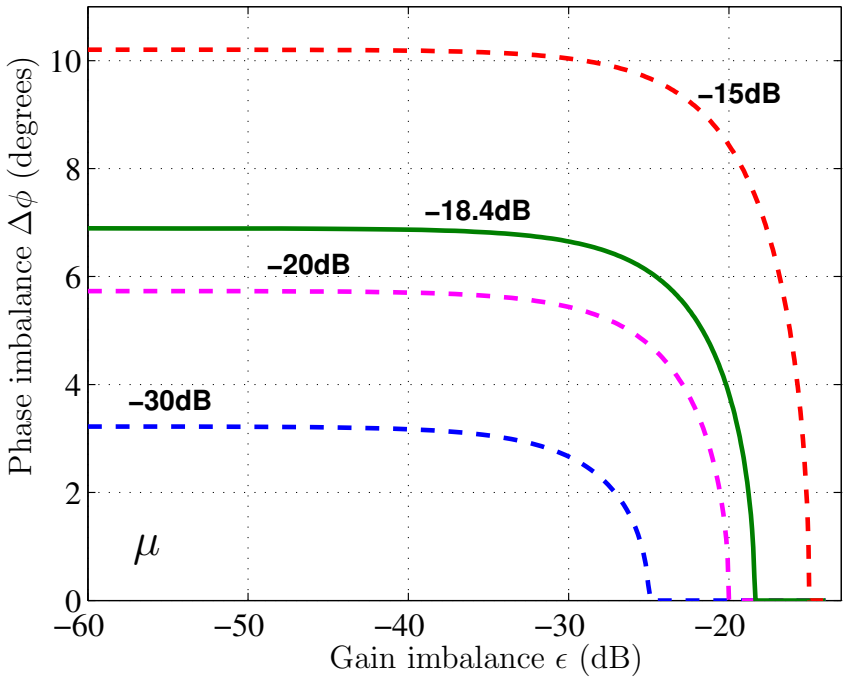

Figure 4.6: Theoretical μ contours with different gain and phase imbalances for the QPSK modulation.

to differentiate the gain/phase imbalances from other distortions for high-order modulation schemes. Rather, it is preferred to observe the constellation diagram of the pilot sub-carriers, which are BPSK modulated, in order to diagnose the problem.

When only the phase imbalance exists, i.e., $\alpha = \cos\Delta\phi$ and $\beta = -j\sin\Delta\phi$, we have

$$Y_k = \alpha X_k + \beta X_k^{\#}, \tag{4.29}$$

where

$$X_k^{\#} = X^*_{(N-k) \bmod N}$$

and $(\cdot)^*$ is the complex conjugate operation. For BPSK symbols, $X_k^{\#} = X_{(N-k) \bmod N}$ and $|X_k^{\#}| = |X_k|$. Hence, $|Y_k| \equiv |X_k|$, which implies $E_k \equiv 0$. On the other hand, $|\phi_k| \equiv |\Delta\phi|$. So, the condition $E[|\phi_k|] >> E[|E_k|]$ is satisfied and the distortion source can be judged to be the phase imbalance by comparing $|\phi_k|$ and $|E_k|$ of BPSK pilot signals.

4.7 Conclusions

In this chapter, we analyzed statistical behaviors of EVM caused by various impairments, including phase noise, amplitude clipping, PA nonlinearities, and gain/phase imbalances. Theoretical μ values for some specific distortion mechanisms were calculated for various impairments. The results were twofold: first, based on the relationship between the phase error and the magnitude error, we demonstrated how the distortion source could be diagnosed; second, using theoretical calculations, we provided concrete thresholds for the amount of allowable distortions from each distortion source to meet EVM requirements.

CHAPTER V

CONSTRAINED CLIPPING

5.1 Introduction

Crest factor reduction (CFR) is an efficient way to improve the power efficiency and reduce the nonlinear distortion in OFDM communication systems. A lot of CFR techniques have been proposed in the literature, see [36, 57, 86] for the overview of existing algorithms. CFR is also applied to other OFDM-based systems, such as coded OFDM [37], multiple-input multiple-output (MIMO) OFDM [12], multi-carrier code division multiplexing access (CDMA) [98], and uplink of the orthogonal frequency division multiplexing access (OFDMA) systems [99]. Among these techniques, distortion-based CFR algorithms are of particular interest.

In Section 2.5, however, we showed that simple clipping is incapable of fulfilling the in-band and out-of-band distortion requirements of the standard. Hence, the objective of the study can be described as follows: obtain the signal after CFR, $\widetilde{x}_n^{(L)}$ in the time domain, or equivalently, $\widetilde{X}_k^{(L)}$ in the frequency domain, such that:

(i) $\text{PAR}\{\widetilde{x}_n^{(L)}\} \ll \text{PAR}\{x_n^{(L)}\}$;

(ii) $\text{EVM}\{\widetilde{x}_n^{(L)}\} \leq Th$;

(iii) $\text{PSD}\{\widetilde{x}_n^{(L)}\} \leq P(\omega),\ \pi/L < \omega < \pi$.

Th is the in-band EVM threshold and $P(\omega)$ is the out-of-band spectral mask.

A constrained clipping algorithm is proposed to work in OFDM systems, keeping both in-band and out-of-band distortions below certain specified values. We consider the case where the out-of-band distortion must not exceed a given spectral mask, and the in-band distortion is not larger than the EVM threshold. The novelty of the proposed constrained clipping algorithm is that it can guarantee that the EVM and spectral mask requirements

are met for each transmitted symbol. Constrained clipping is not an iterative technique; thus its computational complexity is relatively low.

Recall that $\bar{x}_n^{(L)}$ is the result of simple clipping. Suppose that $\widetilde{x}_n^{(L)}$ is the signal that actually gets transmitted, which may be obtained after certain operations on $\bar{x}_n^{(L)}$, satisfying the EVM threshold and the spectral mask requirements in the standard. In calculating $\mathrm{EVM}\{\widetilde{x}_n^{(L)}\}$, we replace $D_k = \bar{X}_k^{(L)} - X_k$ by $\widetilde{D}_k = \widetilde{X}_k^{(L)} - X_k, \quad k \in \mathcal{I}$. Therefore,

$$\mathrm{EVM}\{\bar{x}_n^{(L)}\} = \frac{1}{S_{max}} \sqrt{\frac{1}{N} \sum_{k \in \mathcal{I}} |\widetilde{D}_k|^2}. \tag{5.1}$$

Computational complexity of the constrained clipping is analyzed to demonstrate that the proposed CFR technique is easy to be implemented compared with other CFR algorithms. To utilize constrained clipping in the multiple-user OFDM system, we have extended the in-band processing to calculate and control EVM values for different modulation schemes.

5.2 Proposed In-Band and Out-of-Band Processing Algorithms

The overall structure of the proposed constrained clipping scheme is shown in Fig. 5.1. Assume that the incoming signal is a standard OFDM signal before any CFR has been applied. Fig. 5.2 gives a simplified diagram of constrained clipping with signal notations labeled. First, the signal $x_n^{(L)}$ is simply clipped at some optimized clipping level A_{max} to create $\bar{x}_n^{(L)}$ as in (2.26). Next, the signal is transformed to the frequency domain with an LN-point fast Fourier transform (FFT), which outputs the signal $\bar{X}_k^{(L)}$ as in (2.28). Afterward, separate in-band and out-of-band processing modules generate $\widetilde{X}_k^{(L)}$ from $\bar{X}_k^{(L)}$ to ensure that the EVM and spectral mask requirements are met. Finally, the outgoing low-PAR symbol, $\widetilde{x}_n^{(L)}$, is created with an LN-point inverse FFT operation (replace $X_k^{(L)}$ by $\widetilde{X}_k^{(L)}$ and $x_n^{(L)}$ by $\widetilde{x}_n^{(L)}$ in (2.12)). Next, three components of constrained clipping, in-band processing, out-of-band processing and clipping level optimization, are introduced in detail.

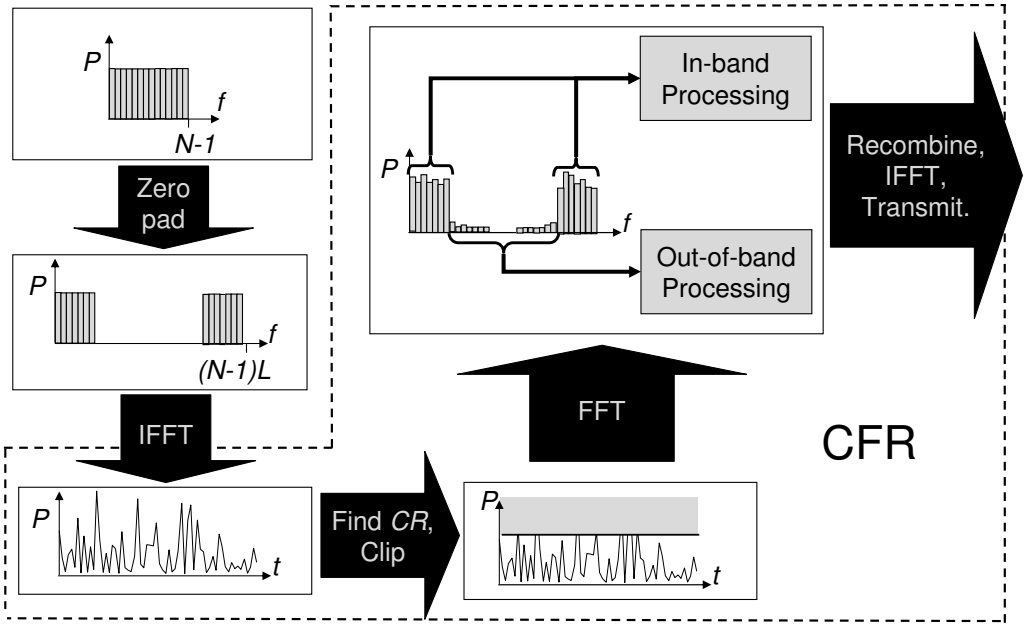

Figure 5.1: Flow chart of the constrained clipping algorithm, which is implemented by the components inside the dashed lines.

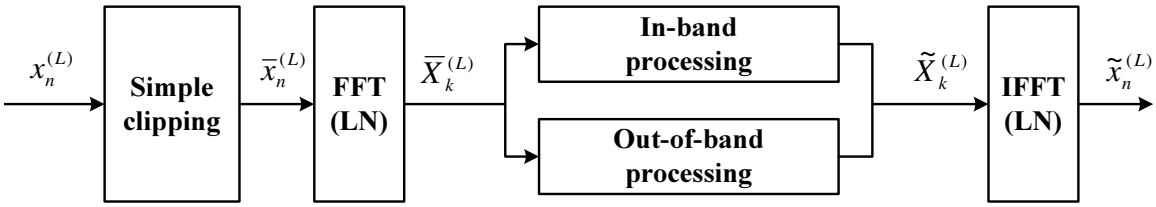

Figure 5.2: Simplified block diagram of the constrained clipping method with signal notations at each processing stage.

5.2.1 In-Band Processing Algorithm

If the clipping is so light that the EVM requirement is already met by the simple clipping signal, i.e., $\text{EVM}\{\bar{x}_n^{(L)}\} \leq Th$, then no in-band processing is necessary and we simply set $\widetilde{X}_k^{(L)} = \bar{X}_k^{(L)}, k \in \mathcal{I}$. If, on the other hand, $\text{EVM}\{\bar{x}_n^{(L)}\} > Th$, our proposed in-band processing algorithm strives to obtain a $\widetilde{x}_n^{(L)}$, whose EVM is below the threshold Th and whose PAR is at a low level.

One way to ensure that the EVM is met is to set

$$\widetilde{X}_k^{(L)} = X_k + D_k \frac{Th}{\text{EVM}\{\bar{x}_n^{(L)}\}}, \quad \forall k \in \mathcal{I}, \tag{5.2}$$

i.e., scale down each D_k to reduce the EVM in $\widetilde{x}_n^{(L)}$, resulting in $\text{EVM}\{\widetilde{x}_n^{(L)}\} = Th$. However, through extensive computer simulations we found that excessive peak regrowth occurs in $\widetilde{x}_n^{(L)}$ as a result of the above scaling operation. Hence, a sorting-based method is used to yield significantly better CFR performance.

In the in-band processing algorithm, we first sort $|D_k|$ in ascending order. If the rms average of the smallest M $|D_k|$ values is less than or equal to $Th \cdot S_{max}$, but the rms average of the smallest $M+1$ $|D_k|$ values is greater than $Th \cdot S_{max}$, we record the value M and collect the sub-carrier indices k that correspond to the M smallest $|D_k|$ values in a set $\mathcal{M}$. In other words, $\mathcal{M}$ is the largest set such that

$$\frac{1}{S_{max}} \sqrt{\frac{1}{M} \sum_{k \in \mathcal{M}} |D_k|^2} \leq Th. \tag{5.3}$$

We assign

$$\widetilde{X}_k^{(L)} = \bar{X}_k^{(L)}, \quad k \in \mathcal{M} \subseteq \mathcal{I}. \tag{5.4}$$

This implies that

$$\frac{1}{S_{max}} \sqrt{\frac{1}{M} \sum_{k \in \mathcal{M}} |\widetilde{D}_k|^2} \leq Th \tag{5.5}$$

as well.

For $k \in \mathcal{I}$ but $k \notin \mathcal{M}$, i.e., $k \in (\mathcal{I} \setminus \mathcal{M})$, the process of obtaining $\widetilde{X}_k^{(L)}$ from $\bar{X}_k^{(L)}$ is explained next. If we make

$$|\widetilde{D}_k| = Th \cdot S_{max}, \quad \forall k \in (\mathcal{I} \setminus \mathcal{M}), \tag{5.6}$$

we infer from (5.5) and (5.6) that

$$\mathrm{EVM}\{\widetilde{x}_n^{(L)}\} = \frac{1}{S_{max}}\sqrt{\frac{1}{N}\sum_{k\in\mathcal{M}}|\widetilde{D}_k|^2 + \frac{1}{N}\sum_{k\in(\mathcal{I}\setminus\mathcal{M})}|\widetilde{D}_k|^2}$$

$$\leq \frac{1}{S_{max}}\sqrt{\frac{M\cdot Th^2\cdot S_{max}^2}{N} + \frac{(N-M)\cdot Th^2\cdot S_{max}^2}{N}} = Th.$$

Thus, (5.6) ensures that the EVM requirement will be met. This means that the vector $\widetilde{X}_k^{(L)}$ should end on the circle that is centered at X_k and that has radius $Th\cdot S_{max}$.

The next consideration is the PAR. Since $\bar{x}_n^{(L)}$ has low PAR, we should make $\widetilde{x}_n^{(L)}$ closely resemble $\bar{x}_n^{(L)}$ so the PAR of $\widetilde{x}_n^{(L)}$ is likely to be low as well. Recalling Parseval's Theorem and (5.4), we infer that

$$\sum_{n=0}^{LN-1}|\widetilde{x}_n^{(L)} - \bar{x}_n^{(L)}|^2 = \sum_{k\in(\mathcal{I}\setminus\mathcal{M})}|\widetilde{X}_k^{(L)} - \bar{X}_k^{(L)}|^2 + \sum_{k\in\mathcal{O}}|\widetilde{X}_k^{(L)} - \bar{X}_k^{(L)}|^2. \tag{5.7}$$

Therefore, we should make $|\widetilde{X}_k^{(L)} - \bar{X}_k^{(L)}|$ as small as possible to ensure a low PAR value in $\widetilde{x}_n^{(L)}$. Jointly considering this and (5.6), we conclude that $\widetilde{X}_k^{(L)}$ should lie at the intersection of the circle and the line connecting vectors X_k and $\bar{X}_k^{(L)}$. In other words,

$$\widetilde{X}_k^{(L)} = X_k + Th\cdot S_{max}\, e^{j\angle D_k}, \quad k\in(\mathcal{I}\setminus\mathcal{M}). \tag{5.8}$$

The procedures from (5.6) to (5.8) to determine $\widetilde{X}_k^{(L)}, k\in(\mathcal{I}\setminus\mathcal{M})$ are illustrated in Fig. 5.3.

5.2.2 Out-of-Band Processing Algorithm

For the out-of-band distortion, the commonly cited method involves filtering the baseband clipped signal with a low-pass filter [11, 55, 60]. In filtering, the out-of-band $|\bar{X}_k^{(L)}|^2$ values are scaled by various constants at each frequency bin k. Since $\bar{X}_k^{(L)}$ is random, the resulting filtered spectrum is random as well so it is difficult to ensure that the spectral mask requirement is always met. Moreover, filtering causes peak regrowth in $\widetilde{x}_n^{(L)}$.

In order to meet the spectral mask, the instantaneous power $|\widetilde{X}_k^{(L)}|^2$ at each out-of-band index ($k\in\mathcal{O}$) must be less than or equal to the spectral mask power P_k. Spectral clipping is used as follows:

$$\widetilde{X}_k^{(L)} = \begin{cases} \bar{X}_k^{(L)}, & |\bar{X}_k^{(L)}|^2 \leq P_k,\ k\in\mathcal{O}, \\ \sqrt{P_k}\, e^{j\angle\bar{X}_k^{(L)}}, & |\bar{X}_k^{(L)}|^2 > P_k,\ k\in\mathcal{O}. \end{cases} \tag{5.9}$$

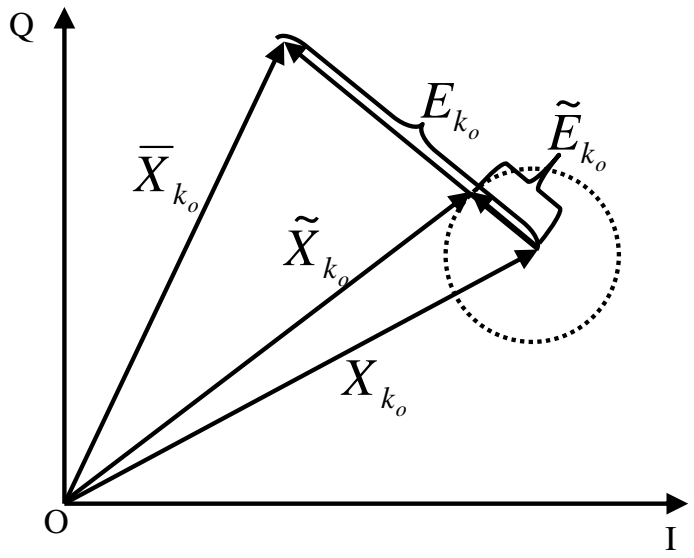

Figure 5.3: Vector diagram to illustrate the in-band processing algorithm, $k \in (\mathcal{I} \setminus \mathcal{M})$.

Note that (5.9) is a deterministic operation that is performed on the out-of-band frequency bins of each symbol $\bar{X}_k^{(L)}$; therefore, PSD$\{\widetilde{x}_n^{(L)}\} \leq P(\omega)$ can be guaranteed for each $\omega = 2\pi k/(LN)$, $k \in \mathcal{O}$.

Spectral clipping resembles the method proposed in [83]; the difference is that with spectral clipping, the out-of-band components that are clipped retain their pre-clipped phases. Similar to time-domain clipping, spectral clipping works by clipping in the frequency domain, the out-of-band parts of the signal that exceed the spectral mask back down to the spectral mask. Note that (5.9) is a deterministic operation that is performed on each out-of-band value of each symbol $\bar{X}_k^{(L)}$.

In summary, the proposed in-band and out-of-band processing algorithm transforms $\bar{X}_k^{(L)}$ into $\widetilde{X}_k^{(L)}$ according to equations (5.4), (5.8) and (5.9). Finally, $\widetilde{X}_k^{(L)}$ is transformed back to the time domain to yield the transmitted signal $\widetilde{x}_n^{(L)}$. The PAR of $\widetilde{x}_n^{(L)}$ will be larger than that of $\bar{x}_n^{(L)}$, but it will still be much lower than the PAR of the original signal $x_n^{(L)}$.

5.2.3 Clipping Level Optimization

Based on empirical studies, the PAR of $\widetilde{x}_n^{(L)}$ has a complex relationship with the initial clipping level, A_{max}. If A_{max} is set too low, large peak regrowths occur when generating $\widetilde{x}_n^{(L)}$ from $\bar{x}_n^{(L)}$, but if A_{max} is set too high, the output signal has a larger PAR than

is necessary. Stated more precisely, the complementary cumulative distribution function (CCDF) of the final PAR is convex in the clipping level A_{max}. Naturally, we want to find the A_{max} that minimizes the output PAR; but because the constrained clipping algorithm is very difficult to theoretically analyze, we have to perform the minimization empirically.

To demonstrate this, we plot the CCDF curves for five different clipping levels in Fig. 5.4. In the plot, $N = 256$, EVM = 6%, the constellation is QPSK, and the spectral mask is taken from the 802.16 standard [4]. Assume that the system calls for an output PAR of 6 dB. That is, any signal with a peak 6 dB above its mean will be clipped by the power amplifier, for instance. If we try to meet the output PAR of 6dB by clipping at a low level of $A_{max} = 3.6$ dB, then 10 percent of the processed symbols $\widetilde{x}_n^{(L)}$ will have a PAR above 6 dB. However, if a moderate $A_{max} = 5.7$ dB is used, only about two percent of the processed symbols $\widetilde{x}_n^{(L)}$ will exceed a PAR of 6dB. Finally, if we set the clipping level to $A_{max} = 6.4$ dB, it can be observed from the plot that virtually every symbol will have an output PAR above 6 dB, which is very undesirable because all symbols with PAR above 6 dB are clipped.

Figure 5.5 is a plot of the probability that the final output PAR of $\widetilde{x}_n^{(L)}$ is above 6 dB for different initial clipping levels A_{max} for $x_n^{(L)}$. From Fig. 5.4, we determined that the optimal clipping level was 5.7 dB for this particular example. Figure 5.5 confirms that the optimal clipping level is 5.7 dB, with about two percent of the output symbols having a PAR above 6dB.

Figure 5.5 demonstrates that it is possible to select the clipping level A_{max} so that the probability of the symbol PAR exceeding 6 dB is minimized. To create a PAR CCDF for our proposed method, it is necessary to find the optimal A_{max} for every possible output PAR. Accordingly, creating a CCDF via Monte Carlo runs will require a great deal of simulation time. However, in a practical system, the optimization only needs to be performed once, off-line, for each set of system parameters (system parameters include the spectral mask, number of sub-carriers, EVM threshold and the type of constellation). For each set of parameters, the off-line optimization will return a clipping level, A_{max}, that will be used in the constrained clipping algorithm. Hence, while the simulation computational complexity is high, the actual complexity when constrained clipping is implemented is very low.

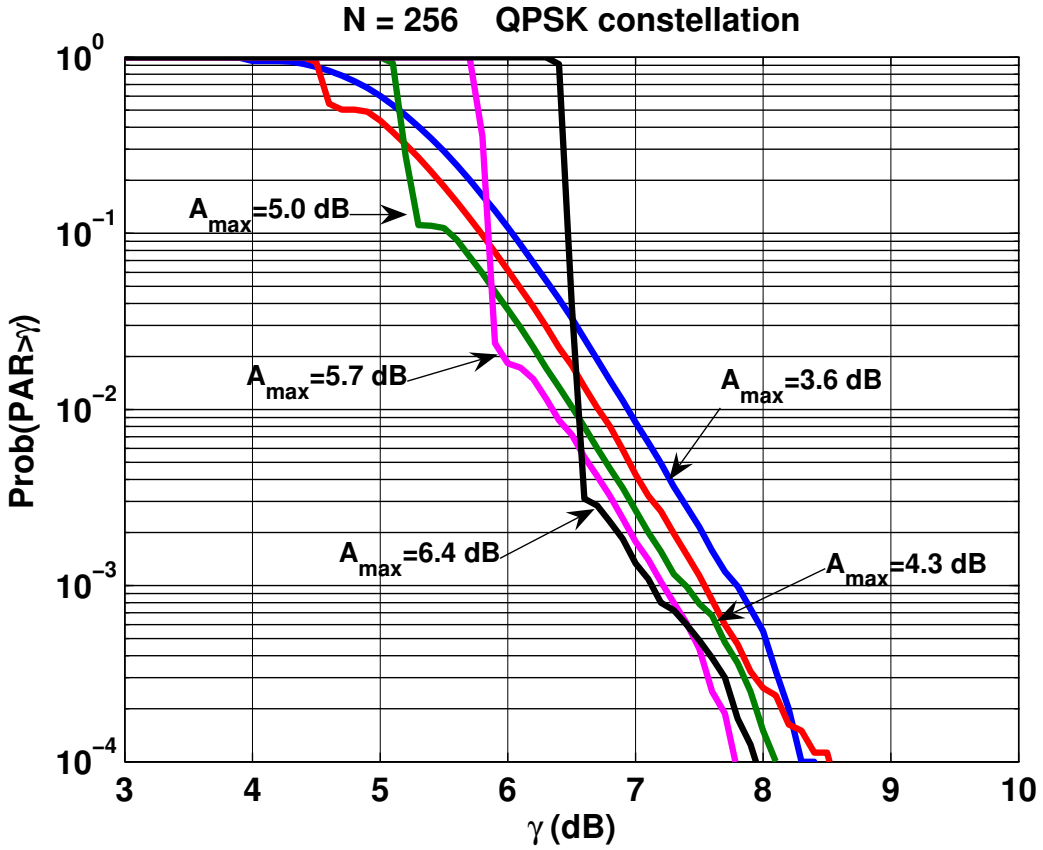

Figure 5.4: CCDF plot of constrained clipping with different initial clipping levels A_{max}, $N = 256$ with a WiMAX spectral mask and EVM = 6%.

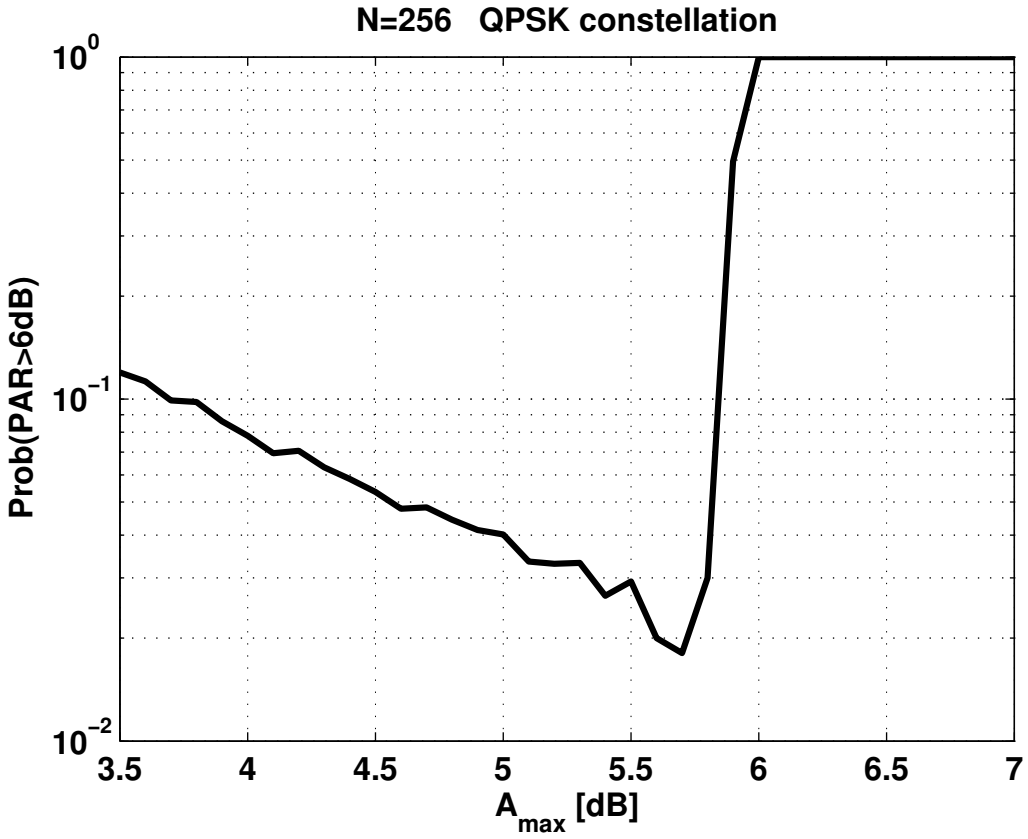

Figure 5.5: Plot of the probability that an OFDM symbol will exceed 6dB in PAR versus the initial clipping level A_{max}, $N = 256$ with a WiMAX spectral mask and EVM = 6%.

Fig. 5.6 is a plot of the CCDF of our proposed method after the initial clipping level A_{max} has been optimized for every output PAR from 4dB to 8dB in increments of 0.1dB. As we can see, an impressive PAR reduction of close to 4.5dB at the 10^{-2} CCDF level is possible while still meeting the spectral mask and EVM constraints. Simulations also indicate that even larger PAR reduction results can be achieved for larger N values with the same EVM and spectral constraints.

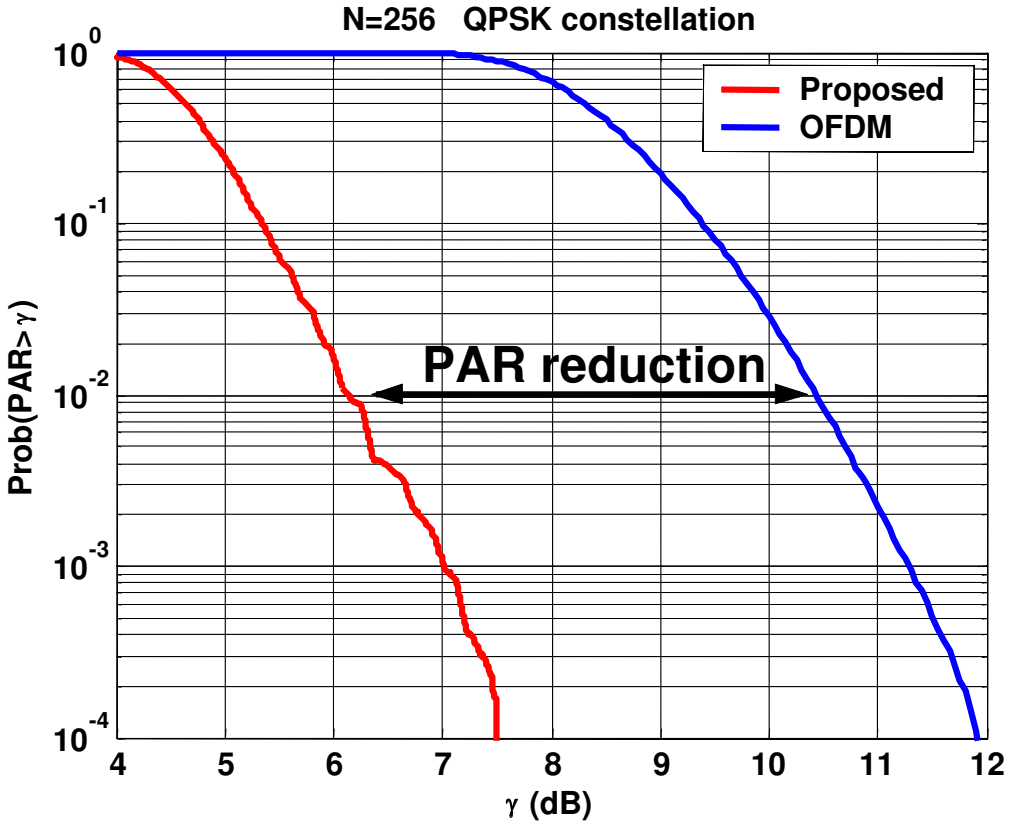

Figure 5.6: CCDF plot for the proposed method after clipping level optimization. $N = 256$ with a WiMAX spectral mask and EVM = 6%.

5.2.4 Performance Results of Constrained Clipping

Ideally, an OFDM symbol, after being processed by constrained clipping, will meet the spectral mask exactly. This is in contrast to the method presented in [10], where all of the out-of-band sub-carriers are set to zero. Figure 5.7 is a simulated PSD plot of the proposed algorithm, Armstrong's algorithm, the spectral mask, and the PSD of the signal after simple

clipping. For the plot, $N = 256$, EVM $= 6\%$, $A_{max} = 5.7$ dB, and the constellation is QPSK. In the plot, we can see that the spectrum of the signal processed by constrained clipping closely follows that of the simple clipping signal for frequencies where the latter does not exceed the spectral mask. For frequencies where the spectrum of the simple clipping signal does exceed the spectral mask, the spectrum of the signal processed by constrained clipping closely follows the spectral mask. This is to be expected, as we intentionally clipped the signal in the frequency domain to exactly meet the spectral mask.

The EVM of the proposed algorithm is designed to never exceed the specified maximum EVM. In Fig. 2.6, it has been shown that some of the symbols processed by Armstrong's method will exceed the allotted EVM. In order to compare the CFR capability of Armstrong's method to constrained clipping, we had to accept a certain probability of EVM-threshold violation from Armstrong's method. In Fig. 5.8 we plot the CCDF of constrained clipping along with the CCDF of Armstrong's method. For the plot a clipping level of 5.7 dB for Armstrong's method is chosen. At this clipping level, symbols processed by Armstrong's method will exceed the EVM threshold about 1.5% of the time, whereas symbols processed by constrained clipping are guaranteed to never exceed the threshold. Despite this handicap, the proposed method still significantly outperforms Armstrong's method in CFR capability.

5.3 Computational Complexity Analysis of Constrained Clipping

In this section, the complexity of the proposed constrained clipping algorithm is investigated. As shown in Fig. 5.2, the main components of the CFR algorithm include

- One inverse fast Fourier transform (IFFT) and one FFT;
- Time-domain clipping;
- In-band and out-of-band processing units.

For each component in the algorithm, the computational complexity will be quantified by the number of instructions per OFDM symbol. Percentage of contribution of each

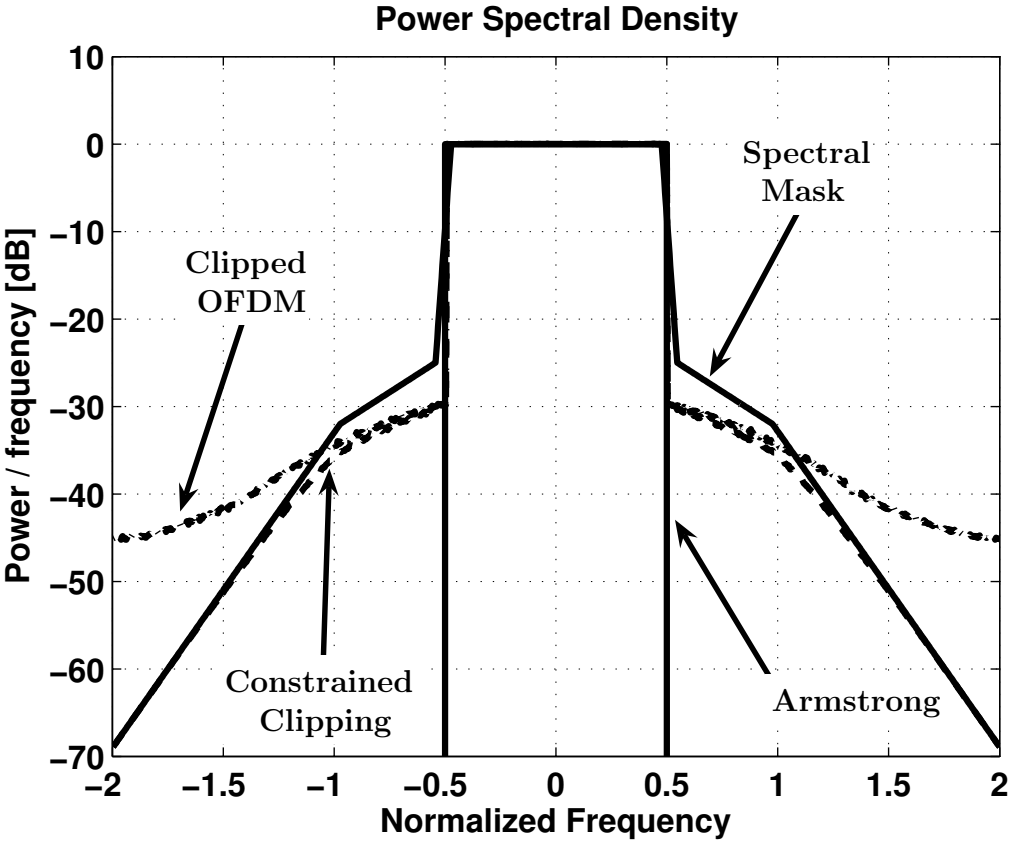

Figure 5.7: Power spectral densities from various clipping methods where the spectral mask from the WiMAX standard is also included.

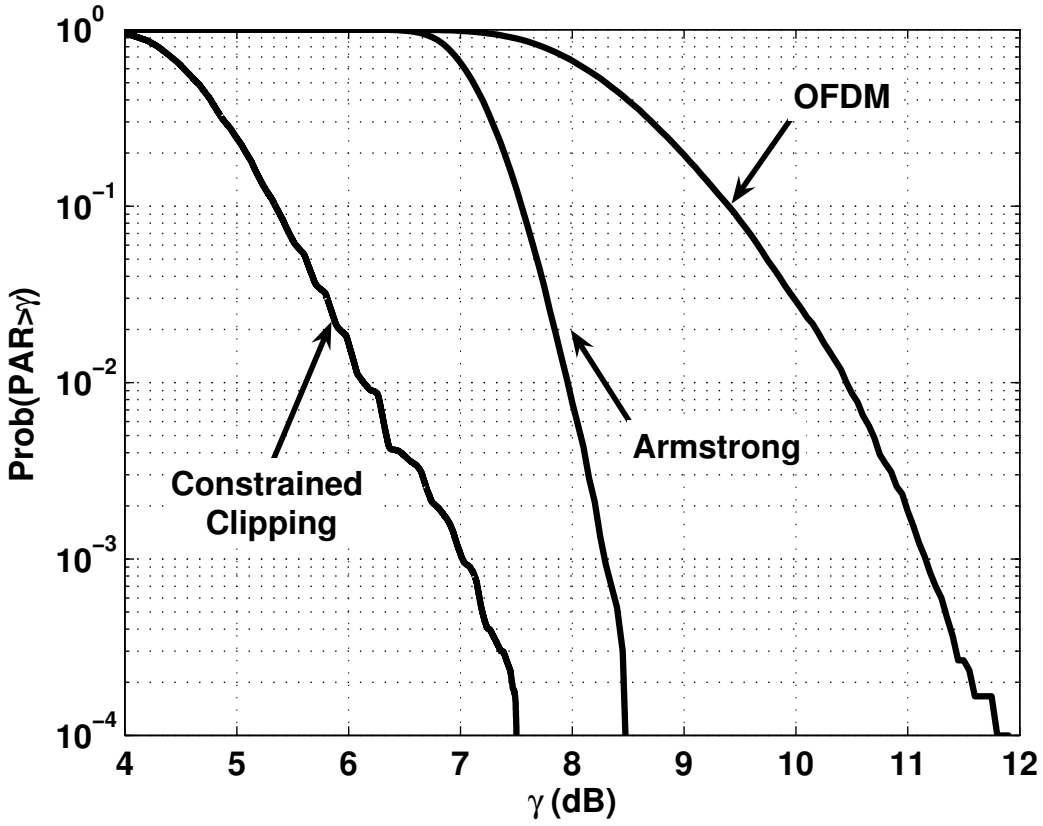

Figure 5.8: CCDF comparison between Armstrong's method and the proposed algorithm. $N = 256$ with a WiMAX spectral mask and EVM = 6%.

component to the complexity will also be given in order to provide a clear understanding about the relative complexity.

In the implementation of constrained clipping, the optimal A_{max} is usually a small value relative to the signal peaks. For this reason, the probabilities of not using time-domain clipping and spectral clipping are negligible. Hence, we assume these two components are called for by every OFDM symbol in the computational complexity analysis.

5.3.1 Complexity of the FFT/IFFT Units

It is known that an LN-point FFT or IFFT requires $(LN/2)\log_2(LN)$ multiplications and $LN\log_2(LN)$ additions. Assuming that a single multiplication operation requires α_M instructions and an addition operation requires α_A instructions, the total number of instructions for carrying out the IFFT and FFT operations is

$$I_{IFFT+FFT} = (\alpha_M + 2\alpha_A)(LN)\log_2(LN). \tag{5.10}$$

5.3.2 Complexity of Time-Domain Clipping

There are LN samples of $x_n^{(L)}$ in the time-domain that pass through the clipping unit. If $|x_n^{(L)}|^2$ is larger than A_{max}^2, the nth sample is clipped and $\bar{x}_n^{(L)} = A_{max}\ x_n^{(L)}/|x_n^{(L)}|$ is the nth sample after clipping.

In order to calculate $|x_n^{(L)}|^2$, $2LN$ multiplications and LN additions are needed. LN comparisons are to be made in order to decide which samples need to be clipped. Assuming that the number of clipped samples is K_t, there are K_t multiplications, K_t divisions and K_t square root operations[1] to obtain the final clipped time-domain signal $\bar{x}_n^{(L)}$. Therefore, the number of instructions required to implement the time-domain clipping is

$$I_{clipping} = 2(\alpha_M + \alpha_A)LN + 7\alpha_M K_t. \tag{5.11}$$

5.3.3 Complexity of In-Band Processing

$\text{EVM}\{\bar{x}_n^{(L)}\}$ in (2.30) is calculated at first in the in-band processing unit which involves $3N$ additions and $2N$ multiplications. In the next step, two cases should be studied separately:

[1]The complexity of a square root operation is assumed to be equivalent to that of five multiplications.

with and without sorting. When $\text{EVM}\{\bar{x}_n^{(L)}\} \leq Th$, sorting is not needed, i.e., the in-band processing step is by-passed. The number of instructions without sorting is

$$I_{ib\ (w/o\ s)} = 3\alpha_A N + 2\alpha_M N. \tag{5.12}$$

When $\text{EVM}\{\bar{x}_n^{(L)}\} > Th$, a sorting algorithm is used, with complexity $O(N \log_2 N)$, to arrange $|D_k|^2$ $(k \in \mathcal{I})$ in ascending order. Hence, we will need about $N \log_2 N$ comparisons which correspond to $\alpha_A N \log_2 N$ instructions. With the sorted $|D_k|^2$ $(k \in \mathcal{I})$, we need $M+1$ additions, $2M+2$ multiplications and $M+1$ comparisons to construct the set $\mathcal{M}$. Once $\mathcal{M}$ is determined, $(N-M)$ $\bar{X}_k^{(L)}$ values should be changed to $\widetilde{X}_k^{(L)}$ as described in (5.8), involving $5(N-M)$ multiplications and $(N-M)$ additions. Therefore, the number of instructions required to implement in-band processing with sorting is

$$I_{ib\ (w/\ s)} = 3\alpha_A N + 2\alpha_M N + \alpha_A N \log_2 N + (N+M+2)\alpha_A + (5N-3M+2)\alpha_M. \tag{5.13}$$

In conclusion, the number of instructions needed to implement in-band processing is

$$I_{ib} = p_i I_{ib\ (w/\ s)} + (1-p_i) I_{ib\ (w/o\ s)}, \tag{5.14}$$

where p_i is the probability of triggering the sorting algorithm (i.e. the probability that $\text{EVM}\{\bar{x}_n^{(L)}\} > Th$).

5.3.4 Complexity of Out-of-Band Processing

Similar to the time-domain clipping, spectral clipping needs $2N(L-1)$ multiplications and $N(L-1)$ additions to calculate $|\bar{X}_k^{(L)}|^2$ $(k \in \mathcal{O})$ and $N(L-1)$ comparisons to determine whether clipping should be taken. Suppose the number of clipped samples is K_f in the spectral clipping, then there are K_f multiplications, K_f divisions and K_f square root operations. Hence, the number of instructions required to implement out-of-band processing is

$$I_{oob} = 2(\alpha_M + \alpha_A)(L-1)N + 7\alpha_M K_f. \tag{5.15}$$

5.3.5 Complexity of the Constrained Clipping Algorithm

The overall computational complexity of the constrained clipping algorithm is

$$I_{CFR} = I_{IFFT+FFT} + I_{clipping} + I_{ib} + I_{oob}, \tag{5.16}$$

depending on various parameters, K_t, p_i, M and K_f. These parameters will change with different A_{max}. Because CFR performance is closely related to A_{max}, the computational complexity varies with different CFR goals.

Typical parameters for the complexity of constrained clipping are given in Table 5.1.

Table 5.1: Example parameters for evaluation of constrained clipping.

Over-sampling rate (L)	4
Number of clipped samples in time-domain clipping (K_t)	J_1
Probability of using sorting algorithm (p_i)	0.1
Number of clipped samples in spectral clipping (K_f)	J_2
M for the in-band processing stage	$0.75N$
# of instructions for addition/substruction/comparison (α_A)	1
# of instructions for multiplication/division/square root (α_M)	2

$J_1 = 0.1NL = 0.4N$, $J_2 = N(L-1)2/3 = 2N$. Parameters are obtained by taking averages on experimental results.

As shown in Fig. 5.9, with $N = 2048$, the IFFT+FFT units account for 71% of the overall computational complexity. Complexity contributions from the other units are out-of-band processing 16%, time-domain clipping 10% and in-band processing 3%.

From the above analysis, it is easy to check that constrained clipping is roughly three times as complex as simple OFDM. Compared with Armstrong's method, which also has IFFT+FFT and time-domain clipping operations, constrained clipping is roughly 25% more complex. The computational complexity of selective mapping (SLM), a popular distortionless-based CFR method, is proportional to the number of used IFFT units. To achieve similar PAR reduction as the constrained clipping, SLM requires approximately 8 IFFT units [13]. So nearly 2/3 computational complexity can be saved by applying the constrained clipping.

5.4 Performance of Constrained Clipping in Multiple-User Environment

5.4.1 EVM Definition in Multiple-User Environment

In the IEEE 802.16 system [4], different users can select appropriate modulation schemes to achieve the optimal transmission performance. Supported modulation schemes include BPSK, QPSK, 16QAM and 64QAM. The constellations shall be normalized by multiplying

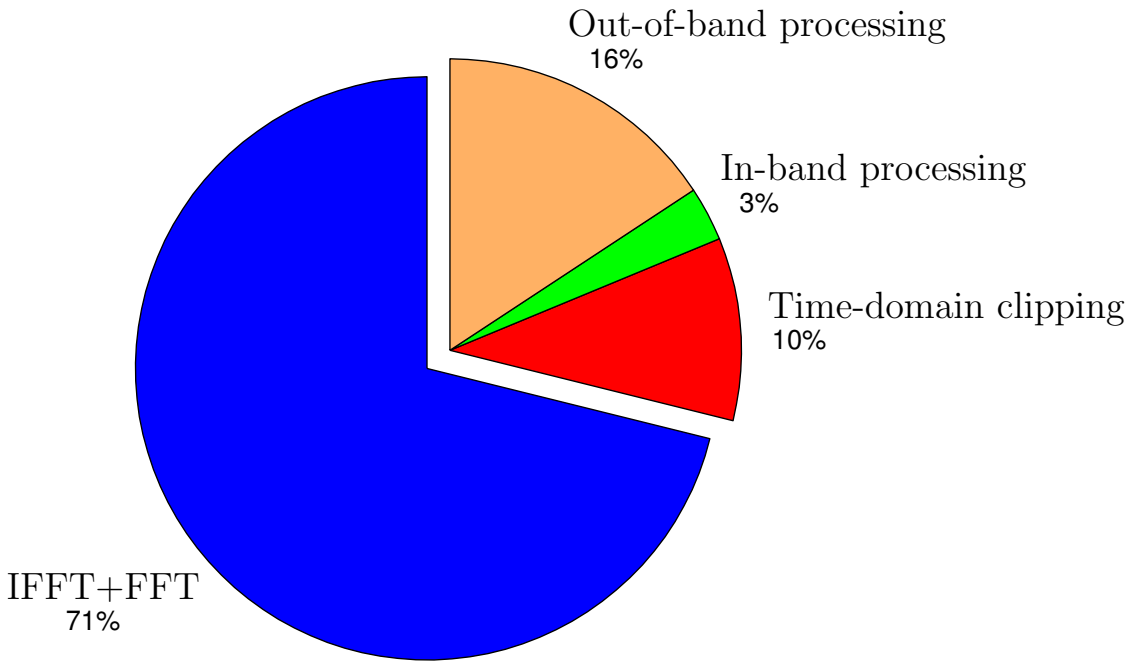

Figure 5.9: Relative computational complexity of constrained clipping, including IFFT+FFT, time-domain clipping, in-band processing and out-of-band processing, $N = 2048$.

the constellation points with a scale factor c to achieve equal average power; for example, $c = 1/\sqrt{2}$ for QPSK, $c = 1/\sqrt{10}$ for 16QAM and $c = 1/\sqrt{42}$ for 64QAM [4]. For the normalized constellations, $S_{max} = 1$ for BPSK and QPSK, $S_{max} = \sqrt{18/10}$ for 16QAM and $S_{max} = \sqrt{98/42}$ for 64QAM. See Fig. 5.10.

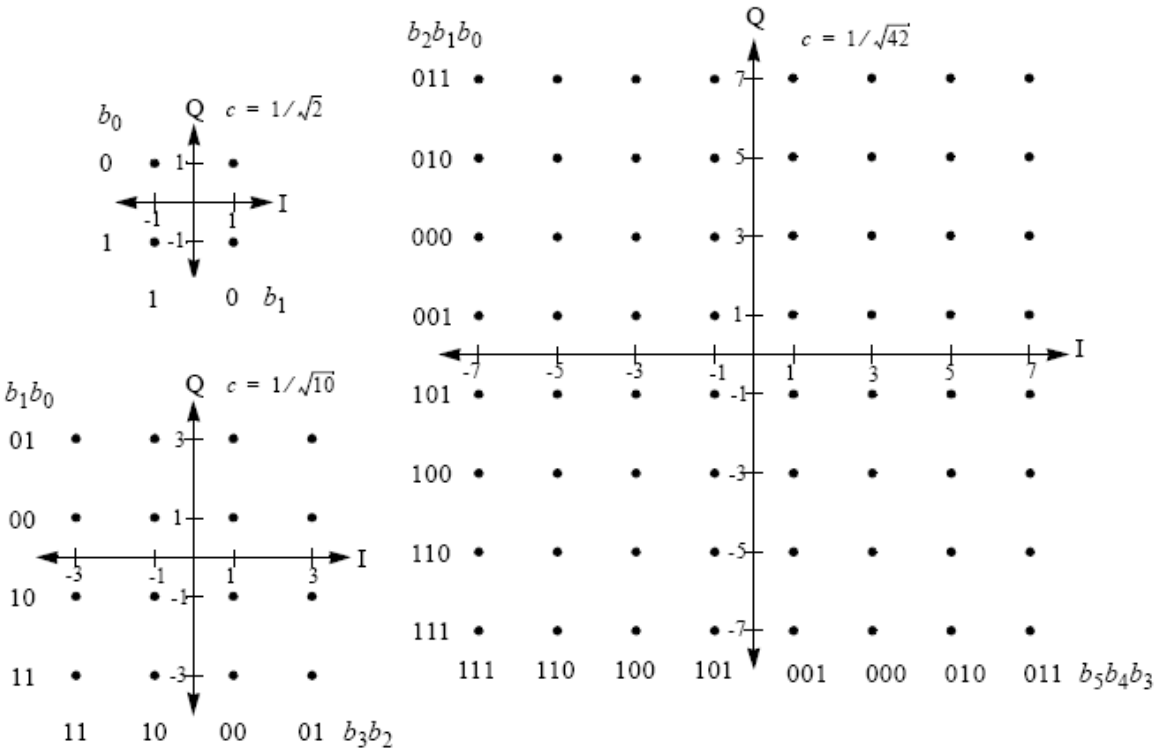

Figure 5.10: Normalized constellations of QPSK, 16QAM and 64QAM supported in WiMAX system [4].

We can divide the data subcarriers into several groups according to the chosen modulation schemes and calculate the corresponding EVMs. Let EVM_{BPSK}, EVM_{QPSK}, $\text{EVM}_{\text{16QAM}}$ and $\text{EVM}_{\text{64QAM}}$ denote the calculated EVM values for the respective constellation. For example, if only QPSK and 64QAM are used, we have

$$\text{EVM}_{\text{QPSK}} = \sqrt{\frac{1}{|\mathcal{N}_{\text{QPSK}}|} \sum_{k \in \mathcal{N}_{\text{QPSK}}} |D_k|^2}, \tag{5.17}$$

and

$$\text{EVM}_{\text{64QAM}} = \sqrt{\frac{42}{98}} \sqrt{\frac{1}{|\mathcal{N}_{\text{64QAM}}|} \sum_{k \in \mathcal{N}_{\text{64QAM}}} |D_k|^2}, \tag{5.18}$$

where $\mathcal{N}_{\text{QPSK}}$ is the set of sub-carrier indices with the normalized QPSK constellation and $\mathcal{N}_{\text{64QAM}}$ is the set of subcarrier indices for the 64QAM constellation, $|\cdot|$ denotes the

cardinality of the set and

$$|\mathcal{N}_{\text{QPSK}}| + |\mathcal{N}_{\text{64QAM}}| = N.$$

The calculated EVM values are compared with the maximum permissible EVM values specified in the standard. We will first compare EVM_{BPSK} to the threshold Th_{BPSK} if BPSK is adopted by some users. If $\text{EVM}_{\text{BPSK}} > Th_{\text{BPSK}}$, in-band processing is employed to make $\text{EVM}_{\text{BPSK}} \leq Th_{\text{BPSK}}$. Similar procedures will be used for QPSK, 16QAM, 64QAM if they are used by some other users.

5.4.2 Performance Results in Multiple-User Environment

Adaptive modulation and coding (AMC) sub-carrier allocation scheme [4] is applied[2], by assuming that there are four users in one symbol and every user occupies 8 sub-channels; the user's modulation was BPSK, QPSK, 16QAM and 64QAM, respectively, for user 1 through 4.

CFR results of different clipping ratios, $\Omega = A_{max}\sqrt{2}/\sigma$ (over-sampling rate $L = 4$), are examined to choose the optimal one for the respective PAR goals. The result is shown in Table 5.2. We can see that Ωs between 4.0dB and 4.8dB all achieved similar PAR reduction results. $\Omega = 4.2$dB is chosen as the optimal clipping ratio for 6-7dB PAR goals at the 10^{-3} CCDF level.

Table 5.2: PARs at the 10^{-3} CCDF level for various Ω's.

Ω (dB)	3.6	3.8	4.0	4.2	4.4	4.8	5.2
PAR (dB)	6.95	6.90	6.81	6.79	6.82	6.84	6.91

Here, CFR capability using the optimal clipping ratio for the multiple-user case is shown. Armstrong's method with $\Omega = 4.2$dB was also included for comparison. In Fig. 5.11, constrained clipping outperformed Armstrong's method by about 0.6dB at the 10^{-3} CCDF level and achieved more than 5dB of PAR reduction at the 10^{-3} CCDF level relative to the original OFDM signal.

[2]The total number of sub-carriers is $N = 2048$, consisting of 48 data sub-carriers per sub-channel $\times$ 32 sub-channels, 192 pilot sub-carriers, 319 null sub-carriers at the band edges, and 1 null sub-carrier at the DC.

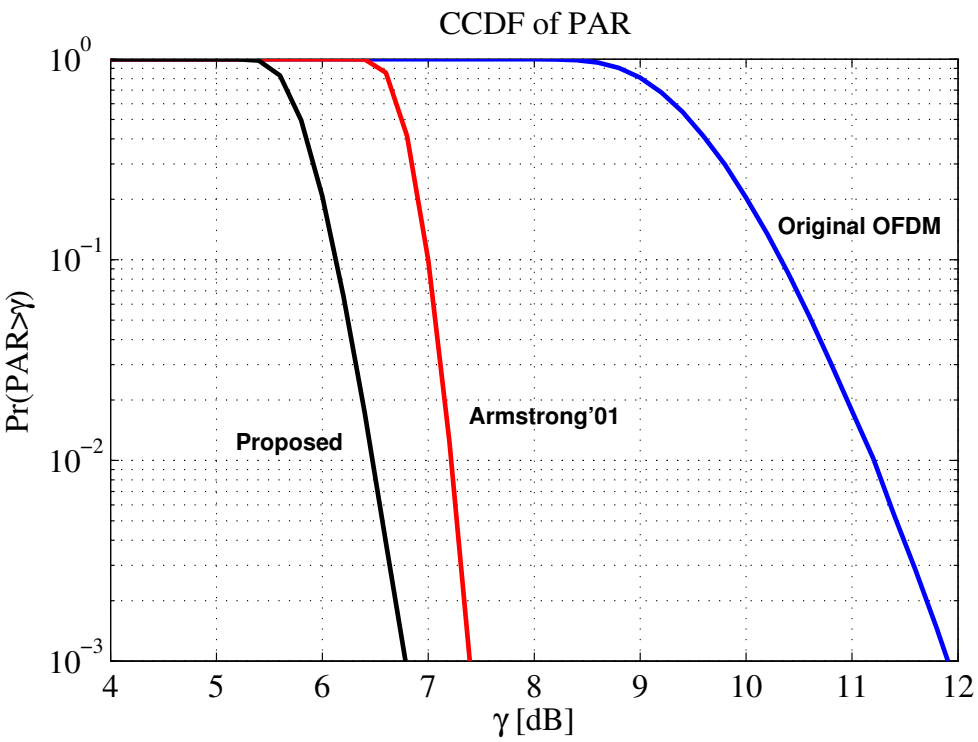

Figure 5.11: Comparison between Armstrong's method and constrained clipping, $N = 2048$ and four-user case.

By using the normalized constellations, the different modulations all have unit average power. Afterwards, we perform spectral clipping to deal with the out-of-band radiation by applying (5.9). Shown in Fig. 5.12 is the power spectral density (PSD) with the constrained clipping method. Also shown are PSDs of the spectral mask, Armstrong's method and the simple clipping method. It is clear that the spectrum of constrained clipping closely follows the spectral mask where simple clipping violates it. Also, we observe from Fig. 5.12 that Armstrong's method is far below the spectral mask by a considerable margin. In contrast, constrained clipping mitigates the out-of-band signal energy to ensure tight spectral compliance without unnecessary use of energy.

Figure 5.13 is a plot of the probability that an OFDM symbol processed by Armstrong's method will exceed the allowed EVM threshold for three different modulations. These curves also represent the probability that constrained clipping will perform in-band processing (i.e. p_i in the in-band processing). By utilizing the proposed constrained clipping algorithm, we can guarantee that EVM requirements for all the modulation schemes can be always met.

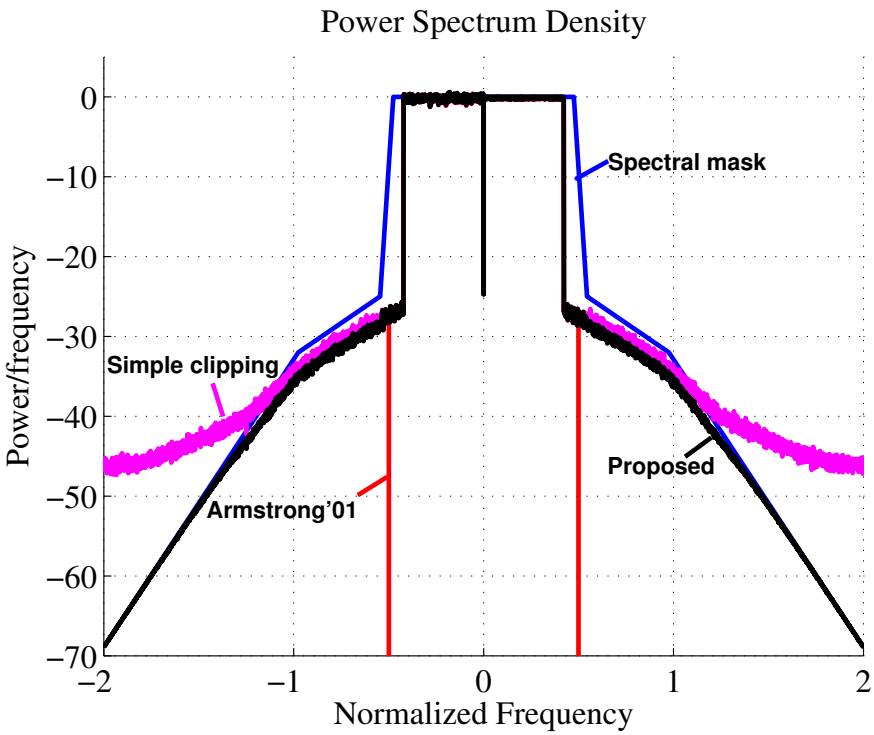

Figure 5.12: PSD plot for four-user case, $N = 2048$ and $\Omega = 4.2$ dB.

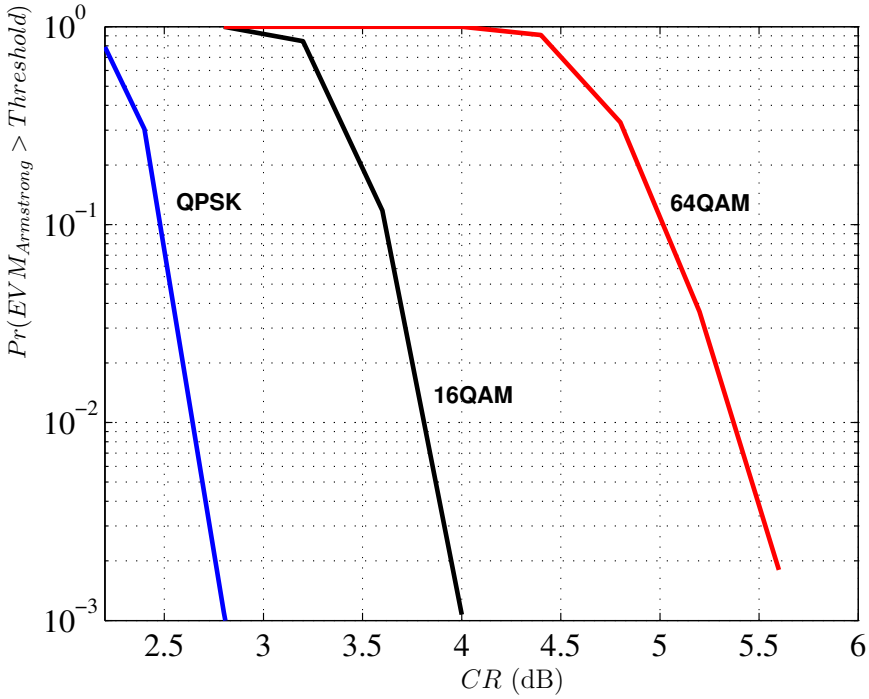

Figure 5.13: Probabilities that Armstrong's method violates the EVM thresholds for different modulation schemes. $Th_{\text{QPSK}} = 12\%$, $Th_{\text{16QAM}} = 6\%$ and $Th_{\text{64QAM}} = 3\%$ [4].

5.5 Conclusions

In this chapter, we proposed constrained clipping, a distortion-based CFR method that is designed to drastically reduce the PAR while satisfying any given EVM and spectral mask constraints. Constrained clipping accomplishes these guarantees by using separate operations for the in-band and out-of-band portions of the signal. With the in-band processing algorithm, the largest error vectors are modified to achieve the desired EVM. In the out-of band processing algorithm, spectral clipping is implemented where the out-of-band signal frequencies that contain more energy than is allowed by the mask are "clipped" down to the mask level. Through extensive simulations we have shown that even for tight EVM and spectral constraints, PAR reductions of some 4.5 dB can be achieved for an OFDM signal with 256 sub-carriers. The distinct advantage of constrained clipping is that all processing is done on the transmitter-side, so no receiver-side modification is necessary.

Computational complexities of various components in constrained clipping was analyzed in terms of the number of instructions for additions and multiplications. From the analysis, constrained clipping is only roughly three times as complex as simple OFDM and only 25% more complex than Armstrong's method. The results demonstrate that constrained clipping, with only small complexity increases, can achieve large CFR and satisfy EVM and spectrum regrowth requirements.

Finally, we demonstrated that constrained clipping can yield excellent CFR results in the multiple-user OFDM environment such as WiMAX. More than 5dB of PAR reduction was achieved at the 10^{-3} CCDF level compared to the original OFDM signal. The EVM and spectrum of the transmitted signals processed by constrained clipping are guaranteed to meet the requirements in the standards.

CHAPTER VI

SNDR ANALYSIS FOR TRANSCEIVER NONLINEARITIES IN AWGN CHANNELS

6.1 Introduction

In broadband high-speed communication systems, the power efficiency and the spectrum efficiency are two key considerations; however, nonlinear devices in the transceiver link usually lead to large signal backoff and spectrum broadening, greatly deteriorating the link performance. Some nonlinearities are inherent, including the nonlinear region of the power amplifier [59], the multiplication in the mixer [59], and the quantization and clipping noise of the DAC [24]. Nonlinearity can also be introduced deliberately, for example, nonlinear system compensation [28,87], distortion-based CFR techniques [14,41,43,65,67,90,91], and baseband nonlinear transformation under the peak-power constraint [73].

The objective of this chapter is three-fold: first, the transceiver SNDR is studied, including the transmitter nonlinearity, the AWGN and the receiver nonlinearity. When transceiver nonlinearities can be expressed or approximated by complex baseband polynomial functions, the closed-form SNDR expression is derived for a complex Gaussian input. Second, when the transmitter nonlinearity is known, we can derive the corresponding nonlinearity at the receiver to maximize the SNDR. Finally, we aim to compare clipping and companding CFR techniques from the following two aspects: (i) we prove that the inverse function pair can only maximize the SNDR when the channel noise power is zero. Therefore, when the SNR is not infinite, the inverse function pair *cannot* yield the best performance in terms of the SNDR. (ii) SNDR values are calculated for typical clipping and companding algorithms, respectively, based on the closed-form expression and the polynomial approximations. From the above analysis, we can claim that companding PAR reduction algorithms which are based on transceiver inverse function pairs are not SNDR-optimal.

The outline of this chapter is as follows: in Section 6.2, the system model with transceiver nonlinearities is presented. Based on this setup, we propose a suitable SNDR definition for the performance evaluation purpose. When the input signal is complex Gaussian distributed, the closed-form SNDR expression is derived in Section 6.3. Three special cases are presented to illustrate calculations of the SNDR under different system configurations. Section 6.4 shows that given the nonlinear function at the transmitter, we can obtain the appropriate function at the receiver to maximize the system SNDR. Moreover, this SNDR-optimizing function may not be the inverse of the transmitter nonlinearity as shown in Section 6.5. Also included in this section is the SNDR performance comparison between clipping and companding. Finally, conclusions are drawn in Section 6.6.

6.2 System Setup and SNDR for Transceiver Nonlinearities

A baseband transceiver model is shown in Fig. 6.1, where $g(\cdot)$ and $s(\cdot)$ represent memoryless nonlinear functions at the transmitter and at the receiver, respectively. x is the complex input to the transmitter nonlinearity with zero mean and variance σ_x^2, and $y = g(x)$ is the transmitter output. Denote by v the additive white Gaussian noise, which has zero mean and variance σ_v^2. The signal arriving at the receiver $w = y + v$ experiences another nonlinearity $s(\cdot)$ to yield $z = s(w)$ for further processing.

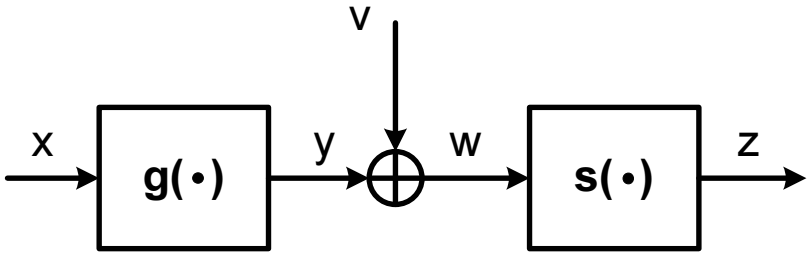

Figure 6.1: An AWGN channel with transmitter nonlinearity $g(\cdot)$ and receiver nonlinearity $s(\cdot)$.

In general, $g(\cdot)$ and $s(\cdot)$ can be two unrelated nonlinear functions (including linear functions as special cases). In companding applications [41,43,90,91], $s(\cdot)$ is usually chosen as the inverse function of $g(\cdot)$, i.e., $s(\cdot) = g^{-1}(\cdot)$.

For the transceiver setup in Fig. 6.1, we again use the Bussgang Theorem to obtain

$$\text{SNDR} = \frac{|E[x^* z]|^2}{\sigma_x^2 E[|z|^2] - |E[x^* z]|^2}, \tag{6.1}$$

where $z = s(y+v) = s\left(g(x)+v\right)$. To compute (6.1), it is necessary to calculate $E[x^* z]$ and $E[|z|^2]$. Since random variables x and v both appear as arguments of the nonlinear mapping $s(\cdot)$, the expectations need to be taken over v and x and the joint PDF $f_{x,v}(x,v)$ must be known. Thus,

$$E[x^* z] = \int_{\mathcal{R}(x,v)} s\left(g(x)+v\right) x^* f_{x,v}(x,v)\ dx\ dv, \tag{6.2}$$

$$E[|z|^2] = \int_{\mathcal{R}(x,v)} |s\left(g(x)+v\right)|^2 f_{x,v}(x,v)\ dx\ dv, \tag{6.3}$$

which is straightforward to calculate numerically for any pair of functions $g(\cdot)$ and $s(\cdot)$.

When the receiver is linear, i.e., when $s(w) = w$,

$$E[x^* z] = E[x^*(y+v)] = E[x^* y], \tag{6.4}$$

$$E[|z|^2] = E[|y+v|^2] = E[|y|^2] + \sigma_v^2. \tag{6.5}$$

Substituting (6.4) and (6.5) into (6.1), the SNDR expression in (2.23) follows.

6.3 Closed-Form SNDR Expression

From this point on, we assume that Fig. 6.1 represents a baseband communication system. If $g(\cdot)$ and $s(\cdot)$ can be modeled by polynomials, we follow the convention of [102] and write

$$g(x) = \sum_{k=0}^{K_g} a_{2k+1} x^{k+1} \left(x^*\right)^k, \tag{6.6}$$

$$s(w) = \sum_{k=0}^{K_s} b_{2k+1} w^{k+1} \left(w^*\right)^k, \tag{6.7}$$

where $a_1, a_3, a_5, ..., a_{2K_g+1}$ are the coefficients that dictate the characteristic of the transmitter nonlinearity $g(\cdot)$ and $b_1, b_3, b_5, ..., b_{2K_s+1}$ describe the receiver nonlinearity $s(\cdot)$. By using curve fitting techniques, these coefficients can be extracted from physical measurements of the device (such as AM-AM and AM-PM measurements of a power amplifier [101]). When v and x are both complex Gaussian distributed; i.e., $v \sim \mathcal{CN}(0, \sigma_v^2)$ and $x \sim \mathcal{CN}(0, \sigma_x^2)$

(such as when x is Nyquist-sampled time-domain OFDM signal), closed-form analysis of the SNDR is feasible since $E[x^*z]$ and $E[|z|^2]$ will be a linear combination of the moments of x and v. By using the complex Gaussian moment Theorem, the moments of a complex Gaussian random variable can be expressed as [76]

$$E[x^k(x^*)^p] = \begin{cases} k!\ \sigma_x^{2k}, & k = p \\ 0, & k \neq p \end{cases}. \tag{6.8}$$

Hence, determining the transceiver SNDR when the polynomial coefficients of $g(\cdot)$ and $s(\cdot)$ are known is simply a matter of expressing $E[x^*z]$ and $E[|z|^2]$ in terms of the moments of x and v.

6.3.1 Closed-Form $E[x^*z]$ and $E[|z|^2]$

The process z in Fig. 6.1 can be expressed as

$$\begin{aligned} z &= s(g(x)+v) = \sum_{k=0}^{K_s} b_{2k+1}\left(g(x)+v\right)^{k+1}\left(g^*(x)+v^*\right)^k \\ &= \sum_{k=0}^{K_s} b_{2k+1} \sum_{l=0}^{k+1} \binom{k+1}{l} g(x)^{k+1-l} v^l \sum_{m=0}^{k} \binom{k}{m} g^*(x)^{k-m}(v^*)^m \\ &= \sum_{k=0}^{K_s} b_{2k+1} \sum_{l=0}^{k+1}\sum_{m=0}^{k} \binom{k+1}{l}\binom{k}{m} g(x)^{k+1-l} g^*(x)^{k-m} v^l (v^*)^m. \end{aligned} \tag{6.9}$$

To simplify the $E[x^*z]$ expression, we first realize that $E[v^l(v^*)^m] \neq 0$ only if $l = m$ (c.f. (6.8)), as a result, the double summation $\sum_{l=0}^{k+1}\sum_{m=0}^{k}$ in the $E[x^*z]$ expression can be reduced into a single summation $\sum_{l=0}^{k}$ and set $m = l$. Consequently,

$$\begin{aligned} E[x^*z] &= \sum_{k=0}^{K_s} b_{2k+1} P_{2k+1} \\ &= \sum_{k=0}^{K_s} b_{2k+1} \sum_{l=0}^{k} \binom{k+1}{l}\binom{k}{l} E\left[x^* g(x)^{k-l+1} g^*(x)^{k-l}\right]\ l!\ \sigma_v^{2l}. \end{aligned} \tag{6.10}$$

It is straightforward that

$$E[x^* g(x)^{t+l} g^*(x)^t] = E\left[x^* \left(\sum_{n=0}^{K_g} a_{2n+1} x^{n+1} (x^*)^n\right)^{t+1} \left(\sum_{n=0}^{K_g} a^*_{2n+1} (x^*)^{n+1} x^n\right)^t\right]$$

$$= \sum_{n_1=0}^{K_g} \cdots \sum_{n_{2t+1}=0}^{K_g} a_{2n_1+1} \cdots a_{2n_{t+1}+1} a^*_{2n_{t+2}+1} \cdots a^*_{2n_{2t+1}+1} E\left[x^{t+1+\sum_{i=1}^{2t+1} n_i} (x^*)^{t+1+\sum_{i=1}^{2t+1} n_i}\right]$$

$$= \sum_{n_1=0}^{K_g} \cdots \sum_{n_{2t+1}=0}^{K_g} a_{2n_1+1} \cdots a_{2n_{t+1}+1} a^*_{2n_{t+2}+1} \cdots a^*_{2n_{2t+1}+1} \left(t+1+\sum_{i=1}^{2t+1} n_i\right)! \sigma_x^{2(t+1+\sum_{i=1}^{2t+1} n_i)}$$

$$= \sum_{n_1=0}^{K_g} \cdots \sum_{n_{2t+1}=0}^{K_g} \left(t+1+\sum_{i=1}^{2t+1} n_i\right)! \ \sigma_x^{2(t+1)} \prod_{i=1}^{t+1} a_{2n_i+1} \sigma_x^{2n_i} \prod_{j=t+2}^{2t+1} a^*_{2n_j+1} \sigma_x^{2n_j}, \tag{6.11}$$

where $t = k-l$. Substituting (6.11) into (6.10), we obtain the closed-form $E[x^* z]$ expression.

Using (6.8) and (6.9), we can calculate the system output power

$$\begin{aligned} E[|z|^2] &= \sum_{k_1=0}^{K_s} \sum_{k_2=0}^{K_s} b^*_{2k_1+1} b_{2k_2+1} Q_{2k_1+1,2k_2+1} \\ &= \sum_{k_1=0}^{K_s} \sum_{k_2=0}^{K_s} b_{2k_1+1} b^*_{2k_2+1} \sum_{l_1=0}^{k_1+1} \sum_{m_1=0}^{k_1} \sum_{l_2=0}^{k_2+1} \sum_{m_2=0}^{k_2} \binom{k_1+1}{l_1} \binom{k_1}{m_1} \binom{k_2+1}{l_2} \binom{k_2}{m_2} \\ &\quad E\left[g^*(x)^{k_1+k_2+1-m_1-l_2} g(x)^{k_1+k_2+1-m_2-l_1}\right] E\left[(v^*)^{l_2+m_1} v^{l_1+m_2}\right] \\ &= \sum_{k_1=0}^{K_s} \sum_{k_2=0}^{K_s} b_{2k_1+1} b^*_{2k_2+1} \sum_{l_1=0}^{k_1+1} \sum_{m_2=0}^{k_2} \binom{k_1+1}{l_1} \binom{k_2}{m_2} \binom{k_1+k_2+1}{l_1+m_2} \\ &\quad E\left[g^*(x)^{k_1+k_2+1-m_2-l_1} g(x)^{k_1+k_2+1-m_2-l_1}\right] (l_1+m_2)! \sigma_v^{2(l_1+m_2)}. \end{aligned} \tag{6.12}$$

Then, the closed-form $E[|z|^2]$ can be obtained from

$$E[g(x)^t g^*(x)^t] = E\left[\left(\sum_{n=0}^{K_g} a_{2n+1} x^{n+1} (x^*)^n\right)^t \left(\sum_{n=0}^{K_g} a^*_{2n+1} (x^*)^{n+1} x^n\right)^t\right]$$

$$= \sum_{n_1=0}^{K_g} \cdots \sum_{n_{2t}=0}^{K_g} a_{2n_1+1} \cdots a_{2n_t+1} a^*_{2n_{t+1}+1} \cdots a^*_{2n_{2t}+1} E\left[x^{t+\sum_{i=1}^{2t} n_i} (x^*)^{t+\sum_{i=1}^{2t} n_i}\right]$$

$$= \sum_{n_1=0}^{K_g} \cdots \sum_{n_{2t}=0}^{K_g} a_{2n_1+1} \cdots a_{2n_t+1} a^*_{2n_{t+1}+1} \cdots a^*_{2n_{2t}+1} \left(t+\sum_{i=1}^{2t} n_i\right)! \sigma_x^{2(t+\sum_{i=1}^{2t} n_i)}$$

$$= \sum_{n_1=0}^{K_g} \cdots \sum_{n_{2t+1}=0}^{K_g} \left(t+\sum_{i=1}^{2t} n_i\right)! \ \sigma_x^{2t} \prod_{i=1}^{t} a_{2n_i+1} \sigma_x^{2n_i} \prod_{j=t+1}^{2t} a^*_{2n_j+1} \sigma_x^{2n_j}, \tag{6.13}$$

where $t = k_1 + k_2 + 1 - m_2 - l_1$.

Substituting (6.10) and (6.12) into (6.1), the closed-form SNDR is expressed in terms of the transceiver nonlinear polynomial coefficients, the signal power σ_x^2 and the noise power σ_v^2.

Next, three special cases are given to demonstrate the calculation of the SNDR. We will investigate (i) the linear transmitter nonlinear receiver case, (ii) the nonlinear transmitter linear receiver case, and (iii) the nonlinear transmitter and nonlinear receiver case. For cases (i) and (iii), we are also interested in finding the optimal receiver nonlinearity to maximize the SNDR when the transmitter nonlinearity is known.

6.3.2 Special Case 1: Linear Transmitter Nonlinear Receiver

When the transmitter is linear, we set $K_g = 0$ in (6.6), i.e., $g(x) = a_1 x$. Hence, the process z in Fig. 6.1 can be expressed as

$$\begin{aligned} z &= s(g(x)+v) = \sum_{k=0}^{K_s} b_{2k+1} \left(a_1 x + v\right)^{k+1} \left(a_1^* x^* + v^*\right)^k \\ &= \sum_{k=0}^{K_s} b_{2k+1} \sum_{l=0}^{k+1} \left(\begin{array}{c} k+1 \\ l \end{array} \right) (a_1 x)^{k+1-l} v^l \sum_{m=0}^{k} \left(\begin{array}{c} k \\ m \end{array} \right) (a_1^* x^*)^{k-m} (v^*)^m. \end{aligned} \quad (6.14)$$

$E[x^* z]$ can be simplified by calculating the moments of the noise v first and reducing the double summation to the single summation. After that,

$$E[x^* z] = \sum_{k=0}^{K_s} b_{2k+1} \sum_{l=0}^{k} \left(\begin{array}{c} k+1 \\ l \end{array} \right) \left(\begin{array}{c} k \\ l \end{array} \right) E\left[x^* (a_1 x)^{k+1-l} (a_1^* x^*)^{k-l} \right] \; l! \; \sigma_v^{2l}. \quad (6.15)$$

Next, we recognize that $E[x^{k+1-l}(x^*)^{k+1-l}] = (k+1-l)! \sigma_x^{2(k+1-l)}$ and simplify $E[x^* z]$ to

$$E[x^* z] = a_1 \sigma_x^2 \sum_{k=0}^{K_s} b_{2k+1} (k+1)! \; \gamma^k, \quad (6.16)$$

where $\gamma = |a_1|^2 \sigma_x^2 + \sigma_v^2$.

To find $E[|z|^2]$, we first realize that $u = a_1 x + v$ is another complex Gaussian r.v. with $E[|u|^2] = |a_1|^2 \sigma_x^2 + \sigma_v^2 = \gamma$. Again utilizing (6.8), we find

$$E[|z|^2] = \sum_{k_1=0}^{K_s} \sum_{k_2=0}^{K_s} b_{2k_1+1}^* b_{2k_2+1} K! \; \gamma^K, \quad (6.17)$$

where $K = k_1 + k_2 + 1$. We can verify the result by setting $K_g = 0$ in the closed-form expression of $E[x^*z]$ and $E[|z|^2]$ in (6.10) and (6.12), respectively.

Substituting (6.16) and (6.17) into (6.1), we can obtain the closed-form SNDR expression

$$\text{SNDR} = \frac{|a_1|^2\sigma_x^2 \sum_{k_1=0}^{K_s}\sum_{k_2=0}^{K_s} b_{2k_1+1}^* b_{2k_2+1} S(k_1,k_2)}{\sum_{k_1=0}^{K_s}\sum_{k_2=0}^{K_s} b_{2k_1+1}^* b_{2k_2+1} T(k_1,k_2)}, \tag{6.18}$$

where

$$S(k_1,k_2) = (k_1+1)!(k_2+1)!\ \gamma^{K-1},$$

and

$$T(k_1,k_2) = \gamma^{K-1}[K!\ \gamma - (k_1+1)!(k_2+1)!\ |a_1|^2\sigma_x^2].$$

For this linear transmitter nonlinear receiver case, we are interested in finding coefficients of $s(\cdot)$ that maximize the SNDR. These optimum b_{2k+1} can be found by setting the partial derivatives of SNDR with respect to b_{2k+1}^* to zero [18]. This allows us to write for example,

$$\frac{\partial |E[x^*z]|^2}{\partial b_{2\tilde{k}+1}^*} E[|z|^2] = \frac{\partial E[|z|^2]}{\partial b_{2\tilde{k}+1}^*} |E[x^*z]|^2, \tag{6.19}$$

where $\tilde{k}$ is a nonnegative integer.

From (6.16) and (6.17), we can calculate

$$\frac{\partial |E[x^*z]|^2}{\partial b_{2\tilde{k}+1}^*} = E[x^*z] a_1^* \sigma_x^2 (\tilde{k}+1)!\ \gamma^{\tilde{k}}, \tag{6.20}$$

and

$$\frac{\partial E[|z|^2]}{\partial b_{2\tilde{k}+1}^*} = \sum_{k_2=0}^{K_s} b_{2k_2+1} (\tilde{k}+k_2+1)!\ \gamma^{\tilde{k}+k_2+1}. \tag{6.21}$$

By substituting (6.20) and (6.21) into (6.19) and assuming $E[x^*z] \neq 0$ [1], we simplify (6.19) to

$$\sum_{k_1=0}^{K_s}\sum_{k_2=0}^{K_s} b_{2k_1+1}^* b_{2k_2+1} (\tilde{k}+k_2+1)!(k_1+1)!\ \gamma^K = \sum_{k_1=0}^{K_s}\sum_{k_2=0}^{K_s} b_{2k_1+1}^* b_{2k_2+1} K!(\tilde{k}+1)!\ \gamma^K. \tag{6.22}$$

The condition to make (6.22) valid is $b_{2k+1} = 0, \forall k \neq \tilde{k}$. Therefore, the possible solutions are $(b_1, 0, 0, \cdots, 0)$, $(0, b_3, 0, \cdots, 0)$, $\cdots$, $(0, 0, \cdots, 0, b_{2K_s+1})$. We substitute these solutions into (6.18) and find that $(b_1, 0, 0, \cdots, 0)$ is the set of coefficients maximizing the SNDR. This

[1] When $E[x^*z] = 0$, SNDR is also zero, which minimizes the SNDR value. Because our objective is to maximize the SNDR, we set $E[x^*z] \neq 0$.

result is quite intuitive, because a linear function at the receiver is intrinsic to be easier to maximize the SNDR when the transmitter is already linear. The maximum SNDR is

$$\text{SNDR}_0 = \frac{\gamma - \sigma_v^2}{\sigma_v^2} = \frac{|a_1|^2\sigma_x^2}{\sigma_v^2}. \tag{6.23}$$

We will obtain the same result by using a different method shown in Section 6.4.

For illustration purposes, let us consider a simple pair of transformations

$$g(x) = a_1 x, \tag{6.24}$$

$$s(w) = b_1 w + b_3 w^2 w^*. \tag{6.25}$$

Assuming that $v \sim \mathcal{CN}(0, \sigma_v^2)$, $x \sim \mathcal{CN}(0, \sigma_x^2)$, the SNDR expression in (6.18) can be shown to simplify to

$$\text{SNDR} = \frac{|a_1|^2\sigma_x^2|b_1 + 2b_3\gamma|^2}{|b_1|^2\sigma_v^2 + 2(b_1^* b_3 + b_1 b_3^*)\sigma_v^2\gamma + 2|b_3|^2\gamma^2(\gamma + 2\sigma_v^2)}. \tag{6.26}$$

Fig. 6.2 is a plot of the SNDR versus b_3, where we assume all the polynomial coefficients are real-valued for simplicity. It is clear that the SNDR is maximized at $b_3 = 0$ (corresponding to a linear receiver) for different b_1 values.

The one-to-one relationship between BER and SNDR is shown in Fig. 6.3 when $b_1 = 1$ is set. The solid SNDR curve is obtained from (6.26) and the theoretical BER for the BPSK modulation can be written as [72]

$$\text{BER} = Q\left(\sqrt{\text{SNDR}}\right), \tag{6.27}$$

where $Q(\cdot)$ is the CCDF of the standard Gaussian distribution. From Fig. 6.3, the minimum BER is obtained at the maximum SNDR when $b_3 = 0$. For some b_3 values, the SNDR values are pretty low and the corresponding BERs reach around 0.5.

The dashed curve in Fig. 6.3 denotes the simulated BER performance when an OFDM system is used with $N = 2048$ and the BPSK modulation. When b_3 is negative, the simulation result is close to the theoretical BER value yielded from (6.27); however, the difference is large for the positive b_3. For $b_1 = 1$, the negative b_3 corresponds to a compressing function and on the other hand, the positive b_3 denotes an expanding function at the receiver.

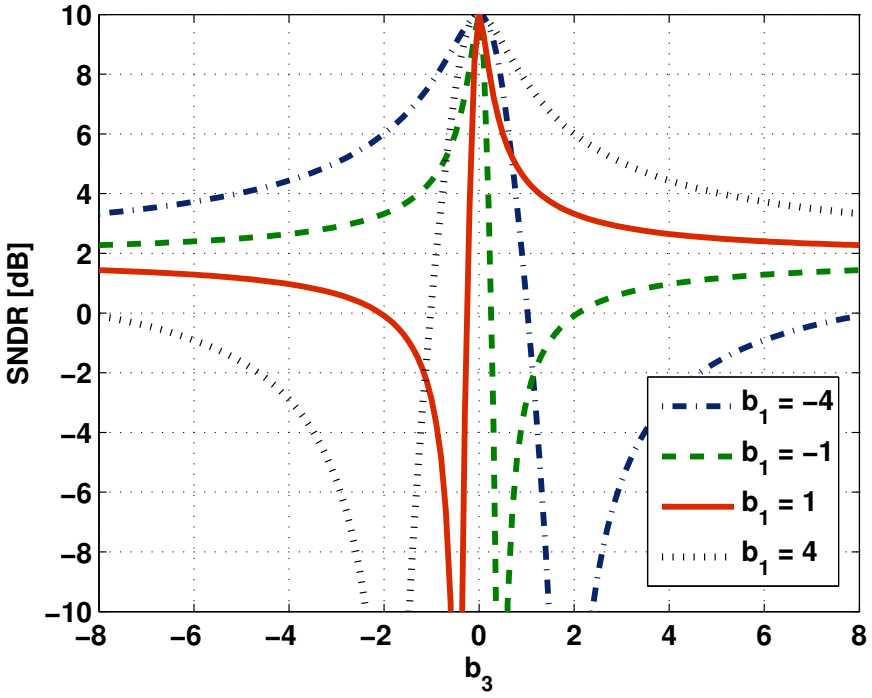

Figure 6.2: SNDR vs. b_3 using equations (6.26). For all lines, $\sigma_x^2/\sigma_v^2 = 10\text{dB}$, $a_1 = 1$, and $\sigma_x^2 = 1$.

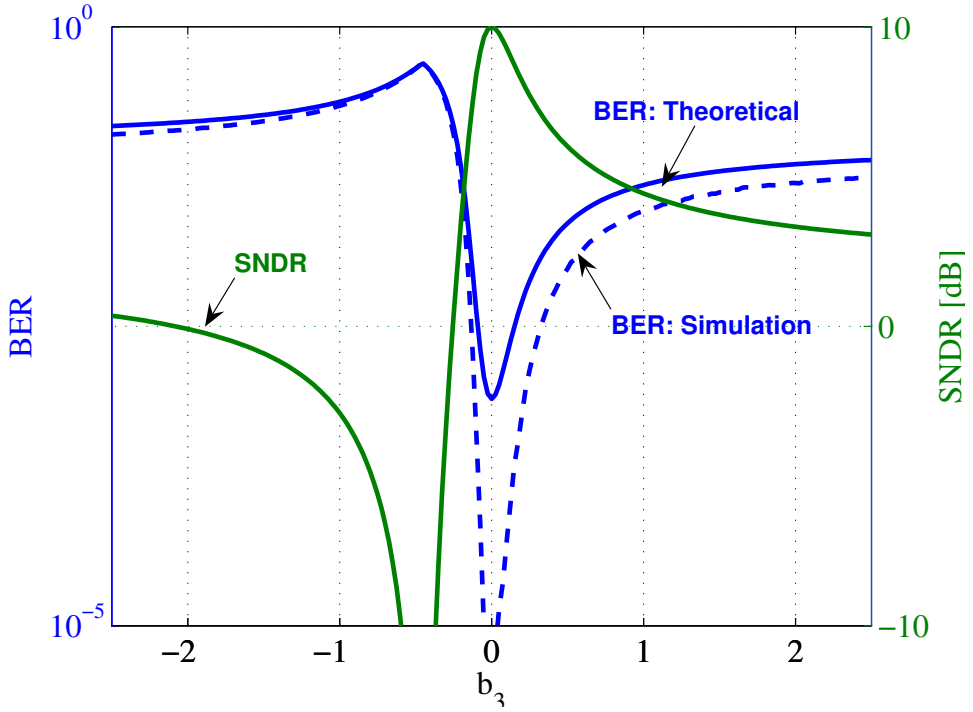

Figure 6.3: Corresponding relationship between BER and SNDR. For all lines, $\sigma_x^2/\sigma_v^2 = 10\text{dB}$, $a_1 = 1$, $b_1 = 1$ and $\sigma_x^2 = 1$.

Because the noise will also be modified by the receiver nonlinearity, (6.27) is not accurate and the derivation is more obvious when the noise is amplified by the expanding receiver nonlinearity. However, we can still use (6.27) since the changing trends of the theoretical and simulated BER curves are very similar. The simulated SNDR curve almost coincides (6.26); hence, we omit it from Fig. 6.3.

6.3.3 Special Case 2: Nonlinear Transmitter Linear Receiver

By setting $K_s = 0$ in (6.7), the receiver is linear, i.e., $s(w) = b_1 w$. So the output process in Fig. 6.1 is

$$z = s(g(x) + v) = b_1 \left(\sum_{k=0}^{K_g} a_{2k+1} x^{k+1} (x^*)^k + v \right). \tag{6.28}$$

By utilizing (6.8), we have

$$E[x^* z] = b_1 \sum_{k=0}^{K_g} a_{2k+1} (k+1)! \sigma_x^{2(k+1)}, \tag{6.29}$$

and

$$E[|z|^2] = |b_1|^2 \left(\sum_{k_1=0}^{K_g} \sum_{k_2=0}^{K_g} a_{2k_1+1}^* a_{2k_2+1} K! \sigma_x^{2K} + \sigma_v^2 \right). \tag{6.30}$$

Substituting (6.29) and (6.30) into (6.1), the closed-form SNDR expression for the nonlinear transmitter linear receiver case can be written as

$$\text{SNDR} = \frac{\sum_{k_1=0}^{K_g} \sum_{k_2=0}^{K_g} a_{2k_1+1}^* a_{2k_2+1} (k_1+1)!(k_2+1)! \sigma_x^{2K}}{\sum_{k_1=0}^{K_g} \sum_{k_2=0}^{K_g} a_{2k_1+1}^* a_{2k_2+1} [K! - (k_1+1)!(k_2+1)!] \sigma_x^{2K} + \sigma_v^2}. \tag{6.31}$$

When the transmitter nonlinearity is cubic, i.e.,

$$g(x) = a_1 x + a_3 x^2 x^*, \tag{6.32}$$

$$s(w) = b_1 w, \tag{6.33}$$

the SNDR expression in (6.31) becomes

$$\text{SNDR} = \frac{\sigma_x^2 |a_1 + 2a_3 \sigma_x^2|^2}{\sigma_v^2 + 2|a_3|^2 \sigma_x^6}. \tag{6.34}$$

Fig. 6.4 is a plot of the SNDR versus a_3, which is assumed to be real-valued for simplicity. Interestingly, the SNDR can exceed the SNR $= \sigma_x^2/\sigma_v^2$ by as much as 0.79 dB when some nonlinear distortion is used. The optimizing a_3 is σ_v^2/σ_x^4, and the corresponding α in (2.20)

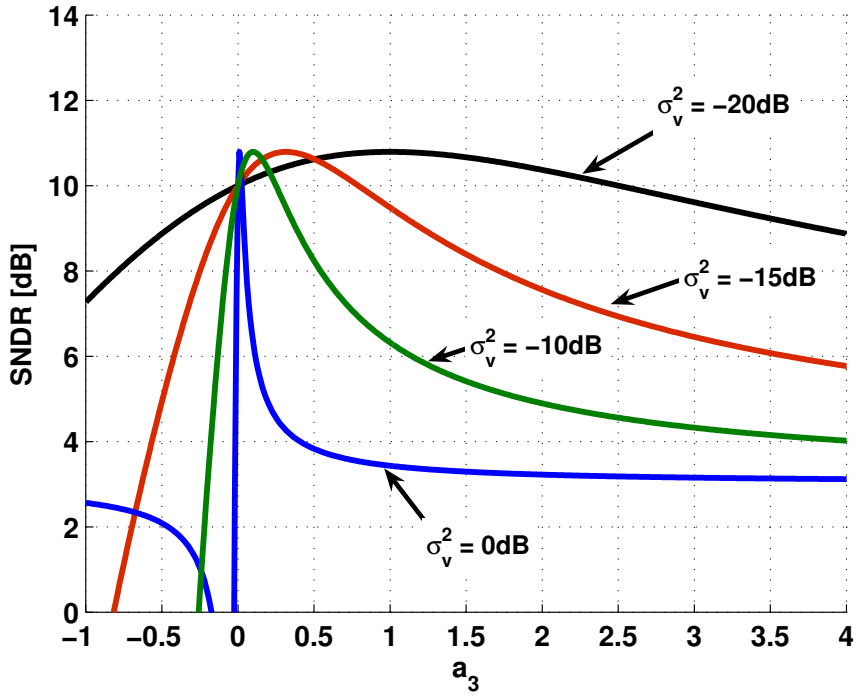

Figure 6.4: SNDR vs. a_3 using equations (6.32) and (6.33). For all lines, $\sigma_x^2/\sigma_v^2 = 10$dB and $a_1 = 1$.

is $1+2/\text{SNR}$ These expanding nonlinearities can increase the useful signal power by making $|\alpha| > 1$, while keeping the distortion power $E[|d|^2]$ relatively small.

For the linear receiver case, the relationship between SNDR and BER is shown in Fig. 6.5, where the theoretical BER curve is calculated from (6.27) with the SNDR in (6.34). One-to-one relationship can be observed between BER and SNDR; moreover, the simulated and the theoretical BER curves are close for most a_3 values.

6.3.4 Special Case 3: Nonlinear Transmitter and Nonlinear Receiver

In reality, nonlinearities can exist at both the transmitter and the receiver. We use the cubic nonlinearities for illustration, which can be written as

$$g(x) = a_1 x + a_3 x^2 x^*, \tag{6.35}$$

$$s(w) = b_1 w + b_3 w^2 w^*. \tag{6.36}$$

By using the derived results in Section 6.3.1, we can simplify the $E[x^* z]$ and $E[|z|^2]$

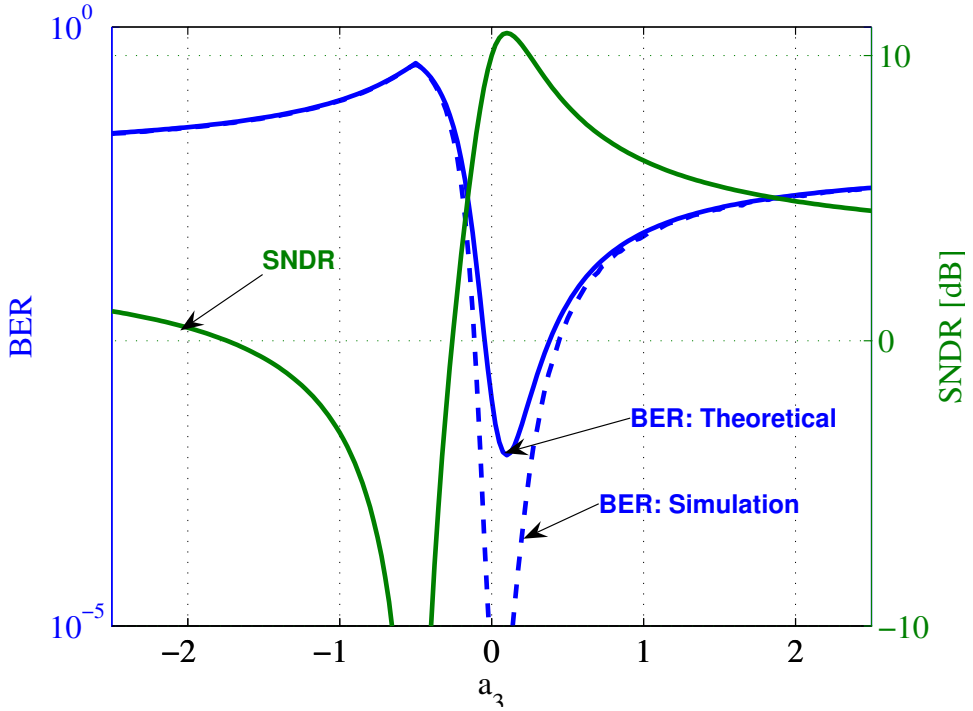

Figure 6.5: Corresponding relationship between BER and SNDR. For all lines, $\sigma_x^2/\sigma_v^2 =$ 10dB, $a_1 = 1$, $b_1 = 1$, $\sigma_x^2 = 1$ and $\sigma_v^2 = 0.1$.

expressions as follows,

$$E[x^* z] = \theta b_1 + (2\theta\sigma_v^2 + \beta) b_3, \tag{6.37}$$

and

$$E[|z|^2] = |b_1|^2(\delta + \sigma_v^2) + (b_1 b_3^* + b_3 b_1^*)(\lambda + 4\delta\sigma_v^2 + 2\sigma_v^4) + |b_3|^2(\zeta + 9\lambda\sigma_v^2 + 18\delta\sigma_v^4 + 6\sigma_v^6), \tag{6.38}$$

where

$$\theta = E[x^* g(x)] = a_1\sigma_x^2 + 2a_3\sigma_x^4,$$

$$\beta = E[x^* g(x)^2 g^*(x)] = 2a_1|a_1|^2\sigma_x^4 + 6(a_1^2 a_3^* + 2a_3|a_1|^2)\sigma_x^6 + 24(a_3^2 a_1^* + 2a_1|a_3|^2)\sigma_x^8 + 120 a_3|a_3|^2\sigma_x^{10},$$

$$\delta = E[g^*(x) g(x)] = |a_1|^2\sigma_x^2 + 2(a_1^* a_3 + a_3^* a_1)\sigma_x^4 + 6|a_3|^2\sigma_x^6,$$

$$\begin{aligned} \lambda &= E[g^*(x)^2 g(x)^2] = 2|a_1|^4\sigma_x^4 + 12(a_1^* a_3 + a_1 a_3^*)|a_1|^2\sigma_x^6 \\ &+ 24(a_1^2(a_3^*)^2 + a_3^2(a_1^*)^2 + 4|a_1|^2|a_3|^2)\sigma_x^8 \\ &+ 240(a_1^* a_3 + a_1 a_3^*)|a_3|^2\sigma_x^{10} + 720|a_3|^4\sigma_x^{12}, \end{aligned}$$

and

$$\begin{aligned}\zeta &= E[g^*(x)^3 g(x)^3] = 6|a_1|^6\sigma_x^6 + 72(a_1^* a_3 + a_1 a_3^*)|a_1|^4\sigma_x^8 \\ &+ 3\times 5!(a_1^2(a_3^*)^2 + a_3^2(a_1^*)^2 + 3|a_1|^2|a_3|^2)|a_1|^2\sigma_x^{10} \\ &+ 6!(a_1^3(a_3^*)^3 + 9(a_1^* a_3 + a_3^* a_1)|a_1|^2|a_3|^2 + a_3^3(a_1^*)^3)\sigma_x^{12} \\ &+ 3\times 7!(a_1^2(a_3^*)^2 + a_3^2(a_1^*)^2 + 3|a_1|^2|a_3|^2)|a_3|^2\sigma_x^{14} \\ &+ 3\times 8!(a_1^* a_3 + a_1 a_3^*)|a_3|^4\sigma_x^{16} + 9!|a_3|^6\sigma_x^{18}.\end{aligned}$$

Substituting (6.37) and (6.38) into (6.1), the closed-form SNDR expression is obtained. In Fig. 6.6, SNDR versus a_3 and b_3 are demonstrated, where the coefficients are assumed to be real-valued for simplicity.

Next, by finding the partial derivatives of the SNDR w.r.t. b_1^* and b_3^* and utilizing (6.19) it is possible to find the optimizing b_1 and b_3 when $a_1,\ a_3,\ \sigma_x^2$, and σ_v^2 are known by solving

$$\theta^* \frac{E[|z|^2]}{(E[x^* z])^*} = b_1(\delta + \sigma_v^2) + b_3(\lambda + 4\delta\sigma_v^2 + 2\sigma_v^4) \tag{6.39}$$

and

$$b_1(\lambda + 4\delta\sigma_v^2 + 2\sigma_v^4) + b_3(\zeta + 9\lambda\sigma_v^2 + 18\delta\sigma_v^4 + 6\sigma_v^6) = (2\theta\sigma_v^2 + \beta)^* \frac{E[|z|^2]}{(E[x^* z])^*}, \tag{6.40}$$

which can be done numerically.

Fig. 6.7 is a plot of AM-AM and AM-PM characteristics of the optimal receiver when a transmitter has $a_1 = 1 - .2j$ and $a_3 = -0.135 + .01j$. For the plot $\sigma_x^2 = 1$ and σ_v^2 is varied to adjust the SNR. The plot shows how the SNDR maximizing cubic curve changes as the noise power changes. The transmitter nonlinearity $g(\cdot)$ is a compressing function. From Fig. 6.7, the optimal receiver nonlinearity $s(\cdot)$ is also compressing for the low-SNR value. An intuitive explanation is that when the noise is salient, i.e., link degradation is mainly determined by the noise rather the nonlinearity, the receiver compressing nonlinearity can also compress some portion of noise; hence, the SNDR can be increased.

More observations are given in Fig. 6.8, where the trend for the optimizing values of b_1 and b_3 is demonstrated as the noise level varies. It is verified that, for SNRs below 12 dB, the real part of b_3 is negative which means that b_3 is a compressing function. When the

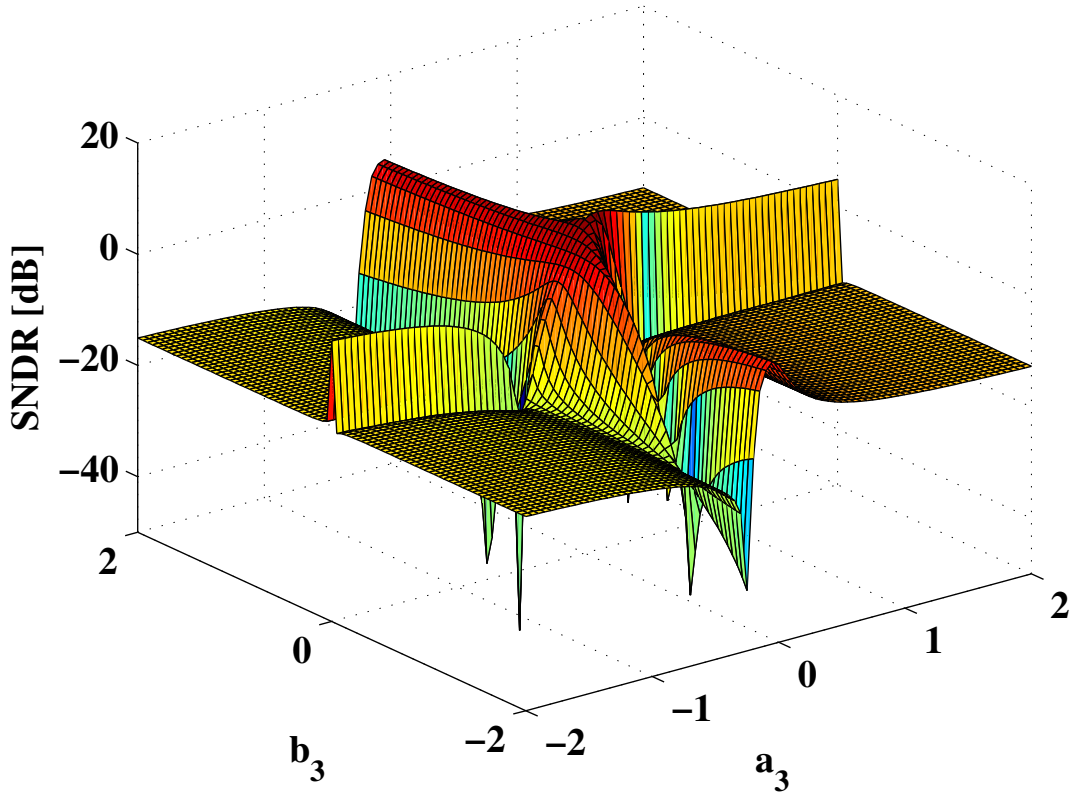

Figure 6.6: SNDR vs. a_3 and b_3 using equations (6.37) and (6.38). For all lines, $\sigma_x^2/\sigma_v^2 = 10$ dB and $a_1 = 1$, $b_1 = 1$.

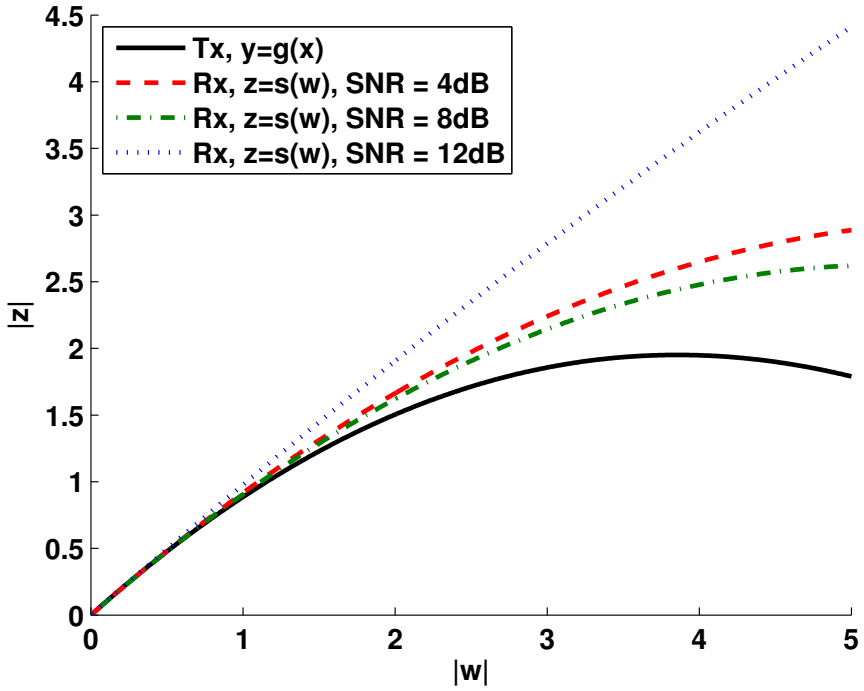

Figure 6.7: Plot of the optimal receiver AM-AM and AM-PM characteristics for the example transmitter characteristic.

SNR is around 12 dB, $b_3 \approx 0$, showing a linear receiver is optimal. For higher SNR values, the receiver nonlinearity is required to be expanding to maximize the SNDR.

6.4 SNDR Maximization

In Section 6.3, interesting results for the receiver nonlinearity are derived to maximize the transceiver SNDR when the transmitter nonlinearity is known. Given the transmitter nonlinearity (the polynomial coefficients a_{2k+1}), the signal power σ_x^2 and the noise power σ_v^2, different receiver nonlinearities will produce different SNDR values, as verified in Fig. 6.2, Fig. 6.4 and Fig. 6.8. Next, we provide an analytical way to calculate the SNDR-optimizing receiver nonlinearity (the polynomial coefficients b_{2k+1}). These optimum b_{2k+1} values can be found by setting the partial derivatives of SNDR with respect to b_{2k+1}^* to zero. This has already been derived in (6.19) and is presented below for convenience,

$$\frac{\partial |E[x^* z]|^2}{\partial b_{2\tilde{k}+1}^*} E[|z|^2] = \frac{\partial E[|z|^2]}{\partial b_{2\tilde{k}+1}^*} |E[x^* z]|^2, \tag{6.41}$$

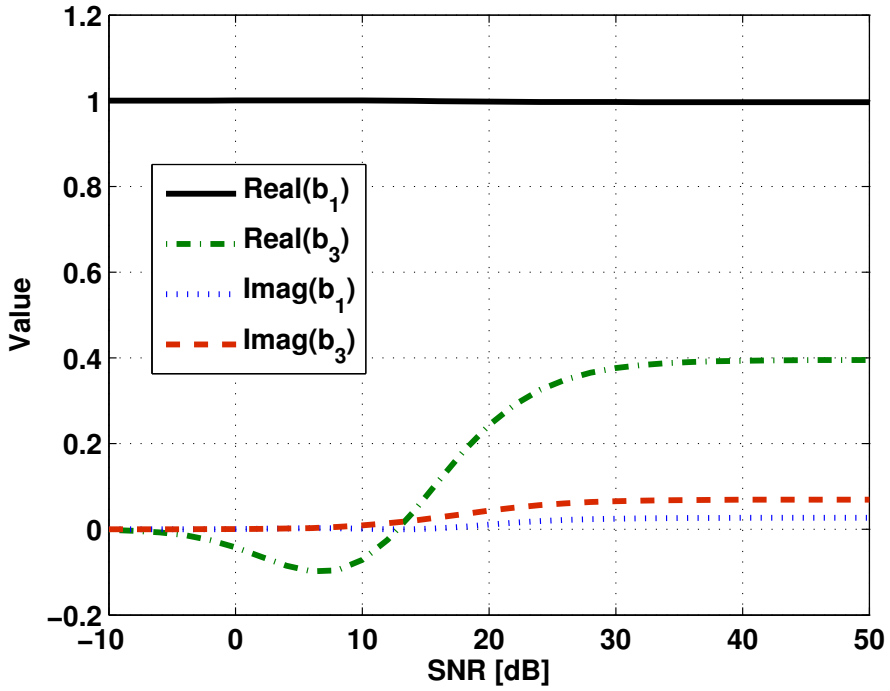

Figure 6.8: Plot of real and imaginary parts of the receiver polynomial coefficients as the SNR varies.

where $\tilde{k}$ is a nonnegative integer. From (6.10), $E[x^*z]$ is not a function of any $b^*_{2\tilde{k}+1}$,

$$\frac{\partial |E[x^*z]|^2}{\partial b^*_{2\tilde{k}+1}} = \frac{\partial (E[x^*z])^*}{\partial b^*_{2\tilde{k}+1}} E[x^*z]. \tag{6.42}$$

It then follows that

$$\frac{\partial (E[x^*z])^*}{\partial b^*_{2\tilde{k}+1}} E[|z|^2] = \frac{\partial E[|z|^2]}{\partial b^*_{2\tilde{k}+1}} (E[x^*z])^*. \tag{6.43}$$

Making use of (6.10) and (6.12), the derivatives in (6.43) can be written

$$\frac{\partial (E[x^*z])^*}{\partial b^*_{2\tilde{k}+1}} = P^*_{2\tilde{k}+1}, \tag{6.44}$$

and

$$\frac{\partial E[|z|^2]}{\partial b^*_{2\tilde{k}+1}} = \sum_{k=0}^{K_s} b_{2k+1} Q_{2\tilde{k}_1+1,2k+1}, \tag{6.45}$$

where P_{2k+1} and $Q_{2k_1+1,2k_2+1}$ are given in (6.10) and (6.12), respectively.

Moreover, from (6.43), we observe that the ratio between (6.44) and (6.45) is constant for various $\tilde{k}$ values, i.e.,

$$\frac{P^*_{2\tilde{k}+1}}{\sum_{k=0}^{K_s} b_{2k+1} Q_{2\tilde{k}_1+1,2k+1}} = \frac{(E[x^*z])^*}{E[|z|^2]}, \tag{6.46}$$

where $\tilde{k} = 0, 1, 2, \cdots, K_s$. Therefore, we can generate K_s equations from (6.46), for example, if taking $\tilde{k} = 0$ and 1,

$$\sum_{k=0}^{K_s} b_{2k+1}[P_1^* Q_{3,2k+1} - P_3^* Q_{1,2k+1}] = 0. \tag{6.47}$$

Because there are $K_s + 1$ unknowns, we can add the additional constraint that $b_1 = 1$ without any loss of generality. In summary, the receiver nonlinearity can be solved from the following equations

$$\mathbf{A}\mathbf{b} = \mathbf{e}, \tag{6.48}$$

where the matrix $\mathbf{A}$ is

$$\begin{pmatrix} 1 & 0 & \cdots & 0 \\ P_1^* Q_{3,1} - P_3^* Q_{1,1} & P_1^* Q_{3,3} - P_3^* Q_{1,3} & \cdots & P_1^* Q_{3,2K_s+1} - P_3^* Q_{1,2K_s+1} \\ P_1^* Q_{5,1} - P_5^* Q_{1,1} & P_1^* Q_{5,3} - P_5^* Q_{1,3} & \cdots & P_1^* Q_{5,2K_s+1} - P_5^* Q_{1,2K_s+1} \\ & & \vdots & \\ P_1^* Q_{2K_s+1,1} - P_{2K_s+1}^* Q_{1,1} & P_1^* Q_{2K_s+1,3} - P_{2K_s+1}^* Q_{1,3} & \cdots & P_1^* Q_{2K_s+1,2K_s+1} - P_{2K_s+1}^* Q_{1,2K_s+1} \end{pmatrix},$$

$\mathbf{b} = [b_1, b_3, \cdots, b_{2K_s+1}]^T$ and $\mathbf{e} = [1, 0, \cdots, 0]^T$. If the matrix $\mathbf{A}$ is full rank, we can obtain the SNDR-optimizing coefficients as

$$\widetilde{\mathbf{b}} = \mathbf{A}^{-1}\mathbf{e}. \tag{6.49}$$

Example 1: Cubic Receiver Nonlinearity

When $K_s = 1$, $\mathbf{A}$ becomes a 2×2 matrix,

$$\begin{pmatrix} 1 & 0 \\ P_1^* Q_{3,1} - P_3^* Q_{1,1} & P_1^* Q_{3,3} - P_3^* Q_{1,3} \end{pmatrix} \begin{pmatrix} b_1 \\ b_3 \end{pmatrix} = \begin{pmatrix} 1 \\ 0 \end{pmatrix}. \tag{6.50}$$

Then, the SNDR-optimizing b_3 is

$$\tilde{b}_3 = -\frac{P_1^* Q_{3,1} - P_3^* Q_{1,1}}{P_1^* Q_{3,3} - P_3^* Q_{1,3}}. \tag{6.51}$$

Example 2: Linear Transmitter

For the linear transmitter, we can set $K_g = 0$ in (6.6), i.e., $g(x) = a_1 x$. From (6.10) and (6.12),

$$P_{2k+1} = a_1 \sigma_x^2 (k+1)! \gamma^k, \tag{6.52}$$

and

$$Q_{2k_1+1,2k_2+1} = (k_1 + k_2 + 1)!\gamma^{k_1+k_2+1}, \tag{6.53}$$

where $\gamma = |a_1|^2\sigma_x^2 + \sigma_v^2$. It is easy to find that $P_1^* Q_{k,1} - P_k^* Q_{1,1} = 0$, which leads to

$$\mathbf{A} = \begin{pmatrix} 1 & \mathbf{0}_{1\times K_s} \\ \mathbf{0}_{K_s\times 1} & \bar{\mathbf{A}} \end{pmatrix}. \tag{6.54}$$

Because the determinant of $\bar{\mathbf{A}}$ is nonzero, $\widetilde{\mathbf{b}} = [1, \mathbf{0}_{1\times K_s}]^T$, i.e., a linear receiver is needed to maximize the transceiver SNDR. If the receiver nonlinearity is cubic, we have $b_3 = 0$, which is in accordance with the result shown in Fig. 6.2.

6.5 Comparison of Clipping and Companding Techniques

Gaussian distribution is an accurate approximation for time-domain signals in multi-carrier or multi-channel transmission schemes, such as OFDM and CDMA; hence, large envelope fluctuations are usually observed. This property is undesirable, for example, when the signal passes through the power amplifier (PA), the large amplitude variations will cause: (i) nonlinear distortions if the signal enters the nonlinear region of the PA; or (ii) low power efficiency if the signal is backed-off from the nonlinear region of the PA. Therefore, the CFR technique is often necessary.

Many CFR techniques have been proposed in the literature, which can be separated into two categories: distortion-based and distortionless-based techniques. Distortion-based CFR algorithms, such as clipping [67, 75] and companding [41, 43, 90, 91], generally require less computational complexity. Nevertheless, the incurred distortion may cause system performance degradations as measured by the SNDR. Distortionless-based methods, on the other hand, can have excellent CFR performance without causing SNDR degradation, but they typically incur large computational complexities, and sometimes side information transmission and receiver-side processing.

The objective of the present study is to carry out SNDR performance comparison of clipping and companding in the AWGN channel to select the high-performance CFR technique

appropriate for communication systems. SNDR analysis for amplitude-limited nonlinearities has been investigated in [75]; it is shown that among all amplitude-limited nonlinearities, clipping with a specific gain is optimal in terms of maximizing the SNDR. We call this method the optimal clipping, which has been reviewed in Section 2.5.2. However, the analysis assumed that the receiver is linear, which is not true for companding techniques. Usually, an inverse nonlinear function is applied at the receiver to recover the signal before compressing.

In this section, we aim to compare the optimal clipping with various companding schemes proposed in the literature. First, the SNDR analysis for inverse functions are performed, which demonstrates that the transceiver SNDR can only be optimized by inverse functions in the noise-free situation. This weakens the usefulness of companding techniques that usually adopt inverse functions to compress and expand signals in the transceiver. Next, we calculate SNDR values of existing companding schemes under the peak-power constraint and compare them with the SNDR value of the optimal clipping. The closed-form SNDR expression and the polynomial approximation are used during the calculation. For the optimal clipping, the optimal SNDR value has been derived in [75].

6.5.1 SNDR of Inverse Functions

In this part, we are interested in studying a special case of the transceiver, where the transmitter nonlinearity $g(\cdot)$ and the receiver nonlinearity $s(\cdot)$ constitute an inverse function pair, i.e., $s(\cdot) = g^{-1}(\cdot)$. This configuration can be regarded as a generalization of various companding PAR reduction algorithms [41, 43, 90, 91], which reduce large amplitude variations by deliberately introducing mutually inverse transceiver nonlinearities. Different companding schemes use different inverse function pairs; however, the transmitter amplitude nonlinearity is always a compressing function (concave with positive slope) and the receiver is always an expanding function (convex with positive slope). One objective of analyzing the SNDR performance for inverse functions is to demonstrate that companding is rarely SNDR-optimal.

For the given transmitter nonlinearity, it has been demonstrated in Section 6.4 that the

receiver nonlinearity should satisfy (6.43) to maximize the SNDR. In the next proposition, we will prove that the condition for inverse functions to optimize the SNDR is the channel noise power should be zero.

Proposition 1. *Given the mutually inverse nonlinearities, the transceiver SNDR is maximized if and only if* $\sigma_v^2 = 0$.

Proof. Without loss of generality, the transmitter nonlinearity is assumed known. First, to maximize the transceiver SNDR, we should design the receiver nonlinearity coefficients $\widetilde{\mathbf{b}}$, such that (6.43) is satisfied. By carrying the conjugation inside the expectation operator (6.43) can be rewritten as

$$\frac{\partial E[xz^*]}{\partial b^*_{2\tilde{k}+1}} E[|z|^2] = \frac{\partial E[|z|^2]}{\partial b^*_{2\tilde{k}+1}} E[xz^*] \tag{6.55}$$

for every $\tilde{k} = 0, 1, 2, \cdots, K_s$.

On the other hand, as the inverse of the given transmitter nonlinearity the receiver nonlinearity coefficients will be the $\mathbf{b}$ that minimizes the mean squared error (MSE) defined by

$$\begin{aligned} \text{MSE} &= E[|s(g(x);\mathbf{b}) - x|^2] \\ &= E[|s(g(x);\mathbf{b})|^2] - E[x^* s(g(x);\mathbf{b})] - E[x s(g(x);\mathbf{b})^*] + E[|x|^2] \\ &= E[|z|^2] - E[x^* z] - E[xz^*] + E[|x|^2], \end{aligned} \tag{6.56}$$

where $\mathbf{b}$ is a vector of the variable coefficients as defined in (6.48) that parameterize $s(\cdot)$. Denote the vector $\mathbf{b}$ that minimizes the MSE as $\overline{\mathbf{b}}$.

When the inverse of $g(\cdot)$ exists, the coefficients $\overline{\mathbf{b}}$ that make $s(\cdot) = g^{-1}(\cdot)$ can be determined by differentiating (6.56) w.r.t. $b^*_{2\tilde{k}+1}$ to get

$$\frac{\partial \text{MSE}}{\partial b^*_{2\tilde{k}+1}} = \frac{\partial E[|z|^2]}{\partial b^*_{2\tilde{k}+1}} - \frac{\partial E[xz^*]}{\partial b^*_{2\tilde{k}+1}}, \tag{6.57}$$

and solving $\partial \text{MSE}/\partial b^*_{2\tilde{k}+1} = 0$. After simplification, we find that $\overline{\mathbf{b}}$ is the set of coefficients that satisfy

$$\frac{\partial E[xz^*]}{\partial b^*_{2\tilde{k}+1}} = \frac{\partial E[|z|^2]}{\partial b^*_{2\tilde{k}+1}}. \tag{6.58}$$

When $\overline{\mathbf{b}} = \widetilde{\mathbf{b}}$ or equivalently when (6.55) and (6.58) are satisfied simultaneously, the inverse function pair maximizes the transceiver SNDR. This requires that $g^{-1}(g(x+v)) = x+v = x$, so that $E[|z|^2] = E[xz^*]$ is satisfied, which only happens when $v = 0$. When $\sigma_v^2 \neq 0$, $E[|z|^2] \neq E[xz^*]$, thus, the criteria for the functions to be inverses of each other in (6.58) and for the SNDR to be maximized in (6.55) are different i.e., $\overline{\mathbf{b}} \neq \widetilde{\mathbf{b}}$, so the inverse functions do not maximize the SNDR. Therefore, when $s(\cdot) = g^{-1}(\cdot)$, the SNDR is maximized if and only if, $\sigma_v^2 = 0$. □

An example is given for the cubic receiver nonlinearity. When b_1 and b_3 are real-valued (only AM-AM conversion exists for $g(\cdot)$ and $s(\cdot)$) and defined as

$$g(x) = R(r)e^{j\angle x}, \tag{6.59}$$

$$s(w) = b_1 w + b_3 w^2 w^*, \tag{6.60}$$

where

$$R(r) = \sqrt[3]{\frac{r}{2b_3} + \sqrt{\frac{b_1^3}{27b_3^3} + \frac{r^2}{4b_3^2}}} + \sqrt[3]{\frac{r}{2b_3} - \sqrt{\frac{b_1^3}{27b_3^3} + \frac{r^2}{4b_3^2}}}, \tag{6.61}$$

and $r = |x|$, we have $s(\cdot) = g^{-1}(\cdot)$. Here, $R(r)$ is obtained by solving the cubic function $T(|w|) = r$, where

$$T(|w|) = |b_1 w + b_3 w^2 w^*| = b_1|w| + b_3|w|^3. \tag{6.62}$$

To calculate the SNDR-optimizing $\tilde{b}_3$, the exact inverse function in (6.61) is difficult to handle, so we calculate its polynomial approximation using the MMSE criteria. For example, when $b_1 = 1$, $b_3 = 0.1$, the 9th-order approximation is

$$g_9(x) = 0.9935x - 0.0811x^2x^* + 0.0113x^3(x^*)^2 - 9.6021\times10^{-4}x^4(x^*)^3 + 3.3286\times10^{-5}x^5(x^*)^4, \tag{6.63}$$

where $E[|s(g_9(x)) - x|^2] = 1.72 \times 10^{-5}$. That is, $g_9(x) \approx R(|x|)e^{j\angle x}$ where $R(\cdot)$ is defined in (6.61).

To evaluate how close the SNDR-optimal $\tilde{b}_3$ is to the $\bar{b}_3$ that makes $s(\cdot) = g^{-1}(\cdot)$, define the relative difference to be $D = \tilde{b}_3/\bar{b}_3 - 1$. When $D = 0$, we have $\bar{b}_3 = \tilde{b}_3$, which is the case where the inverse function pair maximizes the SNDR. Plotted in Fig. 6.9 are the values of

D versus $1/\sigma_v^2$ for two different $\bar{b}_3$ values as shown, where the order of the approximation polynomial is 9.

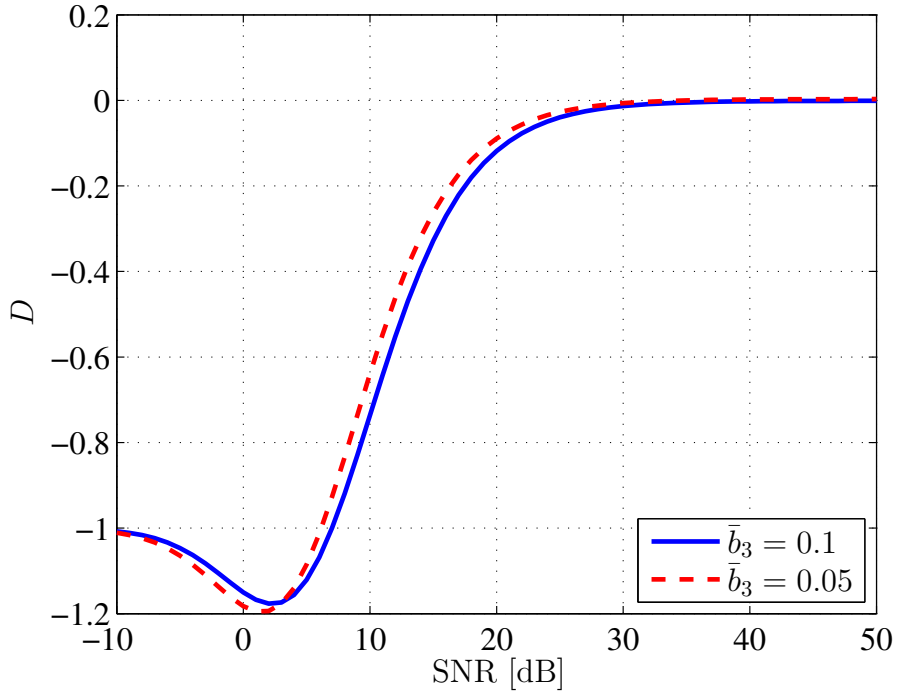

Figure 6.9: Relative difference D for two different $\bar{b}_3$ values by using the 9th-order approximation.

From Fig. 6.9, we verify that the inverse functions *cannot* provide the optimal SNDR performance at the low SNR region. That is to say, the inverse function pair can only obtain the optimal SNDR at high SNR region, where the noise power should be very small which is consistent with Proposition 1.

6.5.2 Comparison under Peak-Power Constraint

In Section 6.5.1, we have shown that the transceiver SNDR is maximized if and only if $\sigma_v^2 = 0$ (noise-free case) for the given mutually inverse nonlinearities. This weakens the usefulness of companding schemes, which apply inverse functions at the transceiver. In this section, we aim at comparing clipping and companding methods in terms of the transceiver SNDR under the peak-power constraint. For detailed companding schemes proposed in the literature, we approximate the companding function using the baseband polynomial model and

calculate their SNDR values using the closed-form expression. Some companding functions are difficult to approximate, because they need many terms to obtain an approximation with low MSE. For these schemes, we use simulations to calculate their SNDR values. On the other hand, the SNDR-optimizing clipping, optimal clipping, has been investigated in [75], where the optimal SNDR has the closed-form expression. We will compare the SNDR values achieved by clipping and companding to find the better PAR reduction method for system implementation.

For companding techniques, we consider four schemes proposed in the literature: μ-law, A-law, NLNST and exponential transform. The inverse functions used in these methods have been presented in Section 2.5.3. See Fig. 2.7 and Fig. 2.8 for typical compressing and expanding curves. Most functions can be approximated by low-order polynomials to obtain small-MSE fittings. For example, if $\mu = 2$ and $B = \sqrt{10}$ are used in the μ-law scheme, we yield

$$g_\mu(x) = 1.4949x - 0.0971x^2x^* + 0.005x^3(x^*)^2, \tag{6.64}$$

$$s_\mu(w) = 0.6369w + 0.0373x^2x^*, \tag{6.65}$$

and the MSEs are both below 10^{-3}.

One exception is the exponential companding, where (2.41) and (2.42) are difficult to be approximated by low-order polynomials because of their sharp transitions. Hence, we will use extensive simulations to calculate the SNDR.

For a specific companding scheme, the μ-law for instance, the transceiver SNDR will vary with different companding factor values. Shown in Fig. 6.10 are SNDR curves for different μ values. SNDR values of the optimal clipping are also included, which are solid lines in Fig. 6.10 because they are independent of μ. For the high PSNR (PSNR = 30 dB), $\mu = 2$ provides the largest SNDR and is only 0.6 dB worse than the SNDR of the optimal clipping. When PSNR = 10 dB, the maximum SNDR is achieved by $\mu = 4$. However, no matter what μ is used, the companding yields much worse performance than the optimal clipping when the PSNR is low. Therefore, we choose $\mu = 2$ as the typical companding factor for the μ-law scheme.

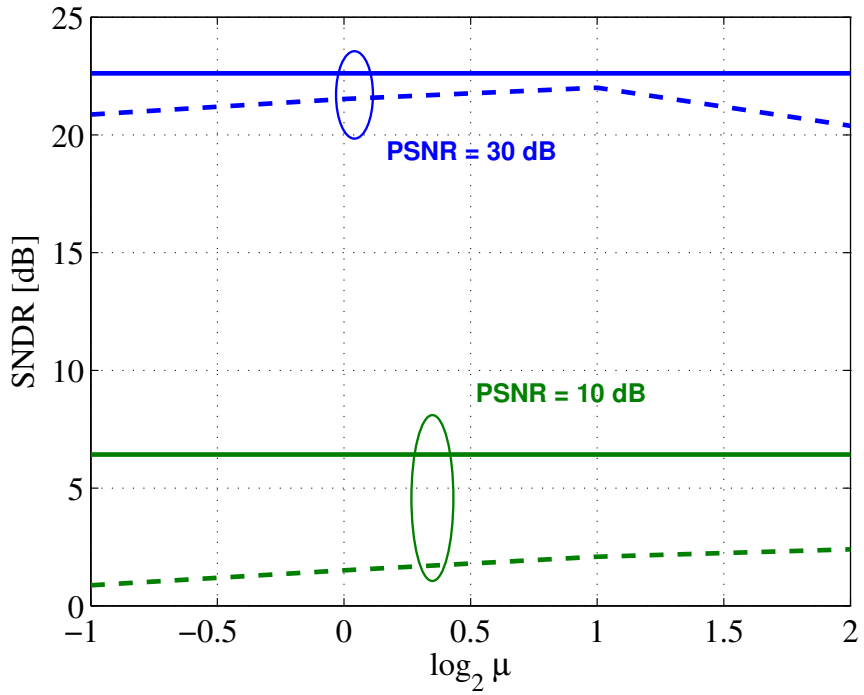

Figure 6.10: SNDR vs. μ for PSNR = 10 dB and 30 dB when the μ-law companding scheme is used.

SNDR results from the optimal clipping and different companding schemes are shown in Fig. 6.11. The SNDR for the optimal clipping comes from [75]. For companding schemes, we yielded the SNDR values from the polynomial fitting and the closed-form SNDR expressions. Typical companding factors are chosen for each companding method and are listed in Fig. 6.11. It is clear that the optimal clipping outperforms companding schemes. For high PSNRs where the noise level is pretty low, the companding methods generates a little bit worse results than the optimal clipping. The performance gap is enlarged at the low PSNR region, because receiver expanding nonlinearities amplify the channel noise. The exponential companding scheme has better SNDR than other companding methods in the low PSNR region; while the situation is reversed for the high PSNR region.

Combining the analysis in Section 6.5.1 and in this section, when the noise is salient, we find that the companding scheme is incapable of achieving the maximum SNDR, and has much worse performance than the clipping. Only when the noise power is pretty low, the companding has comparable SNDR performance with the optimal clipping. Therefore,

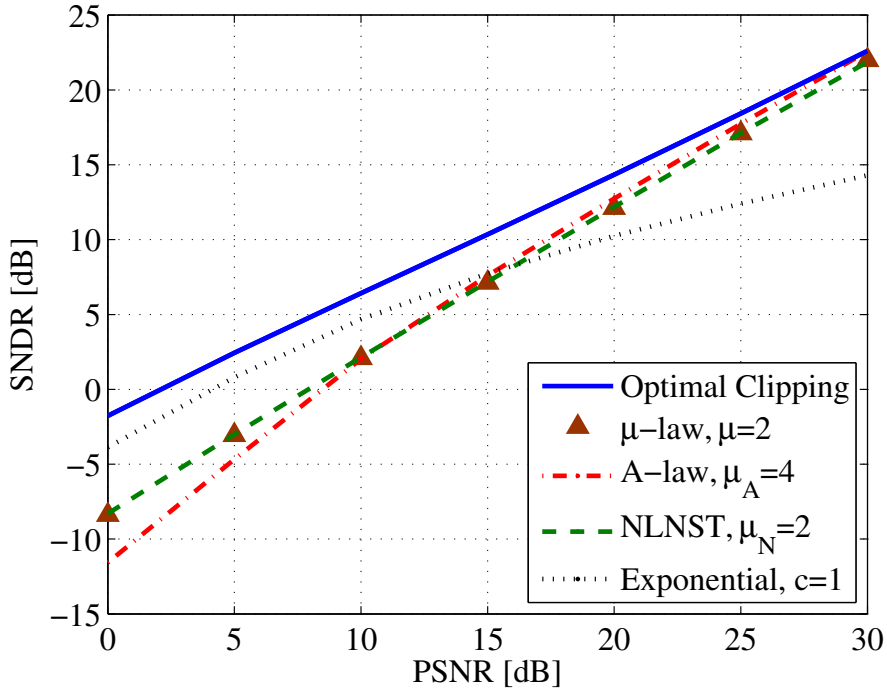

Figure 6.11: Comparison of SNDR values under different PSNRs for the optimal clipping and the different companding schemes.

we advocate to use the optimal clipping PAR reduction algorithm in reality.

6.5.3 Remarks

The above SNDR analysis is under the sample-based framework because of the expectation operator in the SNDR definition, see (6.1). On the other hand, existing companding schemes are proposed for symbol-based transmission (for example, the block-based OFDM modulation), where the peak-power changes per-block. Fortunately, in [16], it was shown that the SNDR difference between the symbol-based and the sample-based schemes is negligible for most practical system parameters. The difference is only observable when the PSNR is high and the block length is small. Hence, the sample-based analysis and comparison presented in this chapter are still valid in reality.

Another aspect is that the spectrum broadening always accompanies the distortion-based CFR methods. Filtering is necessary to constraint the out-of-band spectral regrowth to satisfy standard requirements, such as time-domain filtering [55] and frequency-domain

filtering [10, 14]. The concatenation of the clipping or compressing functions with the filtering makes the transmitter nonlinearity contains memory effects. In [30], the author showed that the Bussgang Theorem is approximately valid under the memory nonlinearity conditions. Therefore, the SNDR analysis based on the memoryless nonlinearities can be still used when the filtering is involved to guarantee the spectrum compliance.

Clipping and companding are two commonly used CFR techniques with little computational complexity. When the receiver is linear, the clipping with gain has been shown to be optimal in terms of SNDR. We extended the SNDR analysis to cope with the nonlinear receiver to study the performance of various companding schemes. Under all the PSNR scenarios studied, clipping always has larger SNDR values than companding, which corresponds to smaller reception error probability. From our result, the optimal clipping is recommended to use in reality for the CFR purpose.

6.6 Conclusions

Nonlinear effects have a significant impact on the link performance in modern communication systems. When considering nonlinear distortion, SNDR should be used to evaluate the reception reliability of the communications link. Previous studies have only focused on a single nonlinearity at either the transmitter or the receiver. In this chapter, SNDR for transceiver nonlinearities is investigated in the AWGN channel. Specifically, three SNDR analyses are presented: i) the closed-form SNDR expression is derived for transceiver nonlinearities that can be represented using the baseband polynomial model; ii) an analytical solution is presented for maximizing the transceiver SNDR for any given set of nonlinear transmitter polynomial coefficients; iii) a proof is provided which establishes that a mutually inverse pair of receiver/transmitter nonlinearities will only be SNDR-optimal when no noise is present. Thus, despite being intuitively appealing, it is only SNDR-optimal to use a receiver nonlinearity that is the inverse of the transmitter nonlinearity in noise-less channels.

CHAPTER VII

CONCLUSIONS

In this dissertation, we studied several aspects of distortion-based crest factor reduction techniques in multi-carrier transmission systems. We started from clarifying the definitions of PAR and analyzing the performance-evaluating metrics. A novel distortion-based CFR algorithm was proposed, which was shown to be efficient, simple and easy to expand. Finally, SNDR analysis helped us to optimize the system design and compare two CFR methods.

7.1 Contributions

Primary contributions of this dissertation are listed as follows:

- Reviewed distortion-based CFR algorithms, including the simple clipping, the optimal clipping and the companding. Performance-evaluating metrics, such as EVM, spectral mask and SNDR, were also introduced.

- Derived the power efficiency maximizing PAR metrics for MIMO-OFDM systems. Relationship between the branch PARs and the overall power efficiency was established.

- Performed the EVM analysis in OFDM systems for various impairments, including phase noise, amplitude clipping, PA nonlinearities, and gain/phase imbalances. Concrete thresholds were also provided for the amount of allowable distortions from each distortion source to meet EVM requirements, based on theoretical calculations.

- Proposed a novel distortion-based CFR technique, constrained clipping, to drastically reduce the PAR while satisfying any given EVM and spectral mask constraints. The computational complexity of constrained clipping was analyzed, showing that it is simple and easy to be implemented. Moreover, constrained clipping was extended to the multiple-user OFDM case.

- Performed SNDR analysis for transceiver nonlinearities in AWGN channels. Closed-form SNDR expression was derived by using Bussgang Theorem and polynomial approximations. When the transmitter nonlinearity was known, we optimized the receiver nonlinearity to maximize the SNDR.

- Compared two CFR algorithms, clipping and companding, using the SNDR analysis. We proved that a mutually inverse pair of receiver/transmitter nonlinearities will only be SNDR-optimal when no noise is present. Moreover, under the same PSNR condition, the optimal clipping was shown to have better SNDR performance than various existing companding schemes.

7.2 Suggestions for Future Research

Some future research directions are listed:

- Design new CFR algorithms for MIMO-OFDM systems. In Chapter 3, PAR definitions are clarified for MIMO-OFDM systems. Based on the proper PAR metrics, we should investigate more efficient and high-performance CFR methods.

- Apply the constrained clipping method to other systems, such as CDMA and wideband CDMA. The main problem is to investigate what proper performance-evaluating metrics are in these systems.

- Compare clipping and companding in detail for other system configurations, for example, in the frequency-selective fading channels. It was shown in [69] that the fading effect should also be considered for the clipping noise; hence, we should utilize the SNDR analysis in the fading channel [74] to compare clipping and companding.

REFERENCES

[1] "IEEE standard for local and metropolitan area networks part 11: wireless LAN medium access control (MAC) and physical layer (PHY) specifications: high-speed physical layer in the 5 GHZ band," *IEEE Std 802.11a-1999*, pp. 1–82, 1999.

[2] "Radio transmission and reception," *GSM Recommendation 05.05*, Dec. 1999.

[3] "Digital video broadcasting (DVB); framing structure, channel coding and modulation for digital terrestrial television," *ETSI EN 300 744 v1.5.1*, pp. 1–64, Nov. 2004.

[4] "IEEE standard for local and metropolitan area networks part 16: air interface for fixed broadband wireless access systems," *IEEE Std 802.16-2004 (Revision of IEEE Std 802.16-2001)*, pp. 1–857, 2004.

[5] "3GPP technical specification group access network," *Base Station Conformance Testing (FDD) (Rel. 99) TS 25.141 V.3.14.0*, 2005.

[6] "Radio broadcasting systems; digital audio broadcasting (DAB) to mobile, portable and fixed receivers," *ETSI EN 300 401 v1.4.1*, pp. 1–197, June 2006.

[7] "Using error vector magnitude measurements to analyze and troubleshoot vector-modulated signals," Agilent PN 89400-14 Product Note, Agilent Technologies.

[8] Aggarwal, A., Stauffer, E. R., and Meng, T. H., "Optimal peak-to-average power ratio reduction in MIMO-OFDM systems," in *Proc. IEEE International Conference on Communications*, vol. 7, pp. 3094–3099, June 2006.

[9] Alamouti, S. M., "A simple transmit diversity technique for wireless communications," *IEEE Journal on Selected Areas in Communications*, vol. 16, pp. 1451–1458, Oct. 1998.

[10] Armstrong, J., "New OFDM peak-to-average power reduction scheme," in *Proc. IEEE Vehicular Technology Conference*, vol. 1, pp. 756–760, May 2001.

[11] Armstrong, J., "Peak-to-average power reduction for OFDM by repeated clipping and frequency domain filtering," *Electronics Letters*, vol. 38, pp. 246–247, Feb. 2002.

[12] Baek, M. S., Kim, M. J., You, Y. H., and Song, H. K., "Semi-blind channel estimation and PAR reduction for MIMO-OFDM system with multiple antennas," *IEEE Transactions on Broadcasting*, vol. 50, pp. 414–424, Dec. 2004.

[13] Bauml, R. W., Fischer, R. F. H., and Huber, J. B., "Reducing the peak-to-average power ratio of multicarrier modulationby selected mapping," *Electronics Letters*, vol. 32, pp. 2056–2057, Oct. 1996.

[14] Baxley, R. J., Zhao, C., and Zhou, G. T., "Constrained clipping for crest factor reduction in OFDM," *IEEE Transactions on Broadcasting*, vol. 52, pp. 570–575, December 2006.

[15] Baxley, R. J. and Zhou, G. T., "MAP metric for blind phase sequence detection in selected mapping," *IEEE Transactions on Broadcasting*, vol. 51, pp. 565–570, Dec. 2005.

[16] Baxley, R. J. and Zhou, G. T., "A comparison of SNDR maximization techniques for OFDM," in *IEEE Statistical Signal Processing Workshop*, Aug. 2007.

[17] Bolcskei, H., "MIMO-OFDM wireless systems: basics, perspectives, and challenges," *IEEE Wireless Communications*, vol. 13, pp. 31–37, Aug. 2006.

[18] Brandwood, D. H., "A complex gradient operator and its application in adaptive array theory," *IEE Proc. Part F and H*, vol. 130, pp. 11–16, Feb. 1983.

[19] Buchholz, M., Schuchert, A., and Hasholzner, R., "Effects of tuner IQ imbalance on multicarrier-modulation systems," *Proc. 3rd IEEE International Caracas Conference on Devices, Circuits and Systems*, pp. T65/1–T65/6, Mar. 2000.

[20] Bussgang, J. J., "Crosscorrelation functions of amplitude distorted Gaussian signals," res. Lab. Elec., MIT, 1952.

[21] Chen, H. and Haimovich, A. M., "Iterative estimation and cancellation of clipping noise for OFDM signals," *IEEE Communications Letters*, vol. 7, pp. 305–307, July 2003.

[22] Cutler, B., "Effects of physical layer impairments on OFDM systems," *RF Design*, pp. 36–44, May 2002.

[23] Dahlman, E., Ekstrom, H., Furuskar, A., Jading, Y., Karlsson, J., Lundevall, M., and Parkvall, S., "The 3G long-term evolution - radio interface concepts and performance evaluation," in *Proc. IEEE 63rd Vehicular Technology Conference*, vol. 1, pp. 137–141, 2006.

[24] Dardari, D., "Joint clip and quantization effects characterization in OFDM receivers," *IEEE Transactions on Circuits and Syst. I: Regular Papers*, vol. 53, pp. 1741–1748, Aug. 2006.

[25] Dardari, D., Tralli, V., and Vaccari, A., "A theoretical characterization of nonlinear distortion effects in OFDM systems," *IEEE Trans. on Commun.*, vol. 48, pp. 1755–1764, Oct. 2000.

[26] Deng, S.-K. and Lin, M.-C., "Recursive clipping and filtering with bounded distortion for PAPR reduction," *IEEE Transactions on Communications*, vol. 55, pp. 227–230, Jan. 2007.

[27] Ding, L. and Zhou, G. T., "Effects of even-order nonlinear terms on power amplifier modeling and predistortion linearization," *IEEE Trans. on Vehicular Technology*, vol. 53, no. 1, pp. 156–162, Jan. 2004.

[28] Dogancay, K., "Blind compensation of nonlinear distortion for bandlimited signals," *IEEE Transactions on Circuits and Syst. I: Regular Papers*, vol. 52, pp. 1872–1882, Sept. 2005.

[29] Ekstrom, H., Furuskar, A., Karlsson, J., Meyer, M., Parkvall, S., Torsner, J., and Wahlqvist, M., "Technical solutions for the 3G long-term evolution," *IEEE Communications Magazine*, vol. 44, no. 3, pp. 38–45, Mar. 2006.

[30] Ermolova, N. Y., "Nonlinear amplifier effects on clipped-filtered multicarrier signals," *IEE Proceedings- Communications*, vol. 153, pp. 213–218, Apr. 2006.

[31] Fischer, R. F. H. and Hoch, M., "Directed selected mapping for peak-to-average power ratio reduction in MIMO OFDM," *Electronics Letters*, vol. 42, pp. 1289–1290, Oct. 2006.

[32] Foschini, G. J., "Layered space-time architecture for wireless communication in a fading environment when using multi-element antenna," *Bell Labs Tech. J.*, vol. 1, no. 2, pp. 41–59, 1996.

[33] Friese, M., "On the achievable information rate with peak-power-limited orthogonal frequency-division multiplexing," *IEEE Transactions on Information Theory*, vol. 46, pp. 2579–2587, Nov. 2000.

[34] Georgiadis, A., "Gain, phase imbalance, and phase noise effects on error vector magnitude," *IEEE Trans. on Vehicular Technology*, vol. 53, no. 2, pp. 443–449, Mar. 2004.

[35] Gradshteyn, I. S., Ryzhik, I. M., Jeffrey, A., and Zwillinger, D., *Table of Integrals, Series, and Products*. Academic Press, 6 ed., July 2000.

[36] Han, S. H. and Lee, J. H., "An overview of peak-to-average power ratio reduction techniques for multicarrier transmission," *IEEE Wireless Communications*, vol. 12, pp. 56–65, Apr. 2005.

[37] Han, S. H. and Lee, J. H., "Modified selected mapping technique for PAPR reduction of coded OFDM signal," *IEEE Transactions on Broadcasting*, vol. 50, pp. 335–341, Sept. 2004.

[38] Hanzo, L., Munster, M., Choi, B. J., and Keller, T., *OFDM and MC-CDMA for Broadband Multi-user Communications, WLANs and Broadcasting*. Wiley-IEEE Press, 2003.

[39] Hara, S. and Prasad, R., "Overview of multicarrier CDMA," *IEEE Communications Magazine*, vol. 35, pp. 126–133, Dec. 1997.

[40] Ho, W. S., Madhukumar, A. S., and Chin, F., "Peak-to-average power reduction using partial transmit sequences: a suboptimal approach based on dual layered phase sequencing," *IEEE Transactions on Broadcasting*, vol. 49, pp. 225–231, June 2003.

[41] Huang, X., Lu, J., Zheng, J., Letaief, K. B., and Gu, J., "Companding transform for reduction in peak-to-average power ratio of OFDM signals," *IEEE Trans. on Wireless Commun.*, vol. 3, pp. 2030–2039, Nov. 2004.

[42] Jayalath, A. D. S. and Athaudage, C. R. N., "Peak power reduction of space-time coded OFDM signals," in *Proc. IEEE 8th International Symposium on Spread Spectrum Techniques and Applications*, pp. 797–801, Sept. 2004.

[43] Jiang, T., Yang, Y., and Song, Y. H., "Exponential companding technique for PAPR reduction in OFDM systems," *IEEE Trans. on Broadcast.*, vol. 51, pp. 244–248, June 2005.

[44] Kenington, P. B., *High Linearity RF Amplifier Design*. Artech House Publishers, 2000.

[45] Kim, D. and Stuber, G. L., "Clipping noise mitigation for OFDM by decision-aided reconstruction," *IEEE Communications Letters*, vol. 3, pp. 4–6, Jan. 1999.

[46] Kim, J. H., Jeong, J. H., Kim, S. M., Park, C. S., and Lee, K. C., "Prediction of error vector magnitude using AM/AM, AM/PM distortion of RF power amplifier for high order modulation OFDM system," *Proc. IEEE MTT-S International Microwave Symposium Digest*, pp. 2027–2030, June 2005.

[47] Krongold, B. S. and Jones, D. L., "PAR reduction in OFDM via active constellation extension," *IEEE Transactions on Broadcasting*, vol. 49, pp. 258–268, Sept. 2003.

[48] Krongold, B. S., Woo, G. R., and Jones, D. L., "Fast active constellation extension for MIMO-OFDM PAR reduction," in *Proc. 39th Asilomar Conference on Signals, Systems and Computers*, pp. 1476–1479, Nov. 2005.

[49] Ku, H., *Behavioral modeling of nonlinear RF power amplifiers for digital wireless communication systems with implications for predistortion linearization systems*. PhD thesis, Georgia Institute of Technology, Oct. 2003.

[50] Kwon, O.-J. and Ha, Y.-H., "Multi-carrier PAP reduction method using sub-optimal PTS with threshold," *IEEE Transactions on Broadcasting*, vol. 49, pp. 232–236, June 2003.

[51] Lee, H., Liu, D. N., Zhu, W., and Fitz, M. P., "Peak power reduction using a unitary rotation in multiple transmit antennas," in *Proc. IEEE International Conference on Communications*, vol. 4, pp. 2407–2411, May 2005.

[52] Lee, K. F. and Williams, D. B., "A space-frequency transmitter diversity technique for OFDM systems," in *Proc. IEEE Global Telecommunications Conference*, Nov. 2000.

[53] Lee, Y. L., You, Y. H., Jeon, W. G., Paik, J. H., and Song, H. K., "Peak-to-average power ratio in MIMO-OFDM systems using selective mapping," *IEEE Communications Letters*, vol. 7, pp. 575–577, Dec. 2003.

[54] Li, H. and Liu, H., "An analysis of uplink OFDMA optimality," *IEEE Transactions on Wireless Communications*, vol. 6, pp. 2972–2983, Aug. 2007.

[55] Li, X. and Cimini, L. J., "Effects of clipping and filtering on the performance of OFDM," *IEEE Communications Letters*, vol. 2, pp. 131–133, May 1998.

[56] Lim, D.-W., Heo, S.-J., No, J.-S., and Chung, H., "A new PTS OFDM scheme with low complexity for PAPR reduction," *IEEE Transactions on Broadcasting*, vol. 52, pp. 77–82, Mar. 2006.

[57] Litsyn, S., *Peak Power Control in Multicarrier Communications*. Cambridge University Press, 2007.

[58] Litsyn, S. and Wunder, G., "Generalized bounds on the crest-factor distribution of OFDM signals with applications to code design," *IEEE Transactions on Information Theory*, vol. 52, pp. 992–1006, Mar. 2006.

[59] Maas, S. A., *Nonlinear Microwave Circuits*. IEEE Press, 1997.

[60] Maattanen, H. L., Ermolova, N. Y., and Haggman, S. G., "Nonlinear amplification of clipped-filtered multicarrier signals," in *Proc. IEEE Vehicular Technology Conference*, vol. 2, pp. 958–962, May 2005.

[61] Mashhour, A. and Borjak, A., "Method for computing error vector magnitude in GSM EDGE systems – simulation results," *IEEE Communications Letters*, vol. 5, no. 3, pp. 88–91, Mar. 2001.

[62] Muller, S. H. and Huber, J. B., "OFDM with reduced peak-to-average power ratio by optimum combination of partial transmit sequences," *Electronics Letters*, vol. 33, pp. 368–369, Feb. 1997.

[63] Nikopour, H., Khandani, A. K., and Jamali, S. H., "Turbo-coded OFDM transmission over a nonlinear channel," *IEEE Transactions on Vehicular Technology*, vol. 54, pp. 1361–1371, July 2005.

[64] Ochiai, H., "Performance analysis of peak power and band-limited OFDM system with linear scaling," *IEEE Transactions on Wireless Communications*, vol. 2, pp. 1055–1065, Sept. 2003.

[65] Ochiai, H. and Imai, H., "Performance of the deliberate clipping with adaptive symbol selection for strictly band-limited OFDM systems," *IEEE Journal on Selected Areas in Communications*, vol. 18, pp. 2270–2277, Nov. 2000.

[66] Ochiai, H. and Imai, H., "On the distribution of the peak-to-average power ratio in OFDM signals," *IEEE Transactions on Communications*, vol. 49, pp. 282–289, Feb. 2001.

[67] Ochiai, H. and Imai, H., "Performance analysis of deliberately clipped OFDM signals," *IEEE Trans. on Commun.*, vol. 50, pp. 89–101, Jan. 2002.

[68] Palomar, D. P., Cioffi, J. M., and Lagunas, M. A., "Joint Tx-Rx beamforming design for multicarrier MIMO channels: a unified framework for convex optimization," *IEEE Transactions on Signal Processing*, vol. 51, pp. 2381–2401, Sept. 2003.

[69] Panta, K. R. and Armstrong, J., "Effects of clipping on the error performance of OFDM in frequency selective fading channels," *IEEE Transactions on Wireless Communications*, vol. 3, pp. 668–671, Mar. 2004.

[70] Papoulis, A. and Pillai, S. U., *Probability, Random Variables and Stochastic Processes*. McGraw-Hil, 4 ed., Dec. 2001.

[71] Pinto, J. L. and Darwazeh, I., "Error vector magnitude relation to magnitude and phase distortion in 8-PSK systems," *Electronics Letters*, vol. 37, pp. 437–438, Mar. 2001.

[72] Proakis, J. G., *Digital Communications*. New York, McGraw-Hill, 4 ed., January 2001.

[73] Qian, H., Raich, R., and Zhou, G. T., "On the benefits of deliberately introduced baseband nonlinearities in communication systems," in *Proc. IEEE International Conference on Acoustics, Speech and Signal Processing*, vol. 2, pp. 905–908, May 2004.

[74] Qian, H., Raich, R., and Zhou, G. T., "Optimization of SNDR in the presence of amplitude limited nonlinearity and multipath fading," in *IEEE Thirty-Eighth Asilomar Conference on Signals, Systems and Computers*, vol. 1, pp. 712–716, Nov. 2004.

[75] Raich, R., Qian, H., and Zhou, G. T., "Optimization of SNDR for amplitude-limited nonlinearities," *IEEE Trans. on Commun.*, vol. 53, pp. 1964–1972, Nov. 2005.

[76] Reed, I. S., "On a moment theorem for complex gaussian processes," *IRE Trans. on Information Theory*, vol. 8, pp. 194–195, Apr. 1962.

[77] Romano, L., Panseri, L., Samori, C., and Lacaita, A. L., "Matching requirements in LINC transmitters for OFDM signals," *IEEE Transactions on Circuits and Systems-I: Regular Papers*, vol. 53, no. 7, pp. 1572–1578, July 2006.

[78] Sandberg, S., LeBlanc, J. P., and Vasic, B., "Receiver-oriented clipping-effect mitigation in OFDM - a worthyt approach?," in *OFDM Workshop*, Aug. 2005.

[79] Saul, A., "Generalized active constellation extension for peak reduction in OFDM systems," in *IEEE International Conference on Communications*, vol. 3, pp. 1974–1979, May 2005.

[80] Schenk, T. C. W., Smulders, P. F. M., and Fledderus, E. R., "The application of spatial shifting for peak-to-average power ratio reduction in MIMO OFDM systems," in *Proc. IEEE 63rd Vehicular Technology Conference*, vol. 4, pp. 1859–1863, May 2006.

[81] Sharif, M. and Khalaj, B. H., "Peak to mean envelope power ratio of over-sampled OFDM signals: an analytical approach," in *Proc. IEEE International Conference on Communications*, vol. 5, pp. 1476–1480, June 2001.

[82] Stuber, G. L., Barry, J. R., McLaughlin, S. W., Li, Y., Ingram, M. A., and Pratt, T. G., "Broadband MIMO-OFDM wireless communications," *Proceedings of the IEEE*, vol. 92, pp. 271–294, Feb. 2004.

[83] Suraweera, H. A., Panta, K. R., Feramez, M., and Armstrong, J., "OFDM peak-to-average power reduction scheme with spectral masking," in *Proc. Intl. Symposium on Communication Systems, Networks and Digital Signal Processing*, pp. 164–167, July 2004.

[84] Tan, M., Latinovic, Z., and Bar-Ness, Y., "STBC MIMO-OFDM peak-to-average power ratio reduction by cross-antenna rotation and inversion," *IEEE Communications Letters*, vol. 9, pp. 592–594, July 2005.

[85] Tarokh, V., Jafarkhani, H., and Calderbank, A. R., "Space-time block codes from orthogonal designs," *IEEE Transactions on Information Theory*, vol. 45, pp. 1456–1467, July 1999.

[86] Tellado, J., *Multicarrier Modulation With Low PAR: Applications to DSL and Wireless*. Kluwer Academic Publishers, 2000.

[87] Tsimbinos, J. and Lever, K. V., "Nonlinear system compensation based on orthogonal polynomial inverses," *IEEE Trans. on Circuits and Syst. I: Fundamental Theory and Applications*, vol. 48, pp. 406–417, Apr. 2001.

[88] Tubbax, J., Come, B., Perre, L. V., Donnay, S., Engels, M., Man, H. D., and Moonen, M., "Compensation of IQ imbalance and phase noise in OFDM systems," *IEEE Trans. on Wireless Communications*, vol. 4, no. 3, pp. 872–877, May 2005.

[89] Vaananen, O., Vankka, J., and Halonen, K., "Effect of baseband clipping in wideband CDMA system," in *Proc. IEEE 7th International Symposium on Spread Spectrum Techniques and Applications*, vol. 2, pp. 445–449, Sept. 2002.

[90] Wang, X., Tjhung, T. T., and Ng, C. S., "Reduction of peak-to-average power ratio of OFDM system using a companding technique," *IEEE Trans. on Broadcast.*, vol. 45, pp. 303–307, Oct. 1999.

[91] Wang, X., Tjhung, T. T., and Wu, Y., "On the SER and spectral analyses of A-law companded multicarrier modulation," *IEEE Trans. on Veh. Techn.*, vol. 52, pp. 1408–1412, Sept. 2003.

[92] Wei, S., Goeckel, D. L., and Kelly, P. E., "A modern extreme value theory approach to calculating the distribution of the peak-to-average power ratio in OFDM systems," in *Proc. IEEE International Conference on Communications*, vol. 3, pp. 1686–1690, Apr. 2002.

[93] Weinstein, S. B. and Ebert, P. M., "Data transmission by frequency division multiplexing using the direct fourier transform," *IEEE Trans. Commun. Tech.*, vol. COM-19, no. 11, pp. 628–634, Oct. 1971.

[94] Wu, S. and Bar-Ness, Y., "OFDM systems in the presence of phase noise: consequences and solutions," *IEEE Trans. on Communications*, vol. 52, no. 11, pp. 1988–1996, Nov. 2004.

[95] Yamanouchi, S., Kunihiro, K., and Hida, H., "An efficient algorithm for simulating error vector magnitude in nonlinear OFDM amplifiers," *Proc. IEEE Custom Integrated Circuits Conf.*, pp. 129–132, Oct. 2004.

[96] Yang, H., "A road to future broadband wireless access: MIMO-OFDM-based air interface," *IEEE Communications Magazine*, vol. 43, pp. 53–60, Jan. 2005.

[97] Yang, L., Chen, R. S., Siu, Y. M., and Soo, K. K., "PAPR reduction of an OFDM signal by use of PTS with low computational complexity," *IEEE Transactions on Broadcasting*, vol. 52, pp. 83–86, Mar. 2006.

[98] You, Y.-H., Jeon, W.-G., Paik, J.-H., and Song, H.-K., "A simple construction of OFDM-CDMA signals with low peak-to-average power ratio," *IEEE Transactions on Broadcasting*, vol. 49, pp. 403–407, Dec. 2003.

[99] You, Y.-H., Jeon, W.-G., Wee, J. W., Kim, S.-T., Hwang, I., and Song, H.-K., "OFDMA uplink performance for interactive wireless broadcasting," *IEEE Transactions on Broadcasting*, vol. 51, pp. 383–388, Sept. 2005.

[100] Yu, H., Chen, M., and Wei, G., "Distribution of PAR in DMT systems," *Electronics Letters*, vol. 39, pp. 799–801, May 2003.

[101] Zhou, G. T. and Kenney, J. S., "Predicting spectral regrowth of nonlinear power amplifiers," *IEEE Trans. on Commun.*, vol. 50, pp. 718–722, May 2002.

[102] Zhou, G. T., Qian, H., Ding, L., and Raich, R., "On the baseband representation of a bandpass nonlinearity," *IEEE Trans. on Signal Processing*, vol. 53, pp. 2953–2957, Aug. 2005.

[103] Zou, W. Y. and Wu, Y., "COFDM: an overview," *IEEE Transactions on Broadcasting*, vol. 41, pp. 1–8, Mar. 1995.

VITA

Chunming Zhao was born in Qingdao, Shandong, China in 1977. He received his Bachelor and Master degrees in Department of Electronic Engineering and Information Science from University of Science and Technology of China (USTC), Hefei, Anhui, China, in 2001 and 2004, respectively. Since then, he has been working towards his Ph.D. degree in Electrical and Computer Engineering at the Georgia Institute of Technology, Atlanta, Georgia, USA.

His general research interests are in the areas of signal processing and communications. Specific current interests include peak-to-average power ratio reduction, error vector magnitude analysis and signal-to-noise-and-distortion ratio analysis.